Use of Soil Nails to Mitigate Infiltration-Induced Slope Failure

by

Dilan Jitesh Gohil

Submitted in partial fulfilment of the requirements for the degree of

Master of Applied Science

At

Dalhousie University

Halifax, Nova Scotia

November 2023

Dalhousie University is located in Mi'kma'ki, the

ancestral and unceded territory of the Mi'kmaq.

We are all Treaty people.

DEDICATION

I owe immeasurable gratitude to my family whose encouragement allowed me to choose the path less traveled, to seek the unknown, and to make a difference.

Table of Contents

List of Tables

List of Figures

ABSTRACT

Natural and man-made slopes are ubiquitous geotechnical structures found in a variety of contexts, such as roads, dams, canals, mines, and riverbanks. The stability of these slopes is critical for the protection of people and infrastructure. Slope failure can have disastrous results due to variables such as earthquakes, rainfall, external stress, or fast groundwater extraction. Landslides have caused substantial damage to property and human life, with the Straight Creek Landslide in the United States being one such current active landslide of concern. This landslide threatens a major roadway, and its failure might lead to fatalities and the long-term closure of the route near the Eisenhower Tunnel. The necessity for proper stabilization solutions to limit the dangers connected with landslides is addressed in this thesis. Soil nailing has gained prominence as a viable method for slope stabilization. However, a thorough study of soil nails' efficacy as a stabilization method, as well as its application under various geological and environmental situations, is still required. The primary goal of this research is to investigate the influence of soil nails on infiltration-induced failures in slopes using long-term modelling of site circumstances. In addition, the study intends to estimate future safety factors using the Excel forecast function and a deep learning model with Long Short-Term Memory (LSTM).

ACKNOWLEDGMENTS

I would like to express my sincere gratitude to Dr Hany El Naggar for his invaluable guidance and support in accomplishing this thesis. I would also like to thank my family and friends for their constant support and encouragement throughout the duration of my study. I would also like to thank my friend Nishit Mistry for helping to understand the Deep learning aspect of coding. Finally, I would like to thank the entire faculty and Civil & Resource Engineering department staff for making my master's degree a smooth and memorable journey.

1. CHAPTER 1: INTRODUCTION

1.1 Background

Slopes, both natural and man-made, are in common geotechnical structures. They can be found on highway embankments, dams, canals, mines, near river banks, and so on. Furthermore, the breakdown of such structures can have catastrophic repercussions for human life and the surrounding infrastructure. As a result, it is critical to ensure that the slopes are stable and do not collapse. The collapse can be induced by a variety of factors, including earthquakes, rains, external stress, or fast groundwater withdrawal. Many landslides have occurred, causing significant damage to property and human lives. In this study, we will be focusing on one such active landslide called Straight Creek Landslide, USA. There is a major highway over the landslide, and failure of the slope can cause loss of lives and long-term closure of the highway just outside of the Eisenhower Tunnel.

1.2 Problem Statement

Landslides endanger human lives, infrastructure, and the environment, needing appropriate stabilization methods. Among the many approaches used, soil nailing has emerged as a potential solution for landslide stabilization. Despite its growing popularity, there is still a need to thoroughly examine the performance of soil nails as a stabilization technology and comprehend its application in various geological and environmental circumstances.

The problem at hand is to simulate the yearly precipitation on the slope and, thereafter, model drains and monitor the change in safety factors. Thus, by implementing soil nails using numerical analysis and doing a parametric analysis on them will yield a comprehensive understanding of the effectiveness and limitations of

soil nails, and the finding will enable engineers to make informed decisions regarding the selection and design of soil nails for mitigation of landslides.

Moreover, a small component of forecasting the safety factor has also been added where the well-known tool Excel has been used and a deep learning method Long Short-Term Memory (LSTM), is used to predict the future values. This will help in integrating the coding in the prediction of safety factors for the concerned engineers.

1.3 Research Objective

The main objective of the thesis is to study the effect of soil nails in improving infiltration-induced failures in slope by long-term modelling of the site conditions and further predict the future safety factor using Excel and LSTM deep learning model.

The objective of this research is to determine the following:

1. To replicate the site conditions using Fully Coupled Flow-Deformation Analysis method of PLAXIS to simulate the yearly change in the groundwater due to infiltration and its effects on the stability of the slope.
2. To study the effect of drain in the upper portion of the slope which intercepts the groundwater and thereby increasing the stability of the slope.
3. Modelling the soil nails in the slope to further increase the stability of the slope and see the effect of the nail spacing and inclination on the stability of the slope.
4. To predict the future safety factors using excel forecast function and LSTM deep learning model.

1.4 Research Approach

Initially the soil properties and geometry of the slope were modelled in the software PLAXIS 2D and safety analysis was done to obtain the FOS. To confirm the

validity of the modelling, it was ensured that the fluctuations in groundwater levels are similar to that of the piezometric readings. Thereafter, the north drain was modelled to observe its effect on the safety factor of the slope. To further increase the safety factor soil nail were installed and parametric analysis was done on the same by changing the inclination and spacing between them. Lastly, the forecasting was done using excel and LSTM model in python.

1.5 Thesis Organization/Arrangement

Thesis is divided into 7 Chapters .

Chapter 1 … Introduction

This chapter gives a bird's eye view of the entire study and summarizes the aim and objectives of the study.

Chapter 2 …Literature Review

In this chapter comprehensive information is provided regarding the landslides, numerical modelling, and the coding aspect of the research. The concepts of matric suction and unsaturated soil is also explained in brief for better understanding of the study.

Chapter 3 …Background

Entire history of the study and list of events that occurred in the case study have been explained here, along with the past remedies and all relevant site data.

Chapter 4 … Methodology

This chapter breaks down the entire study systematically. The instructions from this chapter will enable readers to effectively replicate the things done in the numerical modelling and coding part of the thesis.

Chapter 5 … Results and Discussion

Stepwise explanation of the results of the study are shown here, along with all the logical outcomes and takeaways.

Chapter 6 …Conclusion and Recommendations

A concise explanation of the entire outcome and importance of the study has been mentioned.

Chapter 7 … References

2. CHAPTER 2: LITERATURE REVIEW

1.6 Introduction

Stabilizing the soil slopes is an important aspect in Geotechnical Engineering, as stable slopes facilitate construction of infrastructure over or around it. Slopes can fail due to infiltration, earthquake, geometry, and many other reasons[1]–[3], but here we will be focusing on infiltration-induced slope failure. Infiltration is notorious for causing landslides and slopes failure all over the world. It occurs more often on slopes having less cohesive soil and with slope angles ranging from 25° to 40°. Landslide catastrophes appear to be becoming more common. This is due to the increasing vulnerability and exposure of the population and infrastructure as cities grow in size. Increased human contact, unmanaged land use, and increased forest removal make surface soil more prone to instability [4][5]. To briefly outline the damages due to the slope failure; Natural Resources Canada state that thousands of landslides occur in Canada annually and cause $200 to $400 million in direct and indirect cost[6], in 2018 Japan recorded 161 fatalities and 1505 damaged houses[7] and in US landslides are responsible for $1.6-$3.2 billion in annual losses[8].

Now, to stabilize such slopes various methods have been adopted, such as reducing the slope angle, soil nailing, retaining wall, vegetation, geosynthetics and many more [9], [10].

Due to infiltration the soil loses the matric suction and eventually fails. The matric suction increases the shear strength of the soil by holding the soil particles together. Still, during infiltration, the soil becomes saturated, and that results in the possible failure of the soil slope. In this study, the effect of geogrids on the soil is studied. The soil nails provide reinforcement and hold the soil particles together between the tendons. This results in an increase in the shear strength of the soil.

Moreover, the basics of slope stability analysis are mentioned in this chapter. LE FEA and FDA analysis are briefly explained.

1.7 Landslide: Causes and Consequences

The word "landslide" is often used. The reason for this is that researchers in a wide range of scientific disciplines are interested in the topic of landslides, including sedimentology, oceanography, geomorphology, volcanology, seismology, glaciology, aerology (i.e., geology of Mars), deep-sea structural engineering, highway engineering, soil mechanics, climate change, eustasy, natural hazards, and petroleum exploration and production [11]. Unsurprisingly, each scientific group has developed its own nomenclatural system [12]. In context of geotechnical engineering and for this research we will define it as downward movement of a mass of soil, rock or combination of both, on a sloping stratum triggered when the forces acting on the slope exceed its capacity to resist them and resulting in the movement and displacement in the slope.

Out of all the natural disasters caused the landslides are 7^{th} largest killer [13] and having a mortality rate of about 17% [14]. Landslides inflict an estimated one to 3.6 billion dollars in economic damages in the United States each year, and 25-50 people are killed, making it one of the most expensive disasters in the world [15]. Similarly, Japanese annual losses are estimated to be between $4 and $6 billion USD, with the most severe landslides claiming up to 100,000 people [16], [17]. Due to all these losses and damage, it's important to learn causes of landslides and subsequently find ways to avoid the losses by either stabilizing the slope or entirely avoiding creating a structure over such soil. Following are some of the reasons for landslide to occur:

1. Slope Geology and Geomorphology: The geological characteristics of a slope play a significant role in landslide occurrence. Weak or unstable rock and soil types, such as clay, silt, and loose sand, are more susceptible to landslides. Steep

slopes, rugged terrain, and the presence of fractures or faults can also contribute to instability.

2. Water and Precipitation: Water is a major trigger for landslides. Heavy or prolonged rainfall can saturate the soil, increasing pore pressure and reducing its strength. This leads to a loss of soil cohesion, making it more prone to sliding. Similarly, rapid snowmelt, excessive irrigation, or changes in groundwater levels can contribute to slope instability.
3. Slope Modification and Excavation: Human activities that modify slopes, such as construction, excavation, and mining, can weaken the natural stability of the land. Removing vegetation and altering drainage patterns can disrupt the balance of forces within a slope, making it more susceptible to failure.
4. Earthquakes and Seismic Activity: Earthquakes can induce landslides by imparting strong ground shaking, which destabilizes the slope materials. The shaking can trigger landslides in areas where slopes were already close to failure, or it can generate new landslides by altering the stress distribution within the slope.
5. Vegetation and Root Systems: Vegetation, particularly trees and their root systems, provide essential reinforcement to slopes by binding the soil together and absorbing excess water. Deforestation, wildfires, or the removal of vegetation for development purposes can significantly reduce the slope's stability.
6. Human Activities and Land-Use Practices: Improper land-use practices, such as uncontrolled urbanization, improper slope grading, and inadequate drainage systems, can increase the likelihood of landslides. Poorly planned infrastructure,

such as roads and buildings on unstable slopes, can add weight and stress to the slope, leading to failure.

7. Climate Change: Climate change can influence landslide occurrences through altered precipitation patterns, increased intensity of storms, and melting glaciers. These changes can lead to soil saturation, higher erosion rates, and changes in groundwater levels, all of which contribute to slope instability.

1.7.1 Landslide classification

Historically, the word landslide has been used to refer to nearly any type of mass movement of rocks and regolith at the Earth's surface. David Varnes, a geologist, noticed this imprecise usage in 1978 and developed a new, much stricter framework for classifying mass movements and subsidence processes [18]. Cruden and Varnes improved this approach in 1996,[19] and it was refined by Hutchinson (1988),[20] Hungr et al. (2001),[21] and lastly by Hungr, Leroueil, and Picarelli (2014) [22]. The categorization because of the most recent change is presented below based on the type of movement.

Table 1 Hungr-Leroueil-Picarelli classification [22]

Note: the words in italics are placeholders. Use only one.

Type of movement	**Rock**	**Soil**
Fall	*Rock/ice* fall	*Boulder/debris/silt* fall
Topple	Rock block topple	*Gravel/sand/silt* topple
	Rock flexural topple	
Slide	Rock rotational slide	*Clay/silt* rotational slide
	Rock planar slide	*Clay/silt* planar slide
	Rock wedge slide	*Gravel/sand/debris* slide
	Rock compound slide	*Clay/silt* compound slide
	Rock irregular slide	
Spread	Rock slope spread	*Sand/silt* liquefaction spread
		Sensitive clay spread

Flow	*Rock/ice* avalanche	*Sand/silt/debris* dry flow
		Sand/silt/debris flowslide
		Sensitive clay flowslide
		Debris flow
		Mud flow
		Debris flood
		Debris avalanche
		Earthflow
		Peat flow
Slope deformation	Mountain slope deformation	Soil slope deformation
	Rock slope deformation	Soil creep
		Solifluction

In addition to type of movement, landslides can also be classified on the basis of material involved, triggering mechanism and rate of movement Fig.1.

Based on Material Involved:

a. Rockslides and Rockfalls: These landslides involve the movement of solid rock masses or individual rock blocks. They typically occur on steep slopes and are common in mountainous regions.

b. Debris Avalanches: Debris avalanches involve the rapid movement of a mixture of rock fragments, soil, and other loose debris. They often result from the failure of steep slopes and can travel long distances.

c. Earthflows: Earthflows involve the slow movement of saturated or semi-fluid soil or clay. They have a characteristic viscous behavior and are common in areas with fine-grained materials.

d. Slump: A slump is a form of rotational slide where a block of soil or rock tilts backward and downward along a curved failure surface. The material remains intact during the movement.

Based on Triggering Mechanism:

a. Rainfall-Induced Landslides: These landslides occur as a result of heavy or prolonged rainfall, which saturates the soil, increases pore pressure, and reduces soil strength.

b. Seismically-Induced Landslides: Landslides triggered by earthquakes or seismic activity. The ground shaking from an earthquake can cause slope instability and failure.

c. Human-Induced Landslides: These landslides result from human activities such as construction, mining, or excavation. Alterations to the slope's natural stability through human intervention can trigger landslides.

d. Volcanic-Induced Landslides: Landslides associated with volcanic eruptions, including the collapse of volcanic edifices, pyroclastic flows, and lahars.

Speed class	Description	Velocity (mm/s)	Typ. velocity	Probable destructive significance
7	Extremely fast	5×10^{3}	5 m/s	Disaster of major violence, buildings destroyed by impact of displaced material, many deaths, escape unlikely
6	Very fast	5×10^{1}	3 m/min	Some lives lost; velocity too great to permit all persons to escape
5	Fast	5×10^{-1}	1.8 m/hr	Escape evacuation possible; structures, possessions and equipment destroyed
4	Moderate	5×10^{-3}	13 m/month	Some temporary and insensitive structures can be temporarily maintained
3	Slow	5×10^{-5}	1.6 m/year	Remedial construction can be undertaken during movement; insensitive structures can be maintained with frequent maintenance work if total movement is not large during a particular acceleration phase
2	Very slow	5×10^{-7}	16 mm/year	Some permanent structures undamaged by movement
1	Extremely slow			Imperceptible without instruments, construction possible with precautions

Figure 1 Classification of landslide based on the rate of movement [19], [23]

1.8 Inclinometer

An inclinometer is a device that measures the slope or angle of inclination with respect to the vertical. It is extensively used in engineering, geology, surveying, and construction to monitor changes in slope or tilt. If the inclinometer becomes useless after a particular displacement, it is likely that the device was calibrated for a specified range of movement [24].

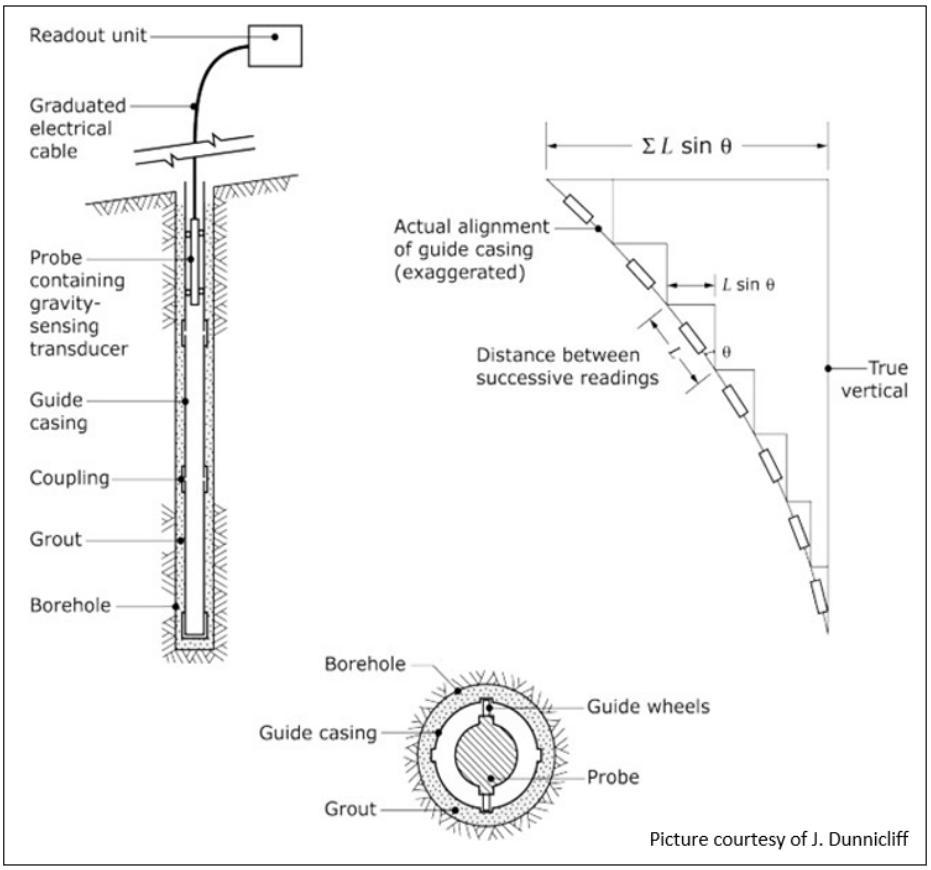

Figure 2 Cross section of inclinometer with its components [24]

1.9 Soil Mechanics for infiltration-based slope failures

Pertaining to this research we will be focusing on the rainfall induced slope failure as our case study experiences failure due to infiltration. Following subtopics give better understanding of the concept behind the slope failure which occurs due to infiltration, or due to increase of water in soil medium.

1.9.1 Introduction

The field of soil mechanics is divided into two parts, one dedicated to saturated soil mechanics and the other to unsaturated soil mechanics. To briefly differentiate between the two, the saturated soil is the soil present below the ground water level and soil above it is called unsaturated soil [25]. Also, most of the world's regions are in semi-arid regions and hence the necessity to consider the later soil. Moreover, unlike the saturated soil which is governed by principle of effective stress by Terzaghi, the unsaturated soil mechanics is governed by normal stress and matric suction [26]. As shown in the figure the water pressure reduces to zero at the groundwater level and then it becomes negative above the groundwater level, thus introducing the concept of matric suction.

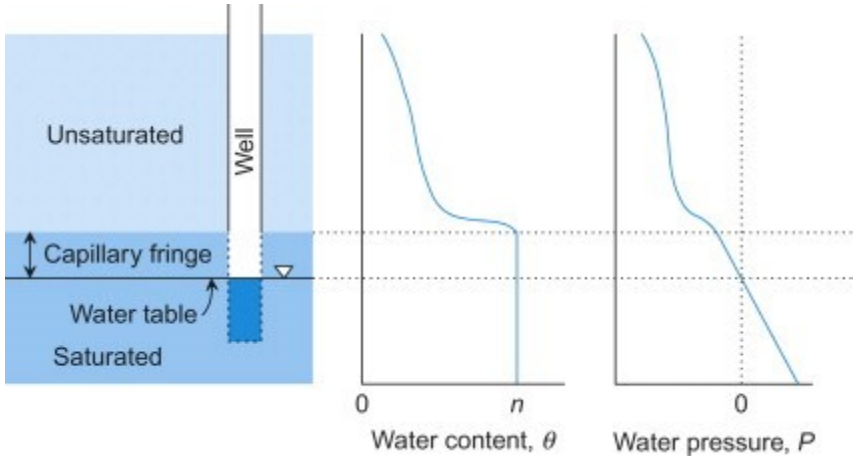

Figure 3 Anatomy of the soil zones beneath the ground

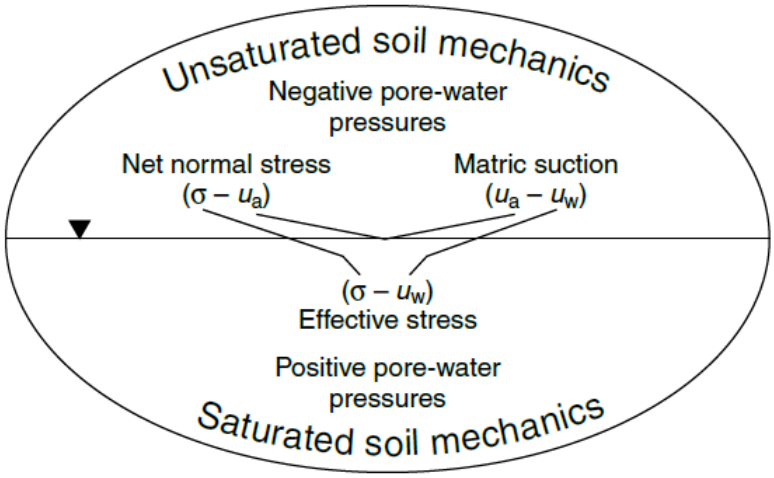

Figure 4 Generalized visual representation of soil mechanics [27]

1.9.2 Saturated and Unsaturated Soil Mechanics

Initially, the shear strength of the soil was given by Mohr-Coulomb empirical equation [28], which gives the shearing resistance of the soil [29], where; τ=shearing resistance, c=cohesion, σ=Normal Stress and φ=friction angle, and later on Karl Terzaghi gave a path to modern-day geotechnical engineering by describing the mechanical behavior of saturated soil and he also gave insight to concept of unsaturated soil mechanics. He revised the shear strength concept by assuming soil to be two phase system, i.e., considering the pore water. In his book "*Theoretical Soil Mechanics*" [29], he discussed the shear strength of the saturated soils and gave insight to the unsaturated soil mechanics which will take some years to evolve.

$$\tau = c + \sigma * tan\varphi \qquad Eq\ 1$$

As the soil was considered as having two phases by Terzaghi he modified the classical shear strength equation of Mohr-Coulomb and replaced the normal stress with the effective stress "σ'"(which is difference of total stress and **pore water pressure)**

and cohesion and Friction angle with their effective counterparts. There is no relation between the effective cohesion and friction angle with cohesion and friction angle, the effective are just the parameters when the pore water is considered in the soil i.e., a two-phase system.

$$\tau = c' + \sigma' * tan\varphi' \qquad Eq\ 2$$

$$\sigma' = \sigma - u \qquad Eq\ 3$$

One of the major issues necessary to create a credible prediction framework for the mechanical behavior of unsaturated soil has been to find a widely applicable and realistically implementable method to quantify the internal stress state[30]. Internal Stress State in unsaturated soil has a certain uniqueness to it as the forces arises from the physicochemical or cementation effects due to the capillary effect of water [30]. The mechanical behavior of unsaturated soil is greatly governed by the degree of saturation, geometry of pores and grain size. Also, total suction in unsaturated soil consists of two components namely, osmotic suction and matric suction [31]. Osmotic suction is the difference in pore water salt concentration within the soil and matric suction is difference between the pore-air pressure and the pore-water pressure [32][33]. Since the osmotic suction changes are less significant in comparison to matric suction, total suction is essentially assumed to be equal to matric suction [34] [32].

Now, for unsaturated soil the shear strength can be given by Eq 4, where "$\sigma - u_a$" is the net normal stress and "$u_a - u_w$" is matric suction. Also, effective stress parameter "χ" is introduced in this equation which ranges from 0 to 1, depending on the saturation of the soil. So, if the saturation is 100% the effective stress parameter will be unity "$\chi = 1$" and the equation will be transformed to Eq 4.

$$s = [(\sigma - u_a) + \chi(u_a - u_w)]tan\varphi' + c' \qquad Eq\ 4$$

Moreover, saturated soil consists of water and soil, while Unsaturated soil contains four components soil, water, air, and air-water interface[35]. The concept of the fourth phase was introduced by Fredlund and Morgenstern [36]. The air-water interface between the particles experiences unbalanced force towards the interior of water, and this develops a tensile full tangential to skin surface to balance the forces that results in added force that keeps the soil particles together. It therefore takes the shape of a catenoid shown in the figure [32]. The shape of the water is catenoid as seen in figure 5, and the shape occupies the least area when bounded by closed space further proof of tensile forces acting in the medium.

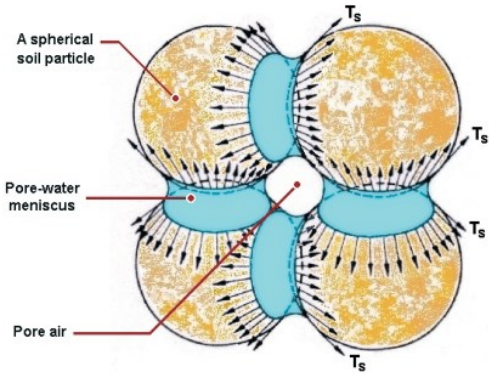

Figure 5 Tensile forces of the water makes the soil particles to stay near each other [32]

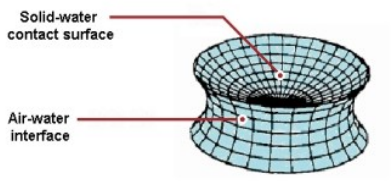

Figure 6 Catenoid shape of the water present between the particles [32]

1.9.3 Effect of infiltration on slope stability

During rainfall or snowmelt, the water infiltrates and creates a wetting front. The gradual seepage of water then increases the groundwater level and results in rise of groundwater level. Traditional slope stability analysis assumes that the failure of the slope was the result of increase in groundwater level due to infiltration [37], [38]. However, in many slopes' failure the advancement of wetting front was the reason for the reduction in the matrix suction, reduction in soil shear strength and eventual slope failure [39]. Thus, for unsaturated soil to include the infiltration in slope stability analysis is very crucial. The effect of infiltration in the unsaturated soil is dramatic and it can significantly reduce the shear strength of the soil eventually leading to failure [40].

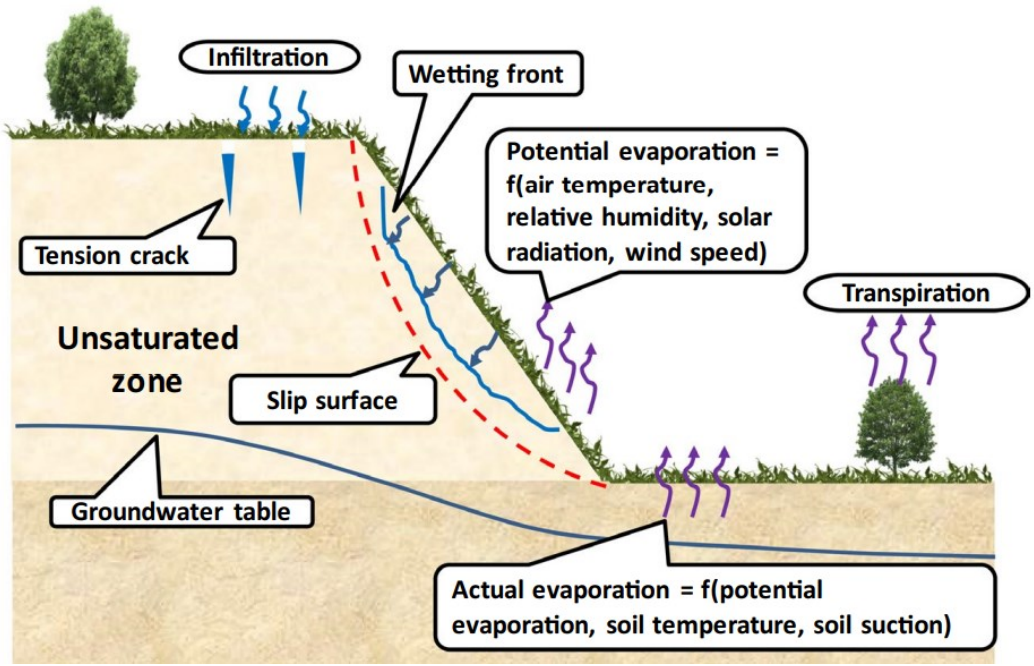

Figure 7 Mechanism of infiltration-induced slope failure [36]

1.10 Slope Stability: Numerical methods

1.10.1 History

Initial numerical modelling can be traced back to 1960s where method of slices, proposed by Fellenius and Bishop independently, was one of the earliest numerical methods for slope stability analysis [41]. It divides the soil mass into vertical slices and applies equilibrium and force/moment equilibrium to each slice. This method facilitated more accurate calculations of factors of safety and critical slip surfaces. Thereafter, Finite Element Analysis (FEA) and Limit Equilibrium Methods (LEM) developed in 1970s both of which are widely used either interchangeably or together depending on type of analysis.

1.10.2 Core Disparity between major numerical methods: Limit Equilibrium Methods, Finite Element Analysis and Finite Difference Analysis

In this section, we will explore the fundamental differences between three major numerical methods commonly used in geotechnical engineering: Limit Equilibrium Methods, Finite Element Analysis (FEA), and Finite Difference Analysis (FDA). These methods have distinct characteristics and approaches, leading to disparities in their underlying principles and application [42].

- Limit Equilibrium Methods: Limit equilibrium techniques are founded on the idea of achieving equilibrium between driving forces (such as gravity forces) and resisting forces (such as shear strength) along probable failure surfaces. They are often used for slope stability analysis and use simplified assumptions such as assuming rigid body behavior and ignoring transient pore water pressure effects. Limit equilibrium

methods are commonly utilized in practice because they give a margin of safety against failure and are reasonably simple to apply.

- Finite Element Analysis (FEA): FEA is a numerical approach for analyzing the behavior of a system under various situations that breaks a large problem into smaller, interrelated pieces. When compared to limit equilibrium approaches, it provides for a more thorough and precise description of the geometry, material characteristics, and boundary conditions. Spatial fluctuations, nonlinear behavior, and complex interactions between soil and structures may all be captured using FEA. However, greater computational resources and knowledge are required to effectively set up and evaluate the findings.
- Finite Difference Analysis (FDA): FDA is another numerical approach that discretizes the problem domain into a grid of nodes and uses difference operators to estimate the derivatives of governing equations. It is extensively used in geotechnical engineering to solve partial differential equations, such as the governing equations for groundwater flow and consolidation analysis. FDA supports the depiction of transitory seepage and consolidation processes, making it appropriate for time-dependent analysis. However, as compared to FEA, FDA may have difficulties in dealing with complicated geometries and boundary conditions.

The fundamental difference between these numerical approaches is reflected in their underlying concepts, assumptions, and capabilities. Limit equilibrium approaches yield simple, conservative estimates of stability, whereas FEA and FDA give more

thorough and extensive assessments capable of capturing complex behaviors and interactions. The approach chosen is determined by the individual problem, available data, necessary precision, and computer resources. Limit Equilibrium, Finite Element Analysis and Finite Difference Methods

1.10.3 Safety Factor of Slope

A slope's safety factor is an important measure used to assess the stability and safety of natural or artificial slopes. It is a fundamental element in geotechnical engineering and indicates the margin of safety against slope failure. Typically, the safety factor is computed by comparing the resisting forces to the driving forces operating on the slope. The shear strength of the soil or rock mass that offers resistance against possible slope breakdown is referred to as the resisting forces. Several elements influence it, including the cohesiveness, friction angle, and internal friction qualities of the soil or rock material. The opposing pressures serve to stabilize the slope and keep it from moving. The driving factors are those that cause slope instability and collapse. The gravitational force acting on the bulk of soil or rock material is the fundamental driving force working on a slope. The slope angle, material weight, and any external loads or pressures operating on the slope all determine the size of the driving force.

By dividing the resisting forces by the driving forces, the safety factor is derived. It may be stated mathematically as:

Safety Factor = Resisting Forces / Driving Forces

The shear strength characteristics of the soil or rock material are often used to represent the resisting forces, while the gravity forces acting on the slope are used to

represent the pushing forces. A number greater than one suggests stability, whereas a value less than one indicates possible slope collapse.

Local safety factor and global safety factor are two often utilised safety factors.

- Local Safety Factor: the local safety factor is a measure of the stability of a specific point or place inside a structure or soil slope. It calculates the margin of safety against failure at that specific place. The local safety factor is computed by dividing the resistive forces at that site by the driving forces.
- Global Safety Factor: The global safety factor, also known as the overall factor of safety, is a measure of the overall stability and safety of the structure or soil slope. It analyses the whole system's stability rather than individual points or regions. The global safety factor compares the total resisting forces to the total driving forces operating on the system to determine the overall stability of the structure or slope.

However, the majority of slope stabilisation standard codes and geotechnical guides rely on global safety criteria. The US Army Corps has specified many safety factors for different slope circumstances, such as **1.5** for typical long-term conditions of embankment and safety factor of 1.3 and up for other slopes where the consequences can be heavy after failure [43].

For example, the safety parameters for soil nail walls are presented in the table below according to FHWA circular 7 [44]. Furthermore, there are no universally agreed criteria for determining the safety factors for a landslide-prone slope; the safety factors are determined based on the consequences of failure, risk tolerance, and site circumstances that may be unclear and represent a danger to stability.

Failure Mode	Resisting Component	Symbol	Minimum Recommended Factors of Safety		
			Static Loads[1]		Seismic Loads[2] (Temporary and Permanent Structures)
			Temporary Structure	Permanent Structure	
External Stability	Global Stability (long-term)	FS_G	1.35	1.5[1]	1.1
	Global Stability (excavation)	FS_G	1.2-1.3 [2]		NA
	Sliding	FS_{SL}	1.3	1.5	1.1
	Bearing Capacity	FS_H	2.5 [3]	3.0 [3]	2.3 [5]
Internal Stability	Pullout Resistance	FS_P	2.0		1.5
	Nail Bar Tensile Strength	FS_T	1.8		1.35
Facing Strength	Facing Flexure	FS_{FF}	1.35	1.5	1.1
	Facing Punching Shear	FS_{FP}	1.35	1.5	1.1
	H.-Stud Tensile (A307 Bolt)	FS_{HT}	1.8	2.0	1.5
	H.-Stud Tensile (A325 Bolt)	FS_{HT}	1.5	1.7	1.3

Figure 8 Safety Factor Requirement for Soil Nail wall [45]

1.10.4 Mechanism of Slope Stabilization

It involves application of various engineering techniques to improve the stability of slope. The selection of the method depends on the type of project, the budget, time required to stabilize the slope and other factors. Following are some of the most used slope stabilization methods:

- Grading and Benching: This is the process of redesigning a slope by cutting or filling it in order to lower its steepness and produce more stable slope angles. The slope has been graded into terraces or benches, which can aid in erosion management and lessen the danger of slope failure.
- Surface Drainage Control: Slope stability is dependent on proper surface drainage. Surface drainage features like ditches, swales, and culverts can assist move water away from the slope and reduce soil saturation, lowering the risk of slope failure.

- Erosion Control Measures: It is critical to use erosion control measures to avoid soil erosion on slopes. Techniques such as the use of erosion control blankets, geotextiles, and revegetation using erosion-resistant plants can aid in the stabilization and protection of the slope.
- Retaining Wall: Constructing retaining walls along the slope can give structural support while also preventing soil movement. Concrete, gabions, and mechanically stabilized earth (MSE) systems are all examples of retaining walls.
- Soil Nailing: Soil nailing is a technique for strengthening a slope by inserting grouted steel bars (nails) at regular intervals into the soil mass. This increases the tensile strength of the soil and helps to stabilize the slope.
- Slope Drainage and Groundwater Control: Proper groundwater control is critical for slope stability. Installing subsurface drainage systems, such as French drains, or horizontal or vertical drains, can assist in lowering the water table and relieving pore water pressure inside the slope.
- Slope anchoring: It is the insertion of anchors or tiebacks into a slope to give additional stability. These anchors, which are often composed of high-strength steel, are typically inserted in the stable soil or rock mass behind the slope.
- Slope Reinforcement: To reinforce the slope, many approaches can be utilized, such as the use of geosynthetics (such as geogrids or geotextiles) to enhance soil strength, slope stabilization mats, or slope mesh systems.

1.10.5 Soil Nails: Remedy to Slope Failure

Soil nails are passive reinforcing devices that are drilled and grouted sub-horizontally in the earth to support excavations in soil or soft and worn rock that: Tension caused by deformation of the retained soil or weathered rock mass contributes to the stability of earth-resisting systems. Tensile loads are transferred to the surrounding ground via shear stresses (i.e., bond stresses) at the grout-ground interface.

History of Soil Nails [46]:

- 1960s: Soil nailing evolved in Europe during the 1960s as a low-cost alternative to traditional slope stabilization technologies. The first applications were mostly from France and Germany.
- 1970s: In the 1970s, soil nailing became popular in France, notably in the building of highway and railway cut slopes. During this time, research and development efforts were focused on developing design methodologies and studying the behavior of soil nails.
- 1980s: Soil nailing became more popular over the world during the 1980s. The approach gained popularity as a means of stabilizing slopes, excavations, and retaining walls. Design processes, building procedures, and the creation of specialized equipment were all improved.
- 1990s: In the 1990s, soil nailing became increasingly frequently used across the world, with applications in a variety of geotechnical projects. The technology has been employed in both temporary and permanent slope stabilization projects, including highway and railway slopes, landslide rehabilitation, and mining applications.

Soil nailing is still a popular and well-established method of slope stabilization in the 2000s and beyond. Soil nails have been shown to be a versatile and effective method of slope stabilization across a wide range of soil types, slope geometries, and ground conditions. They have been utilized successfully in a wide range of geotechnical projects worldwide and have become a standard technique in slope stabilization and earth retention.

1.10.6 Basic components of Soil Nail

The components of soil nails according to FHWA circular no.7 [44]:

- Tendons: Tendons, also known as steel bars, mobilize tensile stress in response to lateral movement and soil deformation. Soil movement can occur during excavation, after excavation (owing to time-dependent deformations), or after excavation in the presence of external loads such as surcharge or traffic loads. Tendons may be solid or hollow bars. After being put into strong drill holes, solid bars are grouted into place. Hollow bars with a sacrificial drill bit are utilised to drill the hole, which then serves as permanent soil nail reinforcement.
- Grout for soil nails is typically composed of Portland cement and water. The grout has three purposes: (i) it transfers shear loads between the deforming ground and the tendons; (ii) it transfers tensile stresses from the tendons to the surrounding stable soil; and (iii) it protects the tendons from corrosion. Using the tremie technique, grout is poured in drill holes by gravity.
- Facing: It is made up of two parts: the first and the last. To offer temporary stability and protection, the first facing is put on the exposed soil at each excavation lift before or after nail installation. The bearing

plate of the soil nail is also received by the first facing. The final facing is built on top of the first face and ensures structural continuity throughout the design life cycle. An aesthetic finish may also be used in the final face. The initial face is often reinforced shotcrete.

- Drainage: Behind soil nail walls, a drainage system is placed to: (i) collect perched groundwater or infiltrated surface water that is present behind the facing; and (ii) move the collected groundwater away from the wall. The drainage system is often made out of composite, geosynthetic drainage strips, also known as geocomposite strip drains. The drainage system does not cover the entire wall surface, but generally 10-20% or more of the excavation face, depending on the strip drain spacing and commercial widths that are available.

1.11 Plaxis 2D for Unsaturated soil

Application of numerical modelling in geotechnical engineering has been proven an effective way to premediate the solutions for various problems, provided that the model is suitably verified and can replicate the complex soil behavior to acceptable extent [47], [48]. Plaxis has the capability to solve the equations of deformation and flow of water simultaneously. It is crucial as the behavior of one depends on the other. More about that is explained in the next section.

1.11.1 Fully Coupled Flow Deformation Analysis

Plaxis uses an iterative solution approach to calculate both water flow and soil deformation in a fully connected study. The program concurrently solves the governing equations for both processes, accounting for the interactions and feedback between

water flow and soil deformation [49]. Here's an overview of how Plaxis calculates water flow and soil deformation together [49], [50]:

- Soil Domain Discretization: The soil domain is discretized into finite elements or finite difference cells. This division allows the soil profile to be represented as a sequence of distinct components or cells, from which the governing equations may be solved.
- Initialization: The analysis begins with a distribution of pore water pressures and saturation degrees. These beginning circumstances are frequently based on the problem's initial conditions or the outcomes of a previous investigation.
- Deformation: Using all the parameters for the soil model plaxis solves the differential equation and gets the deformation in the soil, followed by the flow calculation.
- Flow Calculation: Plaxis solves the Richards equation, which regulates water flow through soil, to compute pore water pressures and gradients of water content in each element or cell. The Richards equation takes into account hydraulic conductivity, gradients of matric suction and water content, and soil storage capacity. Based on the hydraulic parameters and the applied boundary constraints, the flow calculation calculates the redistribution of water within the soil profile. After this the pore pressures are updated for the new deformation calculations, and cycle goes on.
- Coupling Iteration: Plaxis uses an iterative technique to establish convergence between the flow and deformation computations. The flow calculation's computed pore water pressures are utilized to update the

effective stresses and shear strength in the deformation calculation. The updated effective stresses, in turn, alter water flow behavior by influencing hydraulic gradients and pore water pressure distribution. The iteration method is repeated until a consistent solution is produced in which the computed pore water pressures and deformation field meet both the equilibrium conditions and the flow equations at the same time.

- Convergence and Solution: The iterative procedure continues until convergence is reached, which means that the differences in pore water pressures and deformations between subsequent iterations are less than a predetermined tolerance. Plaxis then delivers the final solution, which includes the distributions of pore water pressures, degrees of saturation, deformations, and stresses in the soil profile.

Although linear constitutive models are commonly used in numerical analyses [48], [51]–[55], sometimes to capture the complex behavior of the soil models other than Mohr-Coulomb are used. Here in this study for soils where the displacement needs to be monitored Hardening Soil is used and for the rest Mohr-Coulomb soil type is used. The following sections give brief information regarding the two soil types.

1.12 Analyzing Unsaturated soil with respect to Mohr-Coulomb Soil model

The Mohr-Coulomb (MC) and Soil Water Characteristic Curve (SWCC) parameters are indirectly dependent in fully coupled flow-deformation analysis [50]. The interplay between these factors results from the coupling effect between mechanical behavior and water movement in the soil. The pore water pressure, which is determined by the movement of water through the soil, influences the effective stress in the Mohr-Coulomb model. In turn, the pore water pressure is determined by the

volumetric water content, which is dictated by the SWCC. As a result, the SWCC can indirectly impact the effective stress and, as a result, the shear strength parameters (such as cohesion and friction angle) in the Mohr-Coulomb model. Changes in water content can impact the effective stress state and hence the mechanical behavior of the soil.

1.13 Analyzing Unsaturated soil with respect to Hardening Soil model

The Hardening Soil model was created as a significant development in geotechnical engineering to solve various inadequacies in previous soil models, particularly the traditional Mohr-Coulomb model [56]. The oversimplifications found in prior models, particularly with regard to unsaturated soil behaviour, were the main issues it sought to address. Because of its ability to effectively capture non-linear and time-dependent behaviours, the Hardening Soil model is particularly useful for tracking long-term displacements in soil [57]. The Mohr-Coulomb model, on the other hand, is unsuitable for long-term displacement monitoring because to its extremely simplified assumptions about soil behaviour, which treats it as elastic and fully flexible. This deficiency results in an inaccurate depiction of soil as extremely hard.

1.13.1 Mesh

In FEM, meshing is typically used to discretize the soil or rock domain into fine components. Once the domain has been subdivided into fine elements, they will behave in accordance with the properties provided to them by the user. The mesh is an important component of finite element analysis (FEA) software such as PLAXIS 2D because it allows for numerical approximation of the governing equations that explain soil behavior [58].

PLAXIS 2D has two types of elements for modelling soil layers or other clusters: 6-node and 15-node triangular components (Fig. 15). The element type affects memory usage, computation speed, and accuracy. Nodes are precise spots within the

finite element mesh where analytical computations are conducted. Nodes are often situated near the vertices of the mesh's finite components. These nodes function as control points inside the analytical domain, defining displacements, stresses, strains, and other pertinent characteristics within the soil or rock structure. The 15-node components are chosen for the following 2D-studies to guarantee high accuracy [59], [60]. Also, one can control the density of mesh in the calculations, whether to make it denser or rarer. If the mesh is dense then it will give more accurate results but at the expense of long computational time.

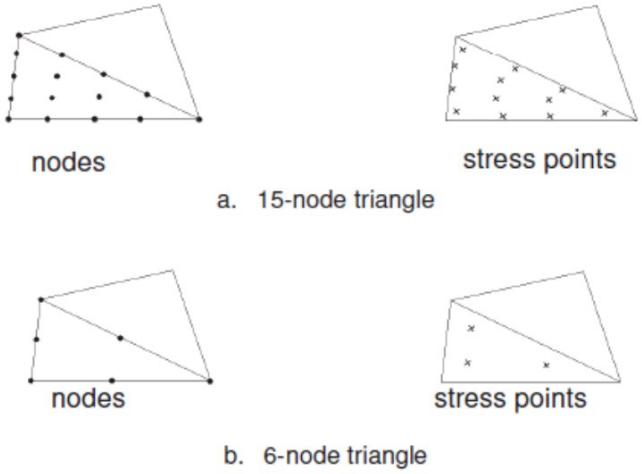

Figure 9 Nodes and Stress points for different soil elements [60]

1.13.2 Safety Analysis in PLAXIS 2D

The Safety calculation type is a PLAXIS 2D option for calculating global safety factors. The shear strength parameters tan and c of the soil, as well as the tensile strength, are gradually lowered in the Safety method until the structure fails. The number of steps is set to 100 by default, however a bigger value up to 10000 can be entered here if necessary.

The FOS is governed by following equation in the software [50]:

$$\Sigma Msf = \frac{tan\varphi'_{input}}{tan\varphi'_{reduced}} = \frac{c'_{input}}{c'_{reduced}} \quad Eq\ 5$$

1.13.3 Numerical modeling parameters of Soil Nails in PLAXIS 2D

In PLAXIS the soil nail can be made using embedded beam feature. In past studies in order to model soil nails plate element or geogrid were used but since the element extended in the Z-axis i.e. perpendicular to the screen [61], without any spacing it would not be accurate to predict the stability as soil nails have some spacing in between them.

So, in this study embedded beam elements are used, where spacing and skin friction along with the material strength properties can be defined. The unit weight was averaged based on the cross-section area of the concrete and tendon. Similarly, the Young's Modulus was also averaged based on the cross-section area. Following formulas represent the unit weight and young's modulus for the soil nail, averages were taken as the material is a composite (concrete and steel).

$$\gamma_{avg} = \gamma_{concrete}\frac{A_{concrete}}{A_{Total}} + \gamma_{Steel}\frac{A_{Steel}}{A_{Total}} \quad Eq\ 6$$

$$E_{avg} = E_{concrete}\frac{A_{concrete}}{A_{Total}} + E_{Steel}\frac{A_{Steel}}{A_{Total}} \quad Eq\ 7$$

Moreover, the skin friction of the soil nails in PLAXIS can be defined in three ways, constant skin friction throughout the length, variable skin friction and lastly layer dependent skin friction. Within the third option, the skin resistance directly relates to the strength of the surrounding soil by the interface strength reduction factor Rinter, which amount of slide between the interface [62].

$$\tau_i = c_i + \sigma_n' tan\varphi_i \qquad Eq\ 8$$

$$c_i = R_{inter} c_{soil} \qquad Eq\ 9$$

$$tan\varphi_i = R_{inter} tan\varphi_{soil} \qquad Eq\ 10$$

$$T_i = 2\pi R_{eq} \tau_i \qquad Eq\ 11$$

To minimize excessive skin resistance, an overall maximum resistance Tmax (constant value along the pile/rock bolt in force per unit pile/rock bolt length) can be defined in the embedded beam material data set as an overall cut-off value.

1.14 Data forecasting methods

Here we have used forecasting to predict the future safety factors based on the data calculated. The following are some of the methods for data forecasting.

1.14.1 Exponential Smoothing

Exponential Smoothing (ETS) is a forecasting approach that is often used to analyze time series data. The ETS method incorporates many algorithms that give varying weights to historical data and provide predictions based on weighted averages [63].

1.14.1.1 Simple Exponential Smoothing

Simple exponential smoothing is one of the most basic methods for forecasting a time series; the only pattern learned from experience is the average value around which demand changes over time. As its final estimate of the level, the exponential smoothing model will project future demand. It is critical to recognise that there is no precise mathematical definition of the level—rather, model must approximate it, but in simple words it is at a given time point, the smoothed value of the series. It represents

the overall baseline or average of the series. The shortcoming of this one is that it does not take into consideration the trend [64].

1.14.1.2 Double Exponential Smoothing

One significant limitation of this simple smoothing is that it can only perceive a level and cannot identify and project a trend. The direction and rate of change of the data over time are represented by the trend. Double exponential smoothing recognizes rising and falling data trends. Trend represents the series' direction and rate of change over time. It detects growing and declining trends in data [64].

1.14.1.3 Excel forecast data function.

The forecast function produces a table with historical and expected data as well as a chart [65]. The prediction forecasts future values using your existing time-based data and the Exponential Smoothing (ETS) algorithm's additive error, additive trend, and additive seasonality (AAA) version. These techniques are intended to detect trends, seasonality, and other patterns in data [64]. So, like double exponential smoothing method, but this adds one more parameter to it, the seasonality. Seasonality represents the data's recurring patterns or cycles, such as daily, weekly, or annual trends.

AAA seasonal the Exponential Smoothing (ETS) algorithm Combines the level, trend, and seasonality components. It is useful for data that exhibits both trend and seasonality.

1.14.2 Long Short-Term Memory (LSTM)

Deep learning is a branch of machine learning that focuses on training artificial neural networks (ANNs) with numerous hidden layers to learn and extract hierarchical data representations. It has received a lot of attention and popularity in recent years

because of its capacity to learn nuanced patterns and features from huge and complicated datasets [66].

The LSTM (Long Short-Term Memory) architecture is a sort of recurrent neural network (RNN) architecture that is meant to overcome the vanishing gradient problem and capture long-term relationships in sequential data. Hochreiter and Schmidhuber developed it in 1997, and it has since been a frequently used model for a variety of applications requiring sequential data, such as time series forecasting, natural language processing [67], speech recognition, and others [68]. Following are brief explanations of open and closed loop forecasting:

- Open Loop: The network in an open loop LSTM creates output entirely dependent on the input sequence. It does not consider the previously expected outcomes. This method considers the LSTM as a separate function that analyses inputs without considering its own past predictions [69].
- Closed Loop: A closed loop LSTM creates output by considering both the input sequence and previously anticipated results. It incorporates feedback from prior forecasts into future predictions. This allows the network to record time-step relationships and produce more context-aware predictions [69].

Here we will be using the closed loop prediction instead of open loop, because the open loop prediction needs true values while the closed loop prediction does not require any true values. Here true value means that if the model has input of 4 years, it will train itself using 3 years and use the last year's data to make the predictions, i.e it will have a target value of true values. In a sense it is forecasting but when the data is

already known. Since we want to forecast the data which is not known we will be using the closed loop prediction.

1.14.3 Working of closed loop LSTM and its training process

A closed loop LSTM (Long Short-Term Memory) architecture features feedback connections, allowing it to create sequential outputs by utilizing its own predictions as input for future predictions. The output of each time step in a closed loop LSTM is supplied back into the model as input for the following time step, forming a feedback loop. To give an example, if the input value for a particular data is 365 days and using that information the LSTM predicts one more day then the new day is again taken into account for second cycle where the first day is no considered and thus forming a loop for prediction.

There are three special gates on the notepad: an input gate, a forget gate, and an output gate [70]. The input gate determines which fresh information should be stored in the memory cell. When anything is significant, it opens the gate and permits the information to be recorded[71]. However, if the information is unimportant, the gate remains closed and the information is disregarded. The forget gate decides what information from the memory cell should be deleted or forgotten. If something is no longer relevant, the gate opens, and the information in the memory cell is deleted[70]. If anything is still vital, the gate remains closed, and the information is saved. Finally, the output gate determines whether or not the information should be shared with others or utilized to make predictions. If anything, helpful is found in the memory cell, the gate opens and the information is transferred. However, if anything is not critical to the present activity, the gate remains closed, and the information is not used.

This allows the model to recall essential patterns in data sequences, forget irrelevant data, and generate accurate predictions based on the remembered data. LSTM has been widely employed for applications like time series forecasting, human language interpretation, and voice pattern recognition. Because of its capacity to capture long-term relationships, it is an effective tool for analyzing sequential data and recognizing patterns that emerge over time.

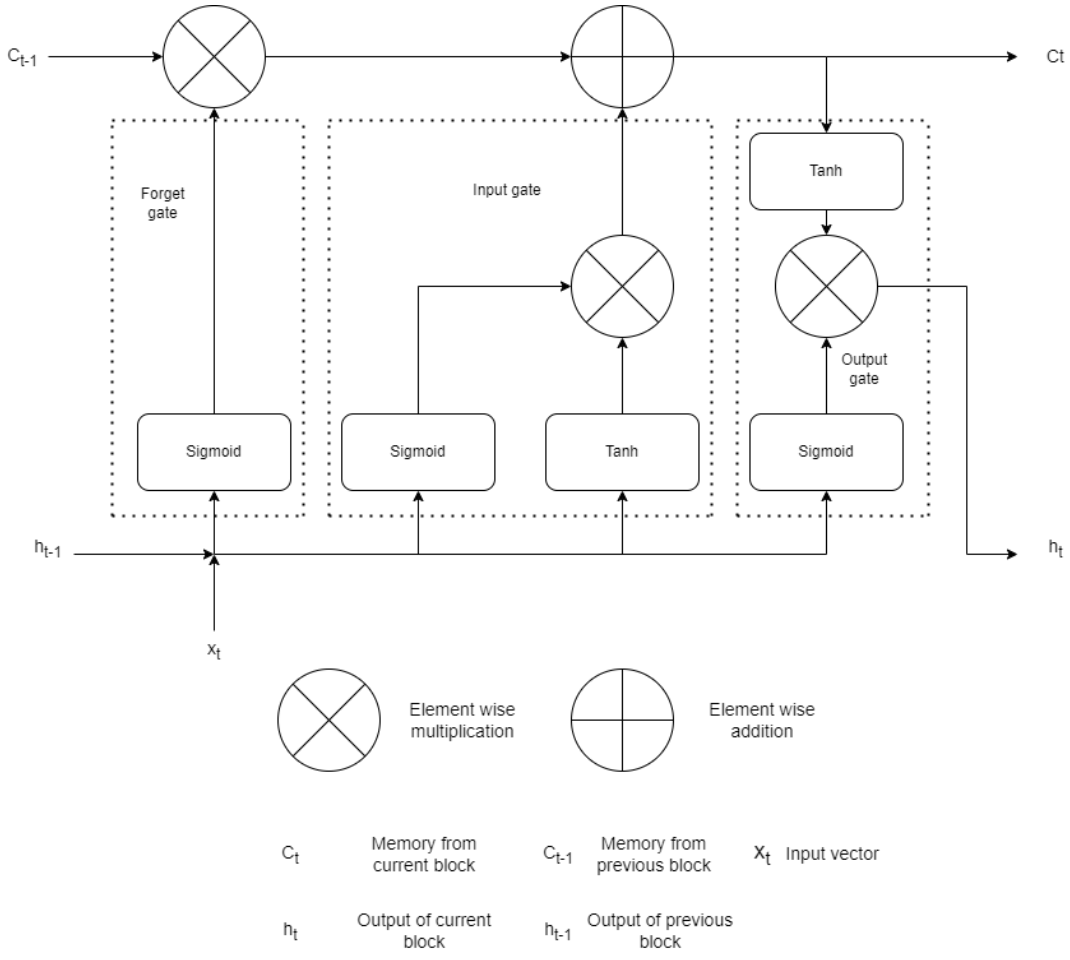

Figure 10 Basic working of LSTM

1.14.4 Mathematical functions used in LSTM

- Tanh Activation: A mathematical function that squashes input values between -1 and 1 is the tanh (hyperbolic tangent) activation function [72]. The tanh activation function is often employed in the LSTM to

control the values that flow through the memory cell. It is applied to the candidate cell state and the output of the memory cell from the previous time step. Tanh activation aids in the management of information flow, preventing it from increasing or vanishing too quickly [73].

- Sigmoid Activation: Another mathematical function that squashes input values between 0 and 1 is the sigmoid activation function. It is widely used to control the flow of information via the gates in the LSTM network. The sigmoid activation is applied to the input gate, forget gate, and output gate in the LSTM. The sigmoid function controls how much information to allow through by returning values between 0 and 1, with 0 representing "close the gate" and 1 representing "open the gate" [73].
- Element-wise Multiplication: Element-wise multiplication is the process of multiplying together the matching elements of two vectors or matrices. To merge information from the previous memory cell state and the candidate cell state in the LSTM, element-wise multiplication is performed. The forget gate output, which selects what information to delete, is element-wise multiplied by the preceding memory cell state. Based on the settings of the forget gate, this action allows the LSTM to selectively maintain or delete information from the prior memory cell state [74].
- Element-wise Addition: As the name implies, element-wise addition entails adding appropriate elements of two vectors or matrices. The information from the input gate and the candidate cell state are combined via element-wise addition in the LSTM. The output of the input gate, which controls what additional information to incorporate, is added to

the modified candidate cell state element by element. The LSTM may use this operation to selectively add new information to the memory cell state based on the values of the input gates [74].

1.15 Case Studies of failure due to infiltration

Slope failures and landslides due to infiltration is a common occurrence throughout world, especially in the regions where the environment is tropical and sub-tropical [75]. In figure 6 [76], the global susceptibility of rainfall-induced landslides is given which was produced by National Aeronautics and Space Administration (NASA) with combination of surface landslide susceptibility and a real-time space-based rainfall analysis system [77]. The Pacific Rim, the Alps, the Himalayas and South Asia, the Rocky Mountains, the Appalachian Mountains, and sections of the Middle East and Africa are highlighted in red and orange, which indicates high-potential landslide risk. According to historical records, China, India, Japan, Singapore, the United States, Italy, Brazil, and Venezuela have experienced the most devastating landslides and debris flows [75]. Landslides in the Appalachian area, USA are caused mostly by heavy rainfall. Hurricanes, cloudbursts, and thunderstorms may produce fast-moving debris flows, which are among the most deadly and catastrophic types of landslides [78].

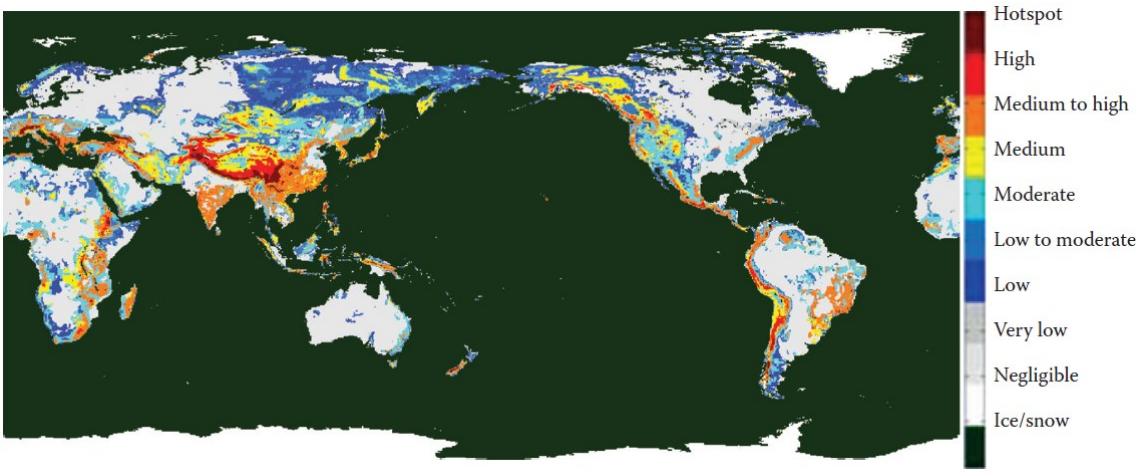

Figure 11 Global susceptibility map of rainfall-induced landslide [75], [76]

Now let us focus on some noteworthy case studies around the globe, which experienced failure due to rainfall.

1.15.1 La Conchita Landslides

La Conchita is located on the southern California coastline midway between Ventura and Santa Barbara. It has a 180-m (600-ft) high bluff having a slope of about 35°. The bluff above La Conchita has produced a variety of landslides over an extended period dating back to 1865 [79]. On March 4, 1995, at 2:03 p.m. PST, the La Conchita landslide failed and moved tens of meters in only a few minutes. The landslide destroyed or severely damaged nine houses. On March 10, a subsequent debris flow damaged five additional houses in the northwestern part of La Conchita. The 1995 slide was 120 m (400 ft) wide, 330 m (1100 ft) long, and covered approximately 4 ha (10 acres). The depth was estimated at greater than 30 m (100 ft), and the volume was estimated at 1.3 million m3 (1.7 million yd3) [80]. The 1995 landslide apparently occurred because the annual rainfall was very high. Mean seasonal rainfall at Ojai (20 km [12 mi] northeast of La Conchita) from October 1 through March 3 (the day before

the landslide occurred) is 390 mm (15.37 in) according to National Oceanic and Atmospheric Administration [81]–[83].

In 2005, it experienced another devastating landslide, it destroyed or severely damaged 36 houses and killed ten people. The 2005 landslide occurred at the end of a 15-day period that produced record and near-record amounts of rainfall in many areas of southern California. To conclude, the effect of infiltration on a slope can result in devastating failure and loss of life and property, further establishing the importance of stability for such slopes.

Figure 6 Aerial photograph of the landslide which occurred in 1995 outlined in blue color and subsequent remobilized area which occurred in 2005 outlined in yellow color [84].

Figure 12 View from the main scarp down the length of 2005 landslide [84].

1.15.2 Po Shan Road landslide

On June 16, 1972, several mud slips were seen along the Po Shan Road [85]. Many structures were inspected, but because it was raining, no substantial evacuation or procedures were implemented. On June 17, a slip occurred across the whole width of the cut slope at the southern face of Inland Lot 2260 on Po Shan Road, destroying almost all the bamboo frame and metal sheet covering. Furthermore, officials observed considerable sinking of numerous houses near Lot 2260 [85]. As a precaution, residents were advised to abandon their homes and flats. On the same day the huge mass broke though the retaining wall on Kotewall Road and following this slip even larger slip occurred. This one knocked off the Kotewall Court and collapsed several flats, killing 67 people and injuring 20. Due to such disaster the roads were affected not to mention

the adverse weather conditions, after hours the first survivors were pulled out of the rubble [85].

Figure 13 Po Shan Road Landslide [86]

1.15.3 Hadong and Pohang engineered cut slope failures

In mountainous regions of Korea, there are many cut slopes, and they experience a lot of failure due to lack of standard regulation and design methods for unsaturated conditions. Due to such negligence and heavy rainfall, two cut slopes failed. The stratum of Cretaceous rocks contains mainly granitic gneiss and weathered granite in Hadong and mudstone and shale in Pohang [87]. The Hadong slope was an engineered cut slope and had been in service for several years, but in July of 2009, after heavy rainfall of 1029mm in span of three months, the slope failed. Like Hadong, Pohang slope failed after experiencing 420mm rainfall for three months, in June 2011. As seen in the figure the slope has angle of around 45° and finite element analysis of

both site showed that the Factor of safety were 0.9 and 1.0 for Hadong and Pohang sites respectively.

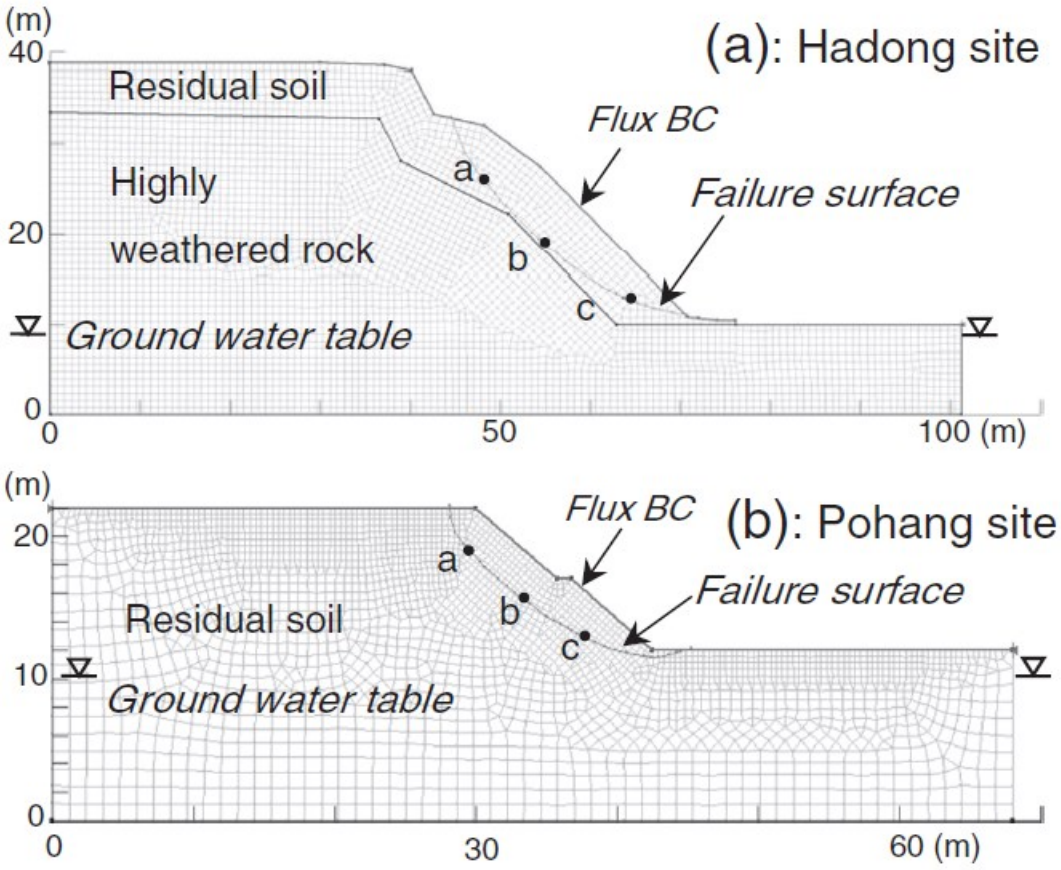

Figure 14 Cross-section of (a) Hadong site and (b) Pohang site [87]

1.15.4 Malda Railway embankment failure

Malda district is a district in West Bengal, India. It lies 347 km north of Kolkata, the capital of West Bengal. The region gets hefty 2000mm-4000mm rainfall per year, most of the precipitation occurs between June to August [88]. The embankment's highest height is 4.4 m. The embankment's side slopes are 2(H):1 (V). The crest's average width is 6.7 m. The railway embankments at Malda are intended to withstand a single axle load of 25 tons from railway locomotives operating on both lines (up and down lines) positioned on top of them. This results in a distributed load of 94.5 kPa on the embankment's crest [89]. Besides the rainfall being the reason for the failure the

engineers also suggested filling up the ponds that develop besides the railway embankment to protect the embankment toes.

Figure 15 Malda Embankment [89]

3. Background and Site Data

1.16 Site Information

The Straight Creek Landslide, located about 80km west of Denver city, Colorado, USA, near the Eisenhower/Johnson Memorial Tunnel is situated between mileposts 212.0 and 212.1 [90]. The GPS coordinates of the site are 39°40’24.98” N and 105°58’00.63” W. The Colorado Department of Transportation deemed it as large landslide, with a width greater than 152m and a depth of 15.2m [91]. The landslide impacted the I-70 highway, which is an important interstate highway in Colorado, with an annual daily average traffic of 20,000 vehicles. The landslide is a recurring failure that alternates between stable and unstable stages, with at least some movement occurring each year. Whereas many landslides fail just once, this repeating slide collapses in basically the same fashion every year, albeit to varied degrees [92].

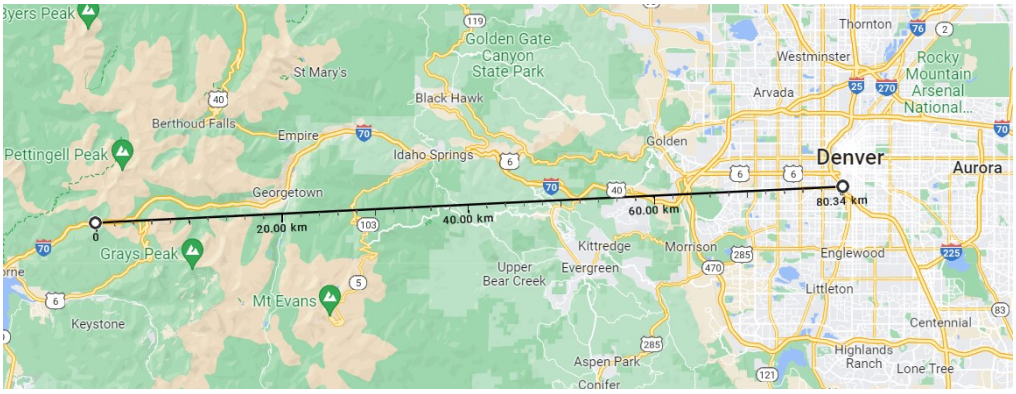

Figure 16 Location of the landslide taken from Google Maps, about 80km west of Denver, CO, USA

Figure 17 Satellite image of the site taken from google earth pro

1.17 Site History

Construction began in late 1963 as the contract for the west approach for the interstate was awarded. The contract of grading and drainage was completed in 1965, but stabilization and paving were delayed until completion of Eisenhower tunnel. But during the grading and drainage stage a ninety-foot cut slope from stations 235 to 242 was cracked and slipped in early June of 1964. As a result of a meeting held in July 1967, Ken R. White Company was selected, and they carried out investigation of the slide. They concluded that the major reason for failure seemed to be groundwater activity. Moreover, in 1970 it was decided to further investigate the site and it was given to Robinson and Associates, which they carried out in 1971. They found out that the groundwater is unevenly distributed throughout the strata and groundwater influenced the stability of the slope significantly also they found out that the embankment was constructed by utilizing the tunnel cuttings from the Eisenhower Tunnel [93], [94].

In 1973, a bulge in the eastbound lanes occurred right above the Straight Creek collapse. Although the Colorado Department of Highways (CDOH) first thought this was a settlement issue and proceeded to remedy the movements with asphalt tops to

preserve a level road surface, the bulge eventually changed into downslope movement [94].

Later, in 1996 Kumar and Associates performed an investigation in the area and they concluded that the failures were due to landslide and not due to settlement. Thus, three inclinometers were installed along the east and westbound shoulders of the highway; the instrument reached its capacity in 2 years. In 1997, five pavement overlays were placed in the area to maintain a level road surface because the settlement of about 60cm happened in 20 years before 1997 based on the asphalt thickness [91]. To remediate the landslide, in 2010 and in 2012 lightweight caissons were installed, along with drains near the toe of the slope in 2012. In addition, Colorado School of Mines and Colorado Department of Transportation drilled three new boreholes and installed three piezometers, each at westbound shoulder, eastbound shoulder and at the toe. The outcome from the readings showed that the landslides were due to rise in groundwater during late spring and early summer months [94].

1.18 Remediation techniques previously used on the slope.

To remediate the landslide lightweight caissons installed under highway pavement in 2010 and 2012. The lightweight caissons were unsuccessful in increasing the stability and marginally increased the factor of safety of the slope. The volume of the caissons was found to be 1.2% of the slide volume, this means reduction of 0.9% slide weight [90]. However, only ~1% increase in factor of safety was seen and it was thought that while the shear stress due to gravity was reduced, the normal stress on the failure plane was also reduced, that could reduce the available friction [95].

The drains were installed in 2012 at the toe and they extended into low hydraulic conductivity bedrock and that resulted into drains having localized effect due to being installed in soil which had less hydraulic conductivity[90]. Also, out of ten drains only

5 have been observed to have any flow and the highest combined flow of drains was approx. 26.5 m^3/day. When we compare the flow over for the entire area it equates to less than 0.1mm of infiltration per day[95].

Since drains and caissons had negligible effect on the stability of the slope they were not considered in the modelling.

1.19 Hydrologic Data

The site's available hydrological data comprises stratigraphy from various boreholes, recorded water table behavior from four piezometers on the hillslope, soil hydrological parameters from laboratory tests, and atmospheric data from a nearby SNOTEL station. Since, the site experiences infiltration in the form of rainfall and snowmelt. Both of those data were taken from nearest SNOTEL station named Grizzly Peak station about 14km away from the site which is managed by United States Department of Agriculture's Natural Resource Conservation Service (NRCS) (USDA) [92][96].

Figure 18 The location of piezometers shown as red dot.

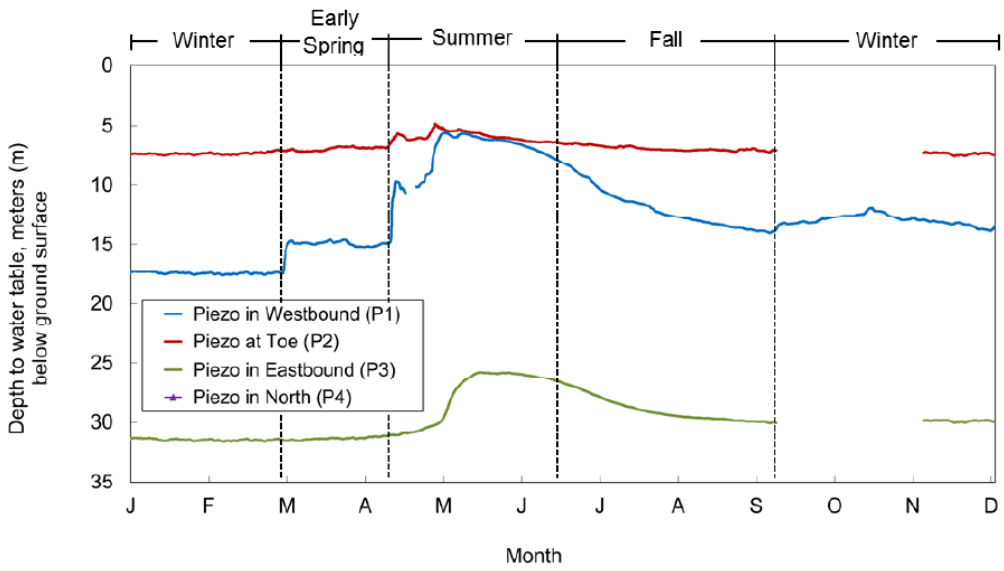

Figure 19 Seasonal change in water table taken from the case study for year 2014 [90]

1.20 Displacement data from inclinometers

The initial equipment on site was two Slope Indicator inclinometers (INC2 and INC3) installed by CDOT in 2008 along the westbound and eastbound shoulders of I-70. The results from these reveal downslope changes of more than 5cm (2 inches) at around 28m (96 ft) depth over the course of a year. The westbound position (INC2) exhibits upslope displacements caused by the rotating character of the breakdown at this point [96] [97].

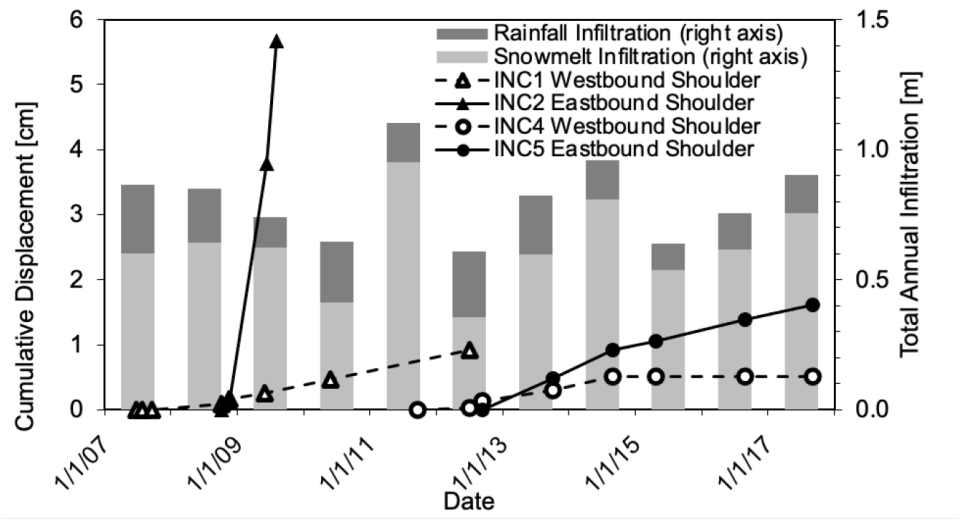

Figure 20 Inclinometer data [97]

During the 2011 examination by CSM/CDOT/USGS-LHP, a second pair of inclinometers (INC4 and INC5) were installed on either side of the roadway and reveal significantly lesser displacements of 0.63cm (0.25 inches) between installation and the most recent reading in April of 2015 (Figure 3.5b). The failure plane in these instruments was measured again at 28m (96 ft) below the eastbound shoulder (INC5), and some upslope movement is noted in the westbound location (INC4) due to the failure mass's continuous rotation. Unfortunately, data from both sets of inclinometers is limited since the boreholes are difficult to reach during the winter months, resulting in just 2-3 measurements per year and making it difficult to pinpoint precise times of movement. Although considerable displacements have been seen throughout the spring and summer seasons [96], [97].

1.21 Soil Data

The properties of soil were derived from the tests conducted by the Colorado Department of Transportation (CDOT), tests such as direct shear for obtaining strength parameters, Transient release and imbibition method (TRIM) for hydrological properties [97]. The following table represents the soil properties in the case study.

Table 2 Soil Properties from the case study [83]

Material	Residual water content	Saturated water content	Inverse air-entry head	Pore size parameter	Saturated hydraulic conductivity	Bulk unit weight	Cohesion	Friction angle	Elastic modulus	Poisson's ratio
	θr	θs	α	n	k_s	γ	c	φ	E	ν
	[-]	[-]	[m^{-1}]	[-]	[m/day]	[kN/m^3]	[kPa]	[°]	[kPa]	[-]
Bedrock	0.06	0.34	1.374	1.72	0.001	23	5638	56	$5.3*10^7$	0.3
Decomposed Gneiss	0.065	0.41	7.5	1.89	1.06	22	25	38	$5.0*10^4$	0.25
Colluvium	0.08	0.33	2.35	2.12	6	20	0	34	$5.0*10^4$	0.25
Alluvium	0.07	0.33	2.35	2.12	3	20	0	30	$5.0*10^4$	0.25
Fractured Gneiss	0.06	0.34	1.374	1.72	40	22	1590	52	$1.0 * 10^7$	0.3
Embankment Fill	0.08	0.33	1.374	2.12	0.5	21	25	35	$3.0*10^4$	0.25
Drain	0.07	0.5	0.5	1.65	1000	Set to match surrounding soil material				

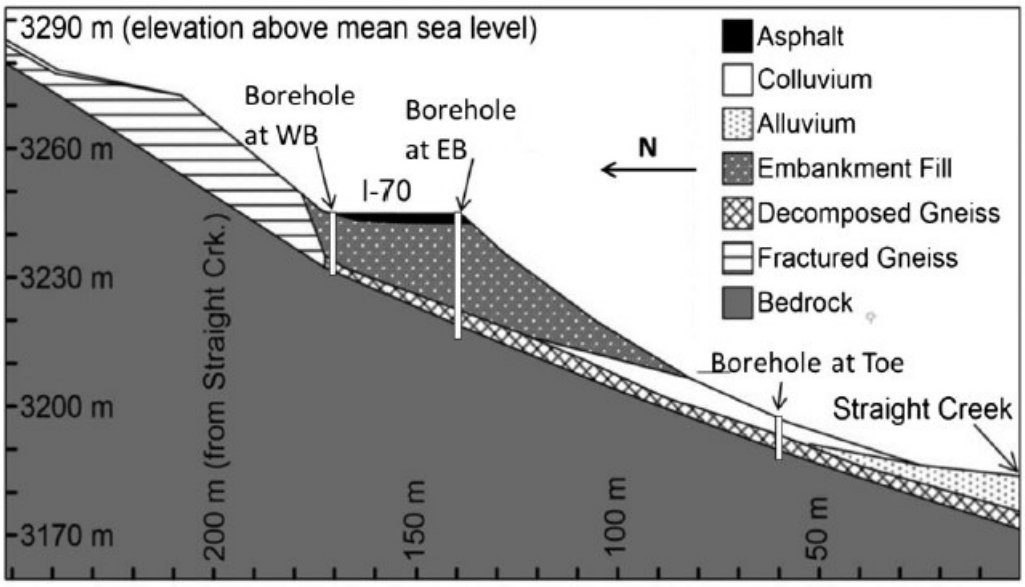

Figure 21 Diagram showing cross-section of the study area from the case study [95]

A layer of fractured and weathered material coming from the same dark gneiss lies over the competent bedrock, ranging in thickness from 1 m to over 30 m. Because the degree of weathering increases as one descends the slope, this layer was separated into two groups for the conceptual and numerical models. The first kind, known as fractured gneiss, is found on the slope above the embankment; it features clean fracture surfaces with little weathering or filling, as well as strong frictional strength and hydraulic conductivity [92].

The slope's surficial soil is made up of colluvial deposits with angular, coarse sand to cobble-sized grains generated from the gneiss bedrock. Straight Creek deposited alluvial material on the valley floor, which is more homogeneous and composed of rounded sand-sized grains. The mechanical characteristics of the two materials are comparable, but the colluvium has better hydraulic conductivity due to decreased in situ density generated by depositional processes [92].

The tunnel-cuttings material utilized for embankment fill is exceedingly heterogeneous, containing big rock pieces and boulders, construction waste (such as shoring decaying timbers), and finer-grained material than the surrounding native soils [98]. Because of the particle’s concentration, the hydraulic conductivity of this material is quite poor. The embankment fill is approximately 14 m thick beneath I-70's westbound shoulder, 29 m thick under I-70's eastbound shoulder and continues approximately 61 m downslope.

1.22 Safety Factors

The previous studies have calculated the local factor of safety using HYDRUS software and global safety factors using bishop method of slices which comes under limit equilibrium analysis. The images below show the local safety factor and global safety factor derived from bishops method. Since, the site undergoes changes and it not constant throughout the year to properly monitor the dynamic changes in slope bishops' method is a simple and quick analysis albeit not as accurate as FEA analysis in PLAXIS 2D. Moreover, majority of codes follow global safety factor for analysis of slope stability, no doubt the local safety factor is very useful and gives insights where there might be potential chances of failure but for overall stability global factor of safety is preferred.

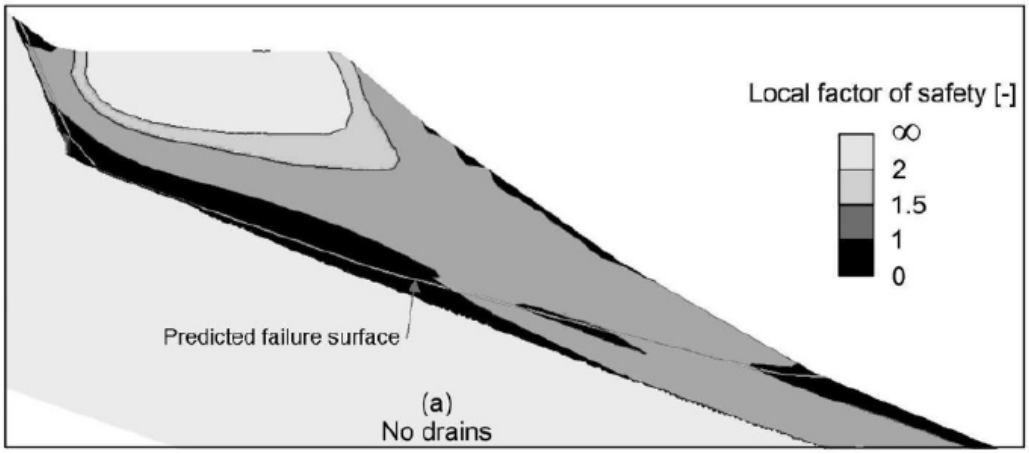

Figure 22 Cross Section of site depecting local safety factor without drains [95]

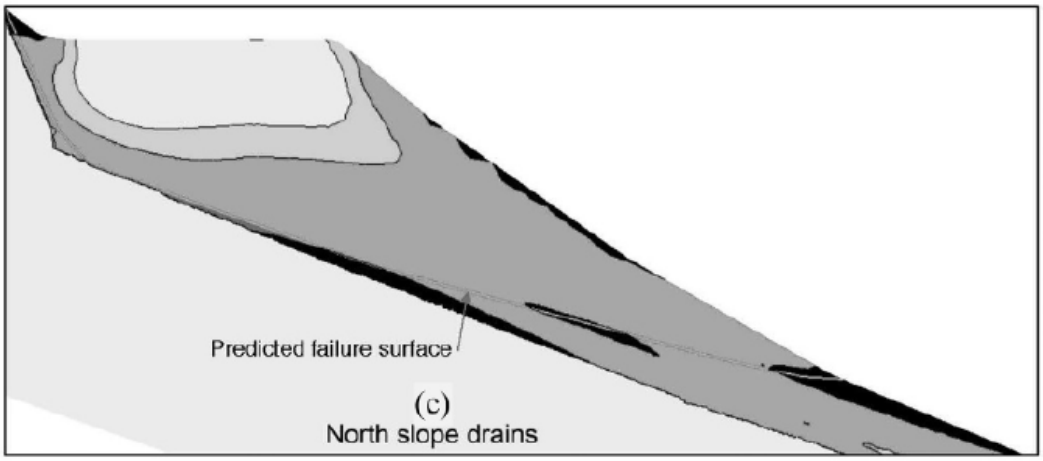

Figure 23 Cross Section of site depecting local safety factor with drains [95]

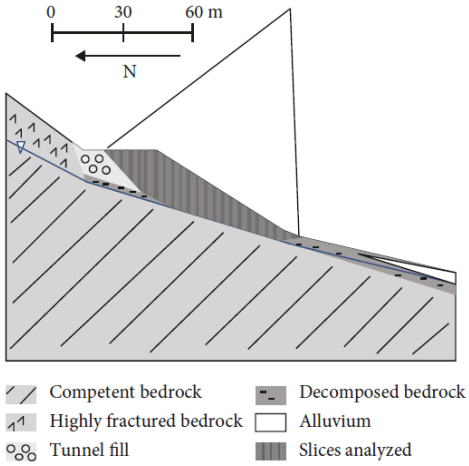

Stage	Season	Factor of safety
I	Winter	1.05
II	Early spring	1.02
III	Spring and early summer	0.94
IV	Fall	1.03

Figure 24 Safety Factor calculated by modified bishop's method [99]

4. Methodology

1.23 Approach

The data was collected from the case study and was quantitative in nature. After data collection the first step was to make sure that the results are like the results of the case study and that will ensure the correctness of the model. So, for that the change in groundwater levels were matched with the case study. Thereafter, remedial measures were taken, and parametric analysis was done on spacing and angle of soil nails.

1.24 Choice of remedial measure

There are many slope stability measures, some require a lot of modification and intervention to the slope geometry and surrounding, while others require few modifications. Some of the measures such as terracing, retaining walls were not considered because of cost and less effectiveness of them in this case. Also, considering the nature of the site and importance of highway a method of less intervention must be selected, for that out of soil nail and ground anchors, soil nails were chosen because the nature of the embankment fill was alkaline and they can cause the ground anchors to corrode, while the soil nail having a better resistance than ground anchors were better choice.

1.25 Data collection

The data for this study was taken from the case study. The geometry of the cross-section was created in AutoCAD and later imported to PLAXIS 2D, which is a finite element analysis software. Similarly, the soil properties were also taken from the case study. The initial step in analysis was to make sure that the factor of safety matched with the case study. All the seasonal data was simulated likewise and fully coupled flow deformation analysis was performed which accounts for the groundwater flow and the deformation of the soil mass all in one phase/step, thereby making the analysis more

accurate. Once the model got validated then the next step was to find remedies and increase the stability of the slope to prevent the landslide. Thus parametric analysis was done using different soil nail layout and lastly safety factor forecasting was done.

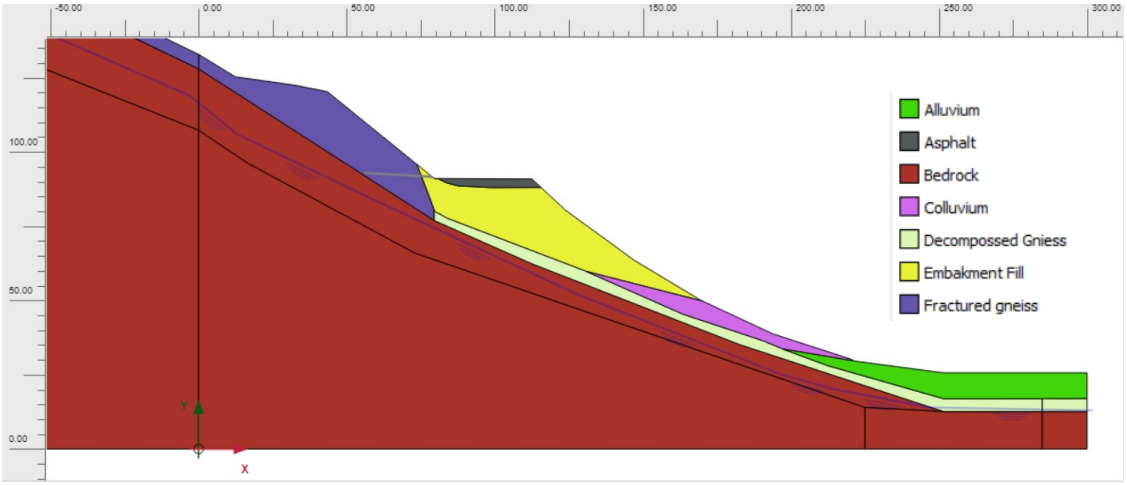

Figure 25 Cross-section of study area viewed in PLAXIS 2D (all scale in meters)

1.26 Numerical framework

For this research Plaxis 2D version 22.02 was used, which is a finite element analysis software to perform deformation and stability analysis for variety of geotechnical problems. For this study plane strain modelling is used, which assumes that the cross-section in 2D extends out of the plane [60].

1.27 Geometry

The geometry of the study was formulated in AutoCAD and later imported to PLAXIS 2D. The geometry was constructed in such a way that entire mountain was considered in the analysis to accurately involve the runoff due to elevation of mountain and enable the water flow in the soil layers not too different than the actual one. The total extent of the slope can be seen in the diagram below, where the distance between maximum and minimum point in X direction is 800m and in Y direction it is 370m. In the figure given below the scales show negative value on left hand side due to the origin

at right hand side as shown with x and y axis symbols. The width of highway is 30m and right below the highway there is a layer of embankment fill, which consist of organic materials and tunnel cutting from the Eisenhower Tunnel not too far from the site.

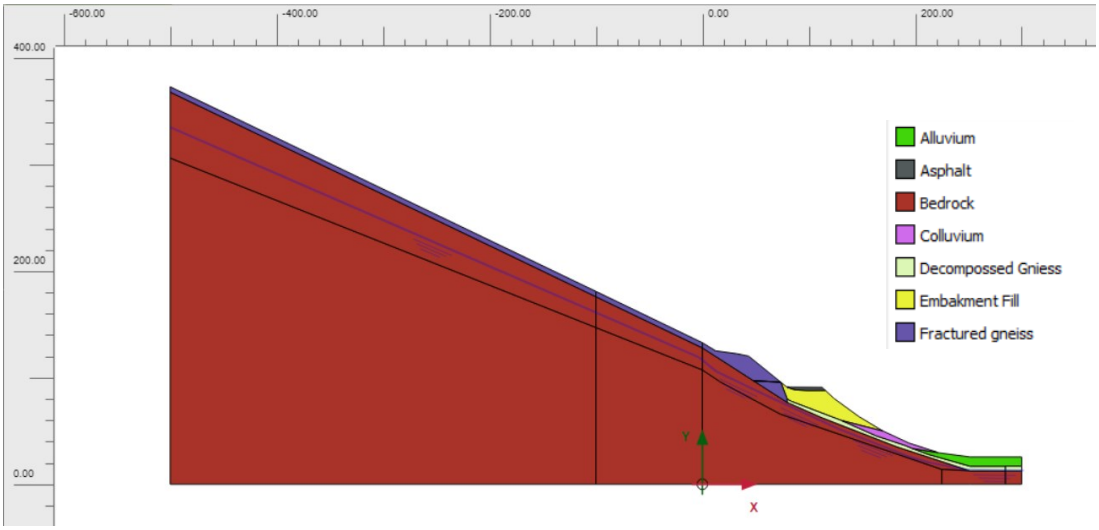

Figure 26 Zoomed out version of cross-section in PLAXIS 2D (all scale in m)

The site has a prominent bedrock primarily Gneiss and it is overlain by layer of decomposed and fractured gneiss. Among both layers the permeability of fractured gneiss is decent, and that is one of the major reasons for instability as it increases the saturation soil and it may result in a catastrophic failure. The angle of slope ranges from 33° near the top to a gentle angle of 5° at the bottom. Initially the groundwater level was kept just below the bedrock as shown in figure 23.

1.27.1 Boundary Conditions

The deformations in the maximum and minimum X directions were kept Normally fixed, the Ymin was fully fixed and Ymax was Free. For groundwater the minimum X and Y directions were kept closed and the maximum directions were open.

1.27.2 Temporary embankments

To consider the practicality of the installation it prudent to add the temporary to access the slope to install the nails. Each has 5 m space for ease of driving large vehicles. Each of them is 5m tall with a gentle angle of 25 degrees. The soil type was kept the same as the embankment type. For each embankment 20 days were assigned for construction and width of about 5m was kept at each for ease of movement of workers and vehicles. The material of embankment was kept with properties of the embankment fill soil. So, it took 80days for creation of embankment and thereafter the soil nails were activated in 50days.

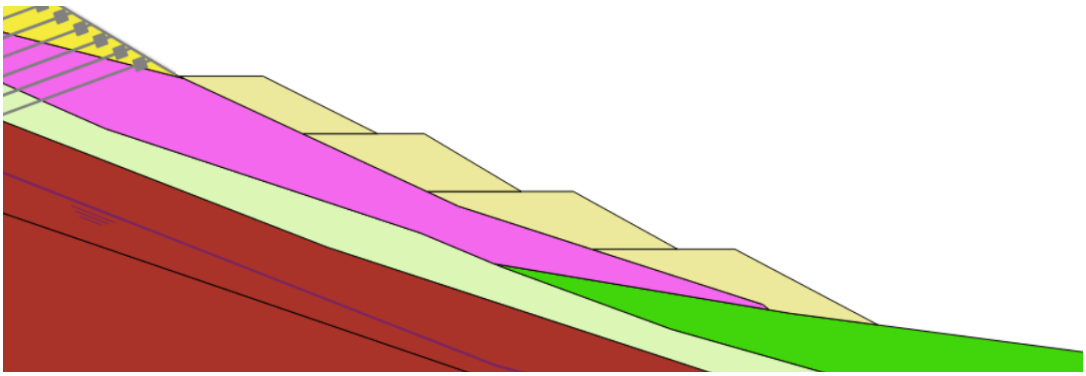

Figure 27 Four temporary embankments near the bottom of the slope

1.28 Soil Model

In this study two soil models were used to calculate and analyze the slope. First being Mohr-Coulomb and Hardening soil model. The latter was used in order to capture the displacements for long term, since one requires non-linear model to replicate the most sophisticated behavior of the soil.

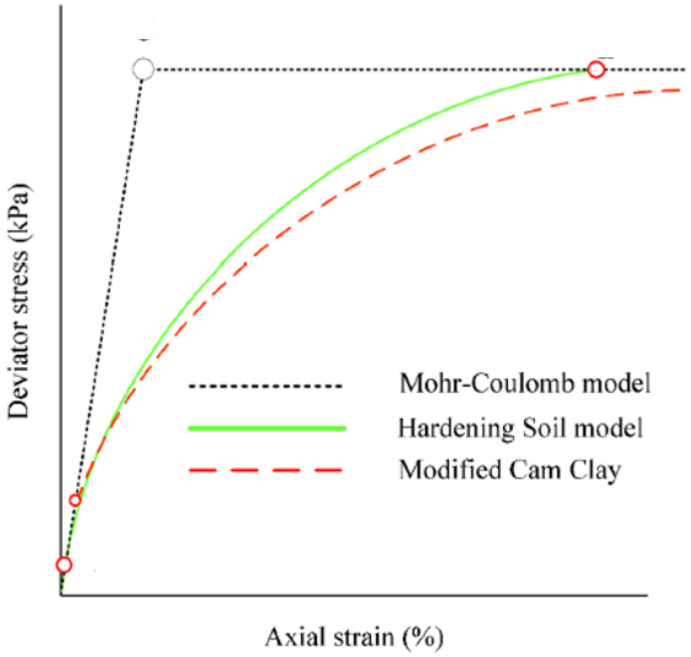

Figure 28 Graph of Deviatoric Stress vs Axial Strain comparing the Mohr-Coulomb, Soil Hardening Soil and Modified Cam Clay model [100].

The figure above of the graph shows the linear model Mohr-Coulomb, Hardening Soil and Modified Cam Clay Soil Model. The actual soil behaviour will be similar to the Hardening or Modified Cam Clay model, hence for long deformation Hardening Soil will be a solid choice.

The Mohr-Coulomb model is a linear elastic perfectly plastic model that was used to approximate normal soil behavior. The basics of this soil model is that when the shear stress at a point on any plane within a soil becomes equal to the shear strength, failure will occur at that point [101]. It requires a total of five parameters (two stiffness parameters namely Young's modulus and Poisson's ratio, and three strength parameters cohesion, friction angle and Dilatancy angle), which are generally familiar to most geotechnical engineers, and which can be obtained from basic tests on soil samples.

The Hardening Soil model is an advanced simulation of soil dynamics. In the Mohr-Coulomb model, limiting states of stress are defined by the friction angle phi, cohesion angle c, and dilatancy angle psi. To reflect soil stiffness more correctly, three

different input stiffnesses are used: the triaxial stiffness E50, the triaxial unloading stiffness Eur, and the oedometer loading stiffness Eoed. The Hardening Soil model, unlike the Mohr-Coulomb model, considers the stress-dependence of stiffness moduli. This demonstrates that when pressure increases, all stiffnesses increase [102].

1.28.1 Soil Properties

The soil properties were taken from the case study (shown in Table 2). The porosity was derived from the saturated moisture content which is also the porosity is already given in the case study, so to calculate the dry unit weight Eq 12 and 13 were used assuming the specific gravity 2.7 The hardening soil properties for the two soil in the table 4 have been decided after lots of trails to achieve closer values of the displacement with the case study.

$$\gamma_{unsat} = \frac{G\gamma_w}{1+e} \qquad \textit{Eq 12}$$

$$e = \frac{n}{1-n} \qquad \textit{Eq 13}$$

Where,

e is void ratio

n is porosity

G is specific gravity

γ_w is the unit weight of water.

γ_{unsat} is unsaturated unit weight of soil.

Table 3 Soil Properties for PLAXIS 2D input [92]

Soil Type	Soil Model	Porosity	Unsaturated unit weight	Saturated unit weight	Effective Young's Modulus	Poisson's ratio	Effective Cohesion	Angle of Friction
		n	γ_{unsat} (KN/m^3)	γ_{sat} (KN/m^3)	E'_{ref} (KN/m^2)	ν	c' (KPa)	ϕ (°)
Alluvium	Mohr-Coulomb	0.33	18.12	20	50000	0.25	0	30
Decomposed Gneiss	Mohr-Coulomb	0.41	15.98	22	50000	0.25	25	38
Bedrock	Mohr-Coulomb	0.34	17.76	23	53000000	0.3	5638	56
Fractured Gneiss	Mohr-Coulomb	0.34	17.76	22	10000000	0.3	1590	52
Asphalt	Linear Elastic	-	0.45	0.45	2100000	-	-	-
Drain	same as surrounding soil properties							

Table 4 Hardening Soil properties for displacement prone soils the stiffness was reduced to match the displacement values from the case study [92]

Soil Type	Soil Model	Porosity	Unsaturated unit weight	Saturated unit weight	Triaxial Stiffness	Odeometric modulus	Triaxial Unloading Stiffness	Poisson's ratio	Effective Cohesion	Angle of Friction
		n	γ_{unsat} (KN/m^3)	γ_{sat} (KN/m^3)	E_{50}	E_{oed}	E_{ur}	ν	c' (KPa)	ϕ (°)
Embankment Fill	Hardening Soil	0.33	18.12	21	26000	26000	78000	0.25	25	35
Colluvium	Hardening Soil	0.33	18.12	20	45000	45000	135000	0.25	0	34

1.28.2 Van-Gretchen Parameters

To represent hydraulic characteristics of groundwater flow in unsaturated zones (typically above the phreatic surface), a Soil Water Characteristic Curve (SWCC) is introduced. The SWCC describes the soil's ability to retain water under various pressures. The soil-water characteristic (or retention) curve (SWCC) is a valuable conceptual tool for evaluating the property functions of unsaturated soil and the accompanying macro-scale behavior (strength, volume change, hydraulic conductivity, fluid flow, diffusivity, and so on) [103]. Here to get SWCC the Van Genuchten model was utilized [104].

$$\theta_w = \theta_{res} + \frac{\theta_{sat} - \theta_{res}}{[1 + (\alpha' \varphi)^n]^m} \qquad Eq\ 14$$

Where,

θ_{res} is residual volumetric water content (dimensionless)

θ_{sat} is saturated volumetric water content (dimensionless)

α' is the reciprocal of the air-entry value with units of $[L^{-1}]$

n is a measure of the pore-size distribution, (dimensionless)

φ is suction pressure ([L] or cm of water).

In PLAXIS, the Van Genuchten parameters can be directly entered to construct these functional forms, or a Spline function can be used to fit smooth curves to tabular data. The parameters are different than one's described in the above formulas, however they can be converted to required format using Eq. 16.

$$S(\psi) = S_{res} + (S_{sat} + S_{res})[1 + (g_a|\psi|)^{g_n}]^{g_c} \qquad Eq\ 15$$

Where,

Ψ = negative ratio of suction pore stress and unit weight of pore fluid

S_{res} = A residual saturation represents a portion of the fluid that stays in the pores even when suction heads are high.

S_{sat} = In general, under saturated circumstances, the pores will not be totally filled with water because air can become trapped, and the saturation, Ssat, will be less than one. The default, however, is Ssat = 1.0.

g_a = A fitting parameter that is connected to the soil's air entry value and must be measured for a specific material. It has a positive value and is measured in 1/L.

g_n = A fitting parameter based on the rate of water extraction from the soil after the air entry value is surpassed. This parameter must be measured for each substance.

$$g_c = (\frac{1 - g_n}{g_n}) \qquad Eq\ 16$$

To convert the parameters as per the above format, which is standards PLAXIS format following equations were used and parameters were changed accordingly.

$$\theta = S\eta \qquad Eq\ 17$$

Where, using the porosity (η) one can convert residual volumetric water content (θ_{res}) and saturated volumetric water content (θ_{sat}) to residual degree of saturation (S_{res}) and saturated degree of saturation (S_{sat}). Also, the reciprocal of the air-entry value (α') and measure of the pore-size distribution (n) are same but labelled differently as g_a and g_n.

Table 5 Van Genuchten parameters for PLAXIS 2D

Soil Type	Residual volumetric water content	Saturated volumetric water content	Reciprocal of the air-entry value	Pore-size distribution parameter	Hydraulic Conductivity
	Sres	Ssat	ga	gn	K (m/day)
Alluvium	0.2121	1.00	2.350	2.120	3
Decomposed Gneiss	0.1585	1.00	7.5	1.890	1.06
Colluvium	0.2424	1.00	2.35	2.120	6
Bedrock	0.06203	1.00	3.830	1.377	3
Fractured Gneiss	0.1765	1.00	1.374	1.720	40
Embankment Fill	0.2424	1.00	1.374	1.720	0.5
Drain	0.07	1.00	0.5	1.650	1000

1.29 Mesh

For this study 15 nodded elements were adopted. The mesh was kept fine near the top boundaries to accurately simulate the infiltration conditions and coarser far from the top boundary. Overall, the mesh was kept medium-sized keeping the analysis time in mind as the simulation is for multiple weeks. The top boundary had the coarseness

factor of 0.1250, which will make the mesh denser near the surface and make the calculation more accurate as there is a component of precipitation in this study. Also, the bedrock layer was divided such that it has more elements near the top and less so in the bottom area which is of less concern.

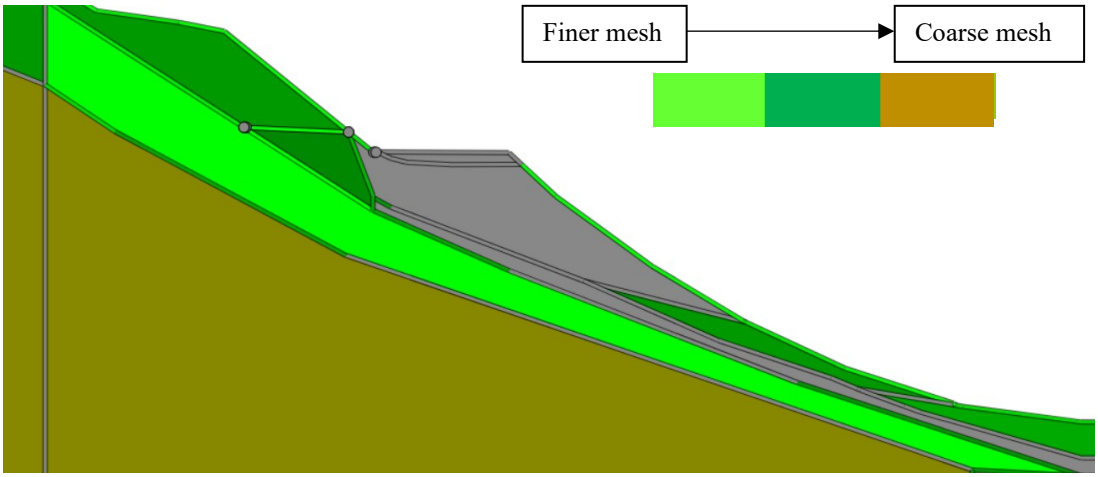

Figure 29 Mesh density distribution

The figure provided below shows the quality of mesh, green means good and redder the color means bad. As seen where the elements are larger in size the quality is not as good, but since the area we are concerned is greener i.e good quality it should not hamper with the accuracy of the results. The obtuse triangle will mean that the mesh will not be accurate to predict the site values hence redder in colour, which acute triangle will be accurate.

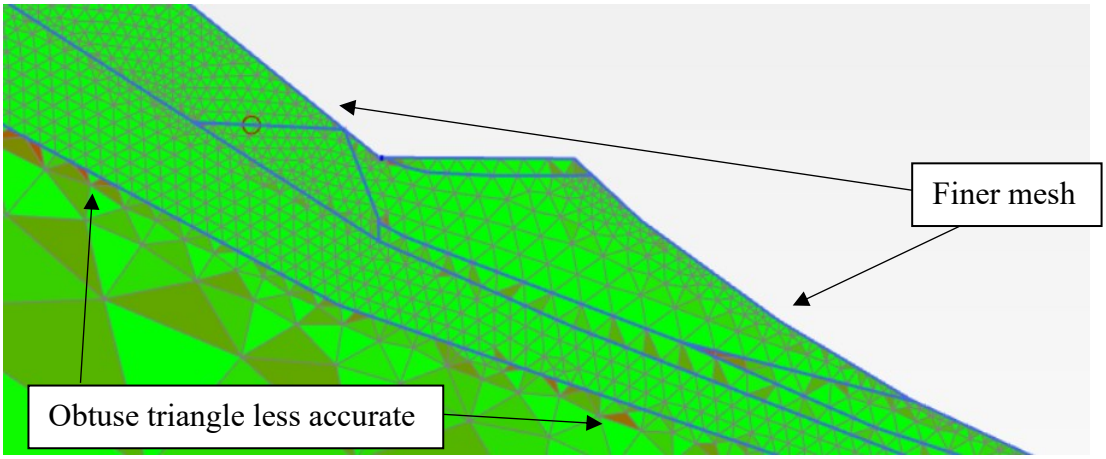

Figure 30 Mesh quality the obtuse triangle will be less accurate than the acute triangles hence redder

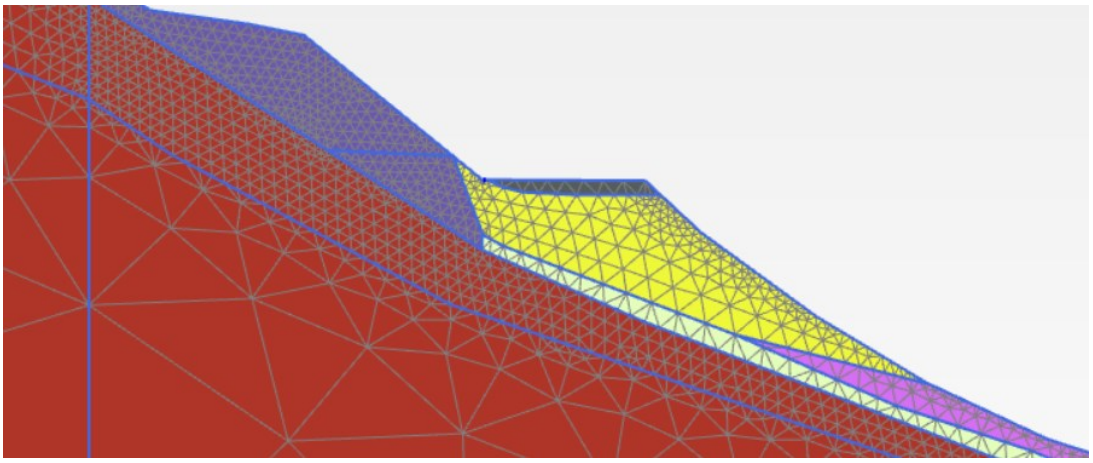

Figure 31 Mesh distribution: It is closer at the surface as there is more activity due to infiltration.

1.30 Integration of SNOTEL data

The data was taken from a SNOTEL station called Grizzly Peak Snotel station. Now, from the station two parameters were extracted and some data cleaning was done so that they can be applied to the study at hand. The two parameters were Snow water equivalent (WTEQ) and rainfall data. The first step was to convert the data into metric units and make it daily from cumulative. Thereafter, the total precipitation was considered whenever the WTEQ data was non-zero and positive during snow, and if WTEQ data was zero i.e., time where there is no snowfall then the rainfall data the total precipitation.

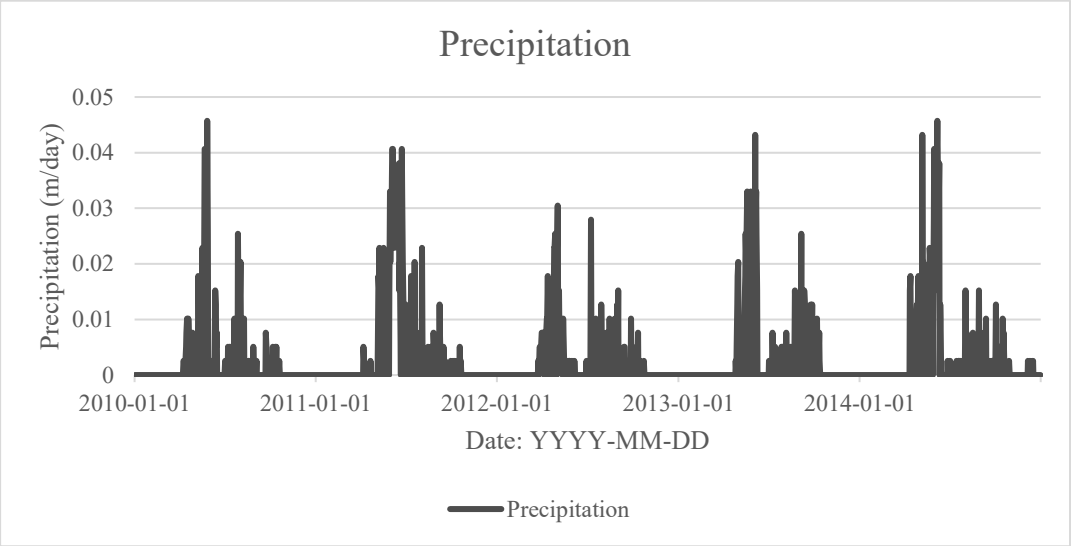

Figure 32 Precipitation data taken from Grizzly peak SNOTEL station.

To insert this data in PLAXIS a discharge function was defined under flow function section, where the data was fed according to seasons for that particular year. Then in the precipitation function of plaxis under the time dependency the respective discharge function was selected depending on date of the precipitation. Also, under model conditions the groundwater flow was closed for X_{min} and Y_{min} boundaries.

1.31 North Drain

The north drain's properties are described in the preceding sections. The diameter of the drain was kept as 6.5cm and a well element was kept at the end to extract the water, so it does not percolate again in the soil medium. The drain was modelled at an angle of 5° and extended till it reached the low permeability bedrock, so that it could intercept all the water traveling towards the highway.

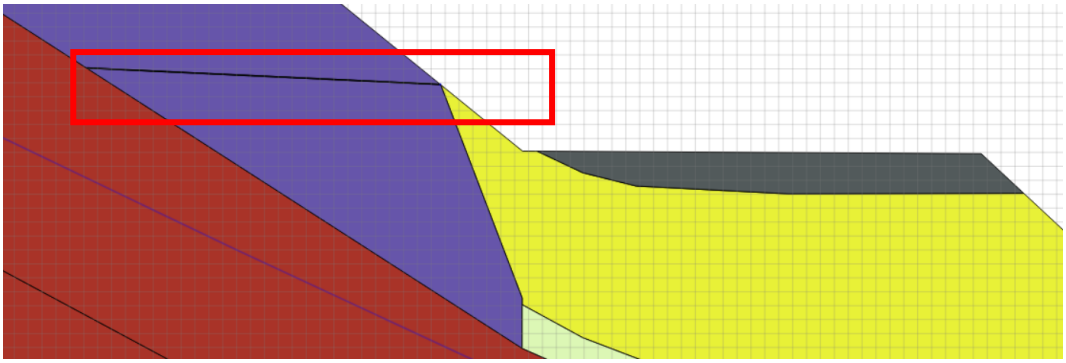

Figure 33 Close up of the North Drain shown in red box.

1.32 Soil Nails

The nails were constructed under embedded beam structure, which allows different spacing in Z direction. Here according to the Soil Nails manual by National Highway institute, USA the bar diameter and bar grades were chosen to be 25mm and grade 75. Also, the hole diameter was suggested in the range of 4-8inch and in this case 4inch was selected that is 10cm. The unit weight and the elastic modulus of the nails were calculated using equations 6 and 7. The skin friction was set to layer dependent, where the skin resistance will be calculated using the equations described in literature review.

Table 6 Properties of Soil Nails for PLAXIS 2D [45]

Property	Value
Material type	Elastic
Unit Weight (KN/m^3)	28.34
Cross section	Solid Circular
Diameter	10cm
Elastic modulus E (kN/m^2)	51.06×10^6
Skin resistance	Layer dependent

Also, the soil nails were arranged in a square array with various spacings such as 1.2m, 1.5m, 1.8m and 2.0m. Moreover, the inclinations were changed from 10°,15° and 20°. The out of plane spacing was same as spacing.

1.32.1 Facing

The facing of soil nails was taken as M25 grade which is recommended by FHWA circular no 7. Here instead of using a plate element which allows the flow of water and which many studies have used previously [61], use of material type concrete was considered with drainage type as non-porous. The facing was extended for 1.5m both at the top and bottom, and the thickness was kept 0.3m considering both initial and final facing.

Table 7 Properties of soil nail facing for PLAXIS 2D [45].

Property	Value
Soil model	Concrete
Drainage Type	Non-porous
Unit weight (kN/m^3)	25
Elastic modulus (kN/m^2)	22.36×10^6
Poisson's ratio	0.2
28-day concrete compressive strength f_{c28}	25×10^3
28-day concrete tensile strength f_{t28}	2500
Φ_{max}	39.50°

Drains were also modelled behind the facing to dissipate the pore pressures, here to model a drain a default drain and well at the base was modelled. As shown in the figure the light blue represents the drain and dark blue is the well. Drain by default has the property to dissipate the pore pressure thereby making water move towards the well and the well extracts the water from the model or the soil. Thus, this system works as a drain to dissipate the excess pore pressure which can be damaging to the soil nail wall.

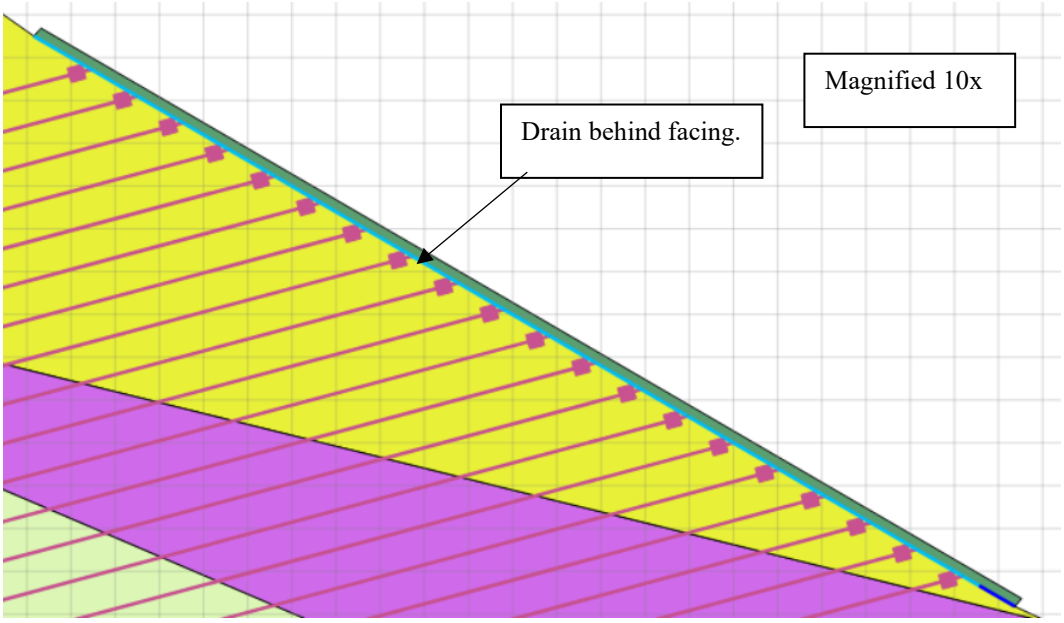

Figure 34 Close up of the soil nail facing which depicts the drain and well behind facing.

1.33 Phases

1.33.1 Initial Phase

Many geotechnical engineering analysis problems need the establishment of a set of initial stresses for non-horizontal layers. The first step is the "Gravity loading," which considers the initial stresses in sloping terrain [60]. The early pressures in a soil body are determined by the weight of the material and the history of its formation.

The following settings were kept for the phase 1 or the gravity loading step.

General	
ID	Initial phase [InitialPhase]
Calculation type	Gravity loading
Loading type	Staged construction
ΣM_{weight}	1.000
Pore pressure calculation type	Phreatic
Thermal calculation type	Ignore temperature
Time interval	0.000 day

Figure 35 Phase setting for initial phase

1.33.2 Phase 1

The second phase aimed to simulate the steady state of the groundwater, where in the context of this study, it means that the groundwater is near the bedrock, thereby

simulating the conditions of the site to create an initial pressure head profile that accurately reflects the water table position observed in the field during winter months [96] and once that is achieved one can further add the steps where actual infiltration data is present. This phase was fully coupled with flow deformation and had a uniform precipitation rate of 0.1000E-3m/day for 7000 days. Since the analysis lasts such a prolonged duration, more than the default step parameter in the numerical and flow control parameters will be required. Thus, the maximum steps were increased to a maximum available number, 10000 steps.

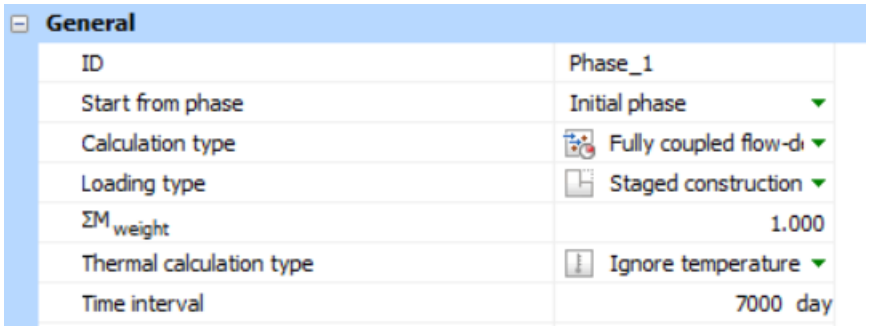

Figure 36 Phase setting for first phase

Numerical control parameters	
Max cores to use	256
Max number of steps stored	1
Use compression for result files	☐
Use default iter parameters	☐
Max steps	10000
Time step determination	Automatic
First time step	Automatic
Min time step	Automatic
Max time step	Automatic
Tolerated error	0.01000
Max load fraction per step	0.5000
Over-relaxation factor	1.200
Max number of iterations	60
Desired min number of iterations	6
Desired max number of iterations	15
Use subspace accelerator	☐
Subspace size	3
Flow control parameters	
Use default iter parameters	☐
Max steps	10000
Tolerated error	5.000E-3
Over-relaxation factor	1.500

Figure 37 Control parameters of the first phase

1.33.3 Following phases and respective safety analysis

After the initial phase and phase 1, the actual precipitation cycle was added. The parameters were kept like the one described above in Phase 1, just as the days were changed according to season. The precipitation values were added via a discharge function. The discharge function was then linked to the precipitation function, changing the precipitation to a time dependent value instead of constant value like in previous phase 1. Thereafter, safety analysis was carried out so that we can obtain the safety factor after each season. Again, for safety analysis the maximum steps were changed due to duration of analysis being long, and the ignore suction box was not checked so to include the matric suction in the calculation.

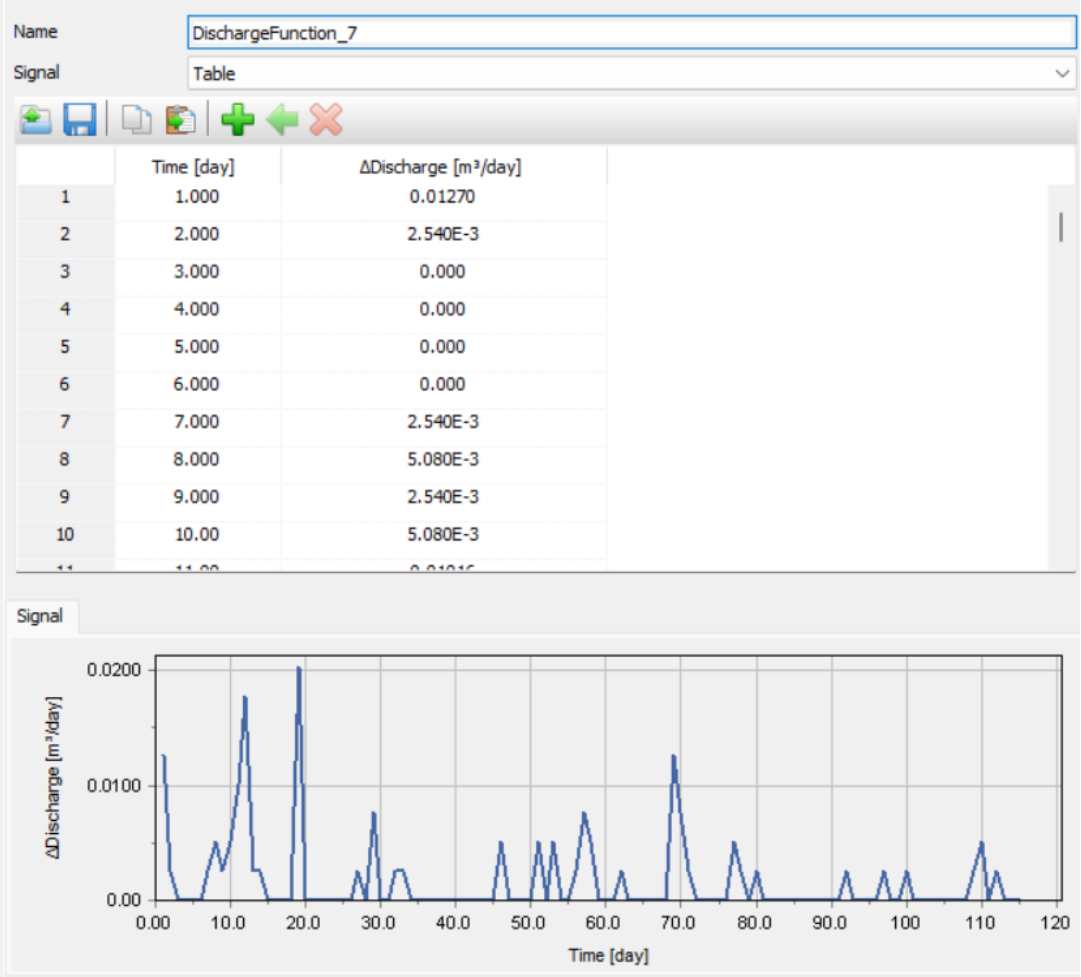

Figure 38 Discharge function tab in PLAXIS 2D

1.34 Data forecasting

The data forecasting was done using two methods, one being the forecast function in excel and other using the LSTM method. For forecasting in excel selecting the columns and the rest of the calculations and graph generations are handled by excel. The only things needed to specify is the future prediction dates.

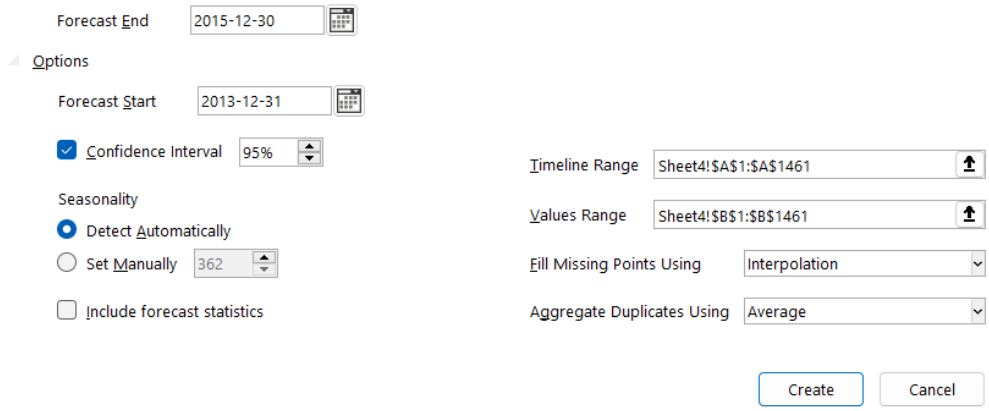

Figure 39 Data forecast panel in excel 2023.

1.34.1 Code breakdown

To predict the data in LSTM the date and safety factors were entered, and a closed loop prediction was done. The data here is thereby univariate because the only variable here is the safety factor. The data was kept univariate and since it predicted it with only one type of data the model was not made complex by adding precipitation. Also, the precipitation values had a lot of zeros and for machine learning model when there are lot of zeros then it will produce inaccuracy in prediction. Overall, for this study univariate data was enough but one can experiment further by adding more variables and playing with type of variables to see where the model will go with the prediction. The code used in this thesis was inspired by the work of user "pkraljnovak" available on Gitlab [105].

Following are some of the basic terminologies which will help understand the code better:

Table 8 Basic terminologies of python

MinMaxScaler	Min-Max scaling: This method scales data to a specific range, usually between 0 and 1. Z-score normalisation (Standardisation) is another approach that centres the data around a mean of 0 and scales it to have a standard deviation of 1. Scaling prevents higher magnitude characteristics from overwhelming

	smaller magnitude features, making the model more effective and guaranteeing fair comparisons across features.
Sequential	Sequential is a type of model in Keras that allows you to build neural networks layer by layer.
LSTM	LSTM is a type of recurrent neural network (RNN) layer
Dense	Dense is a standard fully connected layer, so is a type of layer where every neuron is connected to every neuron in the previous and subsequent layers
mean squared error	These functions are used for evaluating the performance of regression models.
mean absolute error	
epoch	During training, an epoch is a complete trip across the whole dataset. Assume you have a deck of flashcards and wish to remember the information on each card. Going through all of the flashcards at the same time would constitute one era. An epoch in machine learning is defined as providing the full dataset to the model, enabling it to make predictions and alter its internal parameters to enhance its performance.
Batch size	The dataset is partitioned into smaller groups or batches during training, and each batch is handled by the model one at a time. The number of samples or data points in each batch is referred to as batch size. To return to the flashcards analogy, if you want to memorise the flashcards but find it overwhelming to go through them all at once, you may divide them into smaller groups of five cards each. The batch size in this situation is 5. Before going on to the following group, each group allows you to make predictions and refresh your memory based on a smaller collection of facts.
append	means addition to the preexisting data
concatenate	means adding two preexisting data one after the other
DataFrame	It is a two-dimensional data structure in Python supplied by the pandas library. It

	is a flexible and sophisticated data processing and analysis tool. Each column in a DataFrame represents a variable or feature, while each row represents an individual data entry or observation.

Whole code is provided in the appendix.

```
import pandas as pd
import numpy as np
from math import sqrt
from sklearn.preprocessing import MinMaxScaler
from keras.models import Sequential
from keras.layers import Dense
from keras.layers import LSTM
from sklearn.metrics import mean_squared_error, mean_absolute_error
import matplotlib.pyplot as plt
```

The following lines of code import the necessary Python libraries and modules for creating a time series forecasting model with Long Short-Term Memory (LSTM) neural networks. Pandas and NumPy are used for data manipulation and numerical computations, Scikit-Learn's MinMaxScaler is used for data scaling, Keras is used to define the neural network architecture (Sequential, LSTM, and Dense layers), and Scikit-Learn is used to evaluate the model using mean squared error and mean absolute error. It also includes Matplotlib for making visualizations.

```
# Read the data from excel1.xlsx
df1 = pd.read_excel("d:/excel for python/excel3.xlsx")
```

The above line just imports the data from the excel and stores it in a Pandas DataFrame called "**df1**".

```
# Add a date column as the index starting from April 7, 2010
df1["Date"] = pd.date_range(start="2010-04-07", periods=len(df1))
df1.set_index("Date", inplace=True)
```

These lines of code change the DataFrame "df1" by adding a new "Date" column with a series of dates beginning on April 7, 2010, and then making this "Date" column the DataFrame's index. This is important for time series data analysis since it organises the data according on date values, making time-based operations quicker and data exploration more natural.

```
# Frame the inputs as a supervised learning problem
def lstm_super(data, n_in=1, n_out=1, dropnan=True):
    df = pd.DataFrame(data)
    columns, names = list(), list()

    # Input sequence (t-n, ..., t-1)
    for i in range(n_in, 0, -1):
        columns.append(df.shift(i))
        names += [("var(t-%d)" % i)]

    # Forecast sequence (t, t+1, ..., t+n)
    for i in range(0, n_out):
        columns.append(df.shift(-i))
        if i == 0:
            names += [("var(t)")]
        else:
            names += [("var(t+%d)" % i)]

    # Put it all together
    final = pd.concat(columns, axis=1)
    final.columns = names
    return final
```

The given code specifies a Python function named 'lstm_super' for converting time series data into a supervised learning problem [72], which is a typical need for training machine learning models like LSTM networks. The function accepts a dataset (a Pandas DataFrame or Series is assumed) and arguments such as the number of lag observations (n_in) and the number of future time steps to forecast (n_out). It creates a new DataFrame by moving the old data along time steps to generate input-output pairs

where the input consists of past observations (t-n, t-n+1, ..., t-1), and the output is the target to predict (t, t+1, ..., t+n). It then concatenates these columns and gives appropriate column names to provide a structured dataset suitable for supervised learning.

```
# Load the values from the training dataset
values = df1["Safety Factor"].values
```

The code line retrieves information from the DataFrame "df1," which appears to be labelled as "Safety Factor." It takes the values from this column and saves them in a NumPy array called "values." This procedure allows you to isolate and manipulate data from the "Safety Factor" column, making it suitable for use in Python data analysis, modelling, or processing operations..

```
# Convert all data to float data type
values = values.astype("float32")
```

The code snippet changes the data type of the variable "values" to "float32." This is a typical data type conversion technique that is used in data preparation for machine learning and numerical tasks. This is significant because many machine learning methods, such as neural networks, employ floating-point integers, and consistent data formats are required for correct computations and model training.

```
# Normalize features using MinMaxScaler
scaler = MinMaxScaler(feature_range=(0, 1))
scaled = scaler.fit_transform(values.reshape(-1, 1))
```

The MinMaxScaler from the Scikit-Learn module is used to conduct feature scaling on a variable called "values" in this code snippet. Feature scaling is a preprocessing technique that converts data into a specified range, usually between 0 and 1, in order to ensure that all features have similar scales.

```
# Frame the inputs as a supervised learning problem
```

```
lstm_input = lstm_super(scaled, 1, 1)
```

In the context of time series forecasting or sequence modelling, this code snippet frames the input data for a supervised learning task. It use the "lstm_super" function to convert "scaled" data, which represents a time series, into input-output pairs appropriate for training machine learning models.

```
# splitting data into train and test set according to 80:20 policy
train = scaled[:1652]
test = scaled[1652:]
```

The dataset is divided into training and test sets in this code snippet using an 80:20 strategy, which is a standard practise in machine learning for model validation. The previously preprocessed or normalised "scaled" data is separated into two parts. The "train" subset contains the first 80% of the data, or 1652 data points, and is used to train the machine learning model. The "test" subset is made up of the remaining 20% of the data, beginning with the 1653rd data point, and is used to evaluate the model's performance.

```
# split the train and test further into inputs represented by X and
outputs represented by Y
train_X, train_y = train[:-1], train[1:]
test_X, test_y = test[:-1], test[1:]
```

The data is divided into training and testing sets in this code sample, with the goal of constructing input and output pairs for a time series forecasting assignment. The "train" and "test" datasets are usually time series sequences, with the purpose of generating input-output pairs. To do this, the input sequences are represented by "train_X" and "test_X," where "train_X" is produced from the "train" data minus the final element and "test_X" is similarly constructed from the "test" data. "train_y" and "test_y" indicate the comparable output sequences, where "train_y" is made up of the

same "train" data but starts from the second element, and "test_y" is made up of the "test" data with a similar pattern.

```
# reshape the input to be 3D [samples, timesteps, features] as LSTM
requires inputs in 3D format
train_X = train_X.reshape((train_X.shape[0], 1, train_X.shape[1]))
test_X = test_X.reshape((test_X.shape[0], 1, test_X.shape[1]))
```

These datasets are reshaped into a 3D representation by the algorithm. It turns each dataset into a 3D array by invoking "reshape," where each data point (sample) is represented as a 2D array with one time step and many characteristics. This format is required for LSTM networks, which are designed to simulate time-dependent sequences, and this reshaping allows the model to successfully learn and generate predictions based on the data sequence over time. 3D in a sense that instead of two columns of data, it divides it into three namely sample, timesteps and feature. For instance, a sample is a notebook to record measurement of something, each page records it at particular time which is timestep, and lines in notebook has information which is feature.

```
# Design the LSTM model using the Adam optimizer and mean absolute error
(MAE) as the loss function
model = Sequential()
model.add(LSTM(365, input_shape=(train_X.shape[1], train_X.shape[2])))
model.add(Dense(1))
model.compile(loss="mae", optimizer="adam")
```

The Keras library is used to build the model. It starts with a Sequential model, which indicates that we're building a series of layers for the neural network. A single neuron Dense layer is placed after the LSTM layer to provide the model's output. The Adam optimizer, a prominent optimisation technique, is used to create the model, and mean absolute error (MAE) is chosen as the loss function, which evaluates the average absolute difference between predicted and actual values.

`Model = sequential()`	This line creates an empty model object called model using the Sequential class. The Sequential model is a linear stack of layers, allowing us to add layers one after another.
`model.add(LSTM(365, input_shape=(train_X.shape[1], train_X.shape[2])))`	Within this model, an LSTM layer of 365 memory units is introduced, which is a hyperparameter that defines the network's ability to capture patterns. The input_shape is configured to correspond to the dimensions of the training data, specifying the number of timesteps and features.
`Model.add(Dense(units=1))`	The Dense layer is added to the model by this line. The Dense layer is a completely connected layer in which each neuron is linked to every neuron in the preceding layer. It has units=1 in this example, indicating that it contains a single neuron. The Dense layer is in charge of creating the ultimate prediction based on the LSTM layer's output.
`model.compile(optimizer='adam', loss='mae')`	The optimizer and loss function are specified on this line, which builds the model. 'adam', the optimizer, defines how the model is updated depending on the loss and assists in determining the optimum set of weights for the model. The 'mae' loss function calculates the difference between the predicted and actual output. During training, the model attempts to minimise this loss by making predictions that are as near to the actual values as feasible.

```
# Train the model using 50 epochs
history = model.fit(
    train_X,
    train_y,
    epochs=50,
    batch_size=365,
    validation_data=(test_X, test_y),
    verbose=4,
    shuffle=False,
)
```

To train the model with training data (train_X and train_y), use the model.fit function. The epochs option indicates how many times the model iterates over the whole training dataset. A batch size of 365 is also employed, which indicates that the data is divided into batches of 365 samples each to update the model's weights during training. To evaluate the model's performance during training, the validation_data parameter is assigned to the testing data (test_X and test_y). The verbose option is set to 4, indicating that just the most important training progress information is given during training, and the shuffle parameter is set to False, suggesting that the order of training data should not change.

```
# Save the trained model for future predictions
model.save("safety_factor_model.h5")

# Make predictions for future unknown values using the trained model
future_predictions = model.predict(future_X)

# Invert the scaling for the forecasted predictions
future_predictions = scaler.inverse_transform(future_predictions)
```

Here the trained model is saved as "safety_factor_model.h5". The preserved model is then utilised to generate predictions on fresh, previously unseen data represented by "future_X." The anticipated values are first scaled to a certain range for modelling reasons before being transformed back to their original scale with the scaler.inverse_transform function. This scale inversion phase is critical because it guarantees that the anticipated values, such as safety factor predictions, are returned to their original units and can be read and used in their real-world context.

```
# Plot the training loss and validation loss over epochs
plt.plot(history.history["loss"], label="Train")
plt.plot(history.history["val_loss"], label="Test")
plt.xlabel("Epochs")
plt.ylabel("Loss")
plt.legend()
plt.show()
```

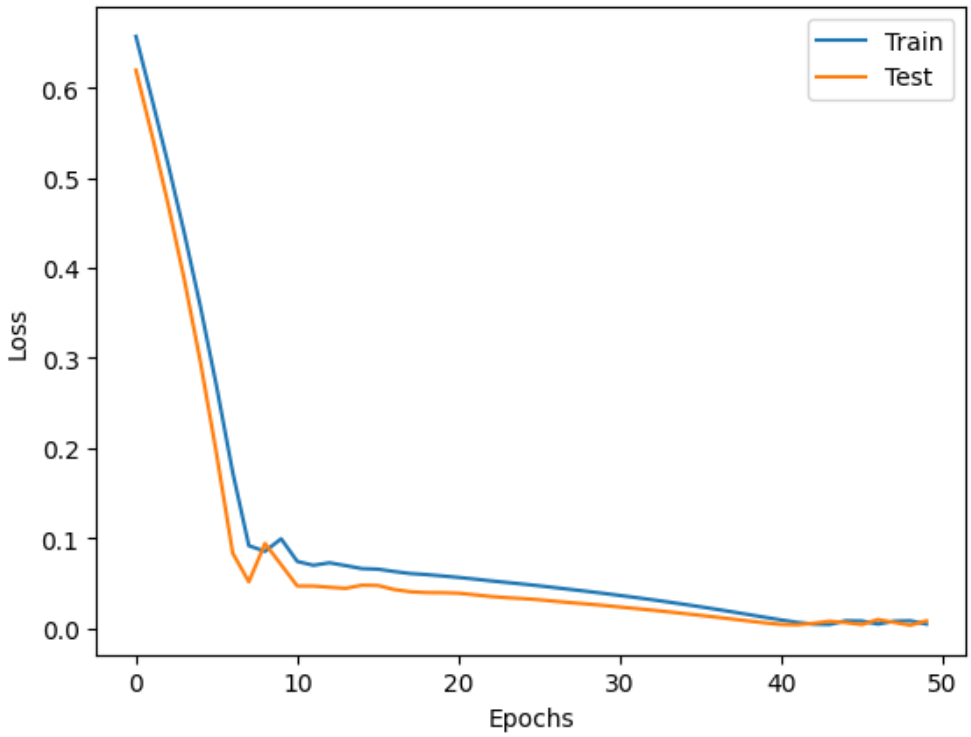

Figure 40 Graph of loss vs epoch

The code above generates a graph of loss vs epochs. The graph shows how the model is learning: ideally, as epochs advance, both training and validation loss should decrease, suggesting increased model performance.

```
# Convert the NumPy array to a DataFrame
test_predicted = pd.DataFrame({'Predicted Safety Factor':
test_predictions.flatten()})


# Save the DataFrame to an Excel file
test_predicted.to_excel('E:/New folder (2)/soil mode/excel for
predictions/Pythonpredicted_data5.xlsx', index=False)
```

The NumPy array containing anticipated safety factor values is turned into a Pandas DataFrame named "test_predicted." This conversion aids in the organisation

and possibly subsequent analysis of the expected data. The code then saves this DataFrame to an Excel file called 'Pythonpredicted_data5.xlsx' in the directory 'E:/New folder (2)/soil mode/excel for predictions/'. The option 'index=False' guarantees that the DataFrame is stored without the default index column.

5. Results and Discussion

1.35 Model Validation

The initial step was to make sure that the results of the analysis align well with the case study. The geometry and the soil properties are same as in the case study so for proper validation the change in groundwater was checked with the case study.

1.35.1 Displacement

The model was meticulously made and all the geotechnical parameters, dimensions and the weather conditions were replicated, but to further ensure that it is like the field conditions the displacement was measured. The values of westbound and eastbound shoulder were taken from the cross-section feature in Plaxis and then it was compared with the values of the study. Now, from the graphs given below the results of finite element analysis closely matched with the field data. The maximum deviation from the original data was at most 0.5cm which when considering the entire length of just the moving mass, which is 100m and that would make the deviation of 0.005m.

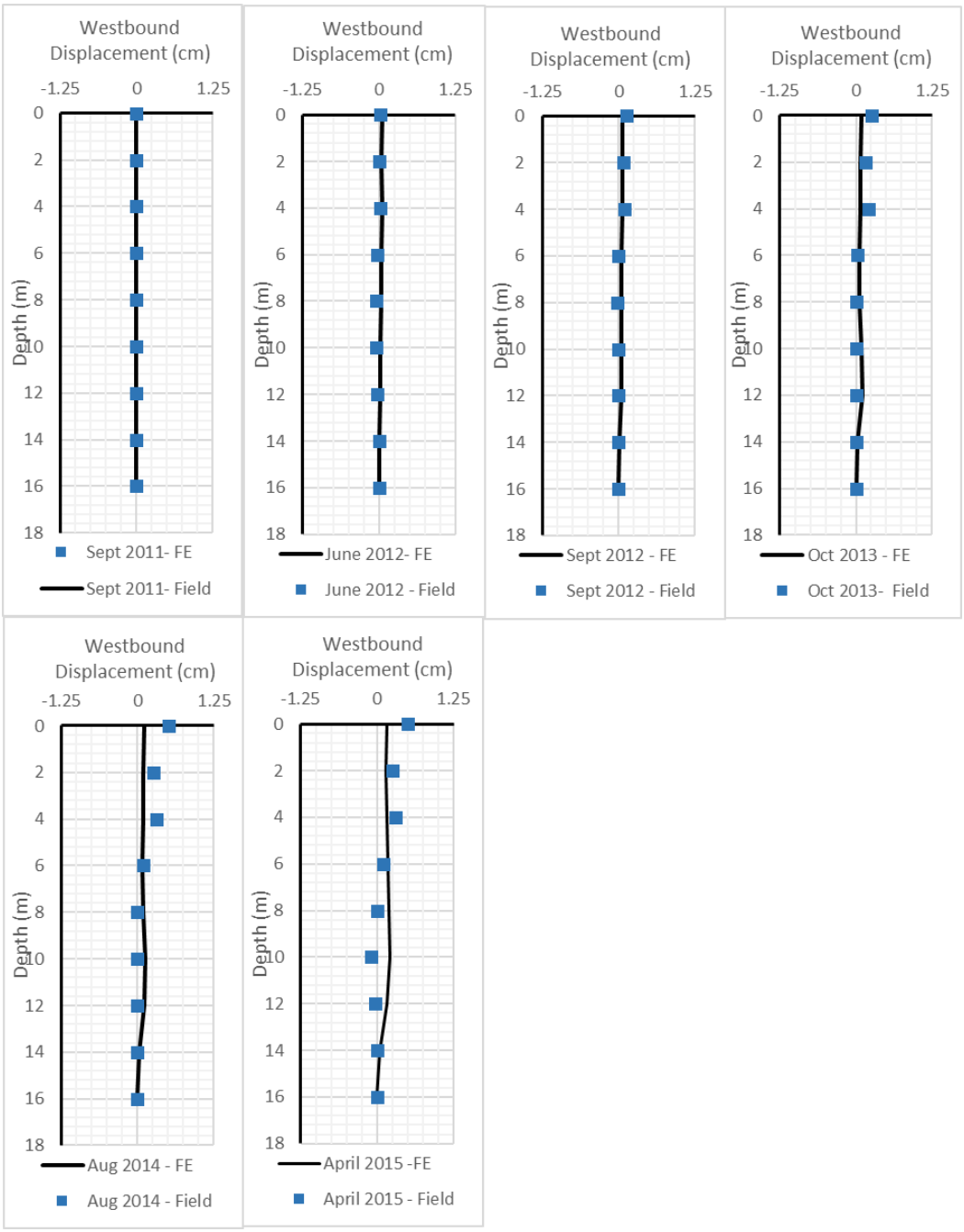

Figure 41 Displacements in the westbound shoulder

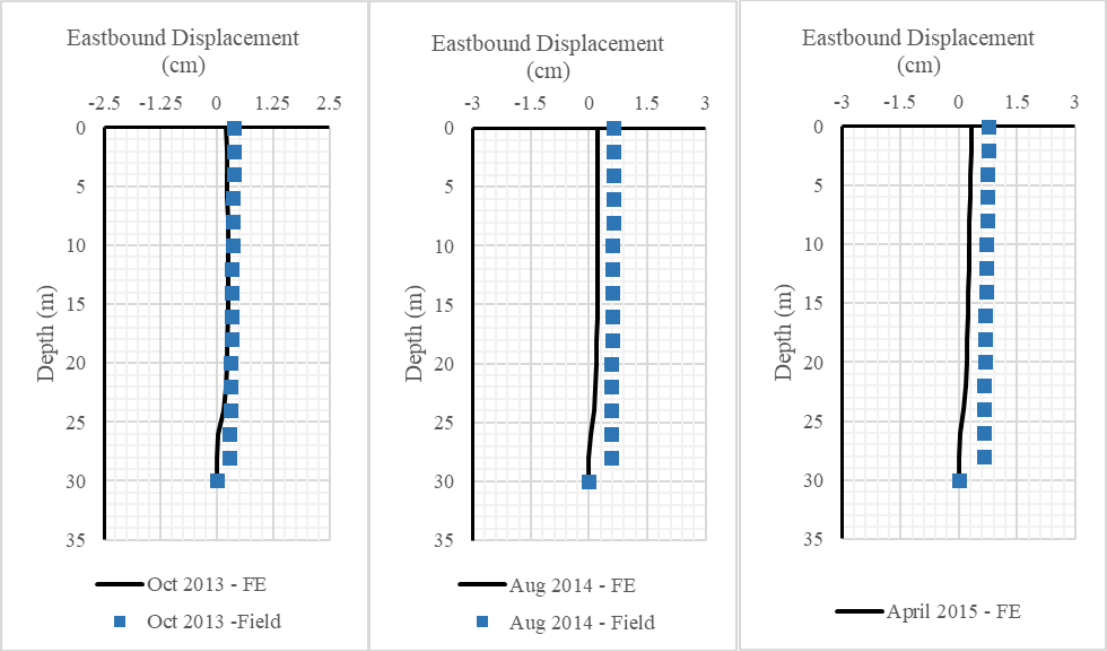

Figure 42 Displacement in eastbound shoulder

1.35.2 Depth to water

The change in the depth of the groundwater was monitored from the year 2010 to the end of 2015. The main aim was to match the seasonal changes in the groundwater so that the model would match the conditions on the site. Also, since the properties of soil and geometry are entered according to the case study, replicating the change in groundwater will ensure that the model is responding to the change in precipitation values. Below is a graph showing the change in depth to water for two positions, Westbound shoulder, and Eastbound shoulder of the highway. Both were measured from the surface to bedrock. As one can see the changes are cyclic, the groundwater level increases at mid-year and gradually decreases till the end.

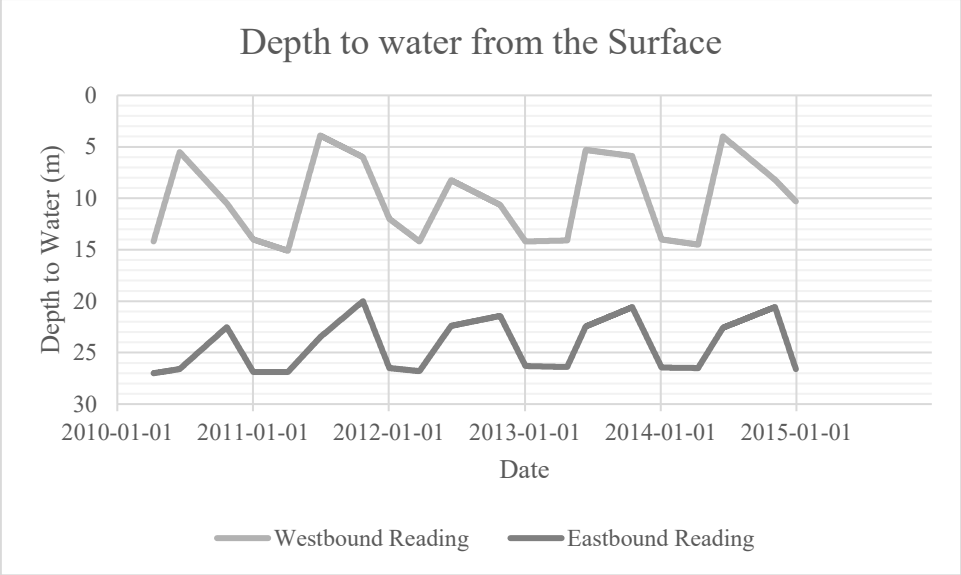

Figure 43 Depth to water for westbound and eastbound shoulder of the highway

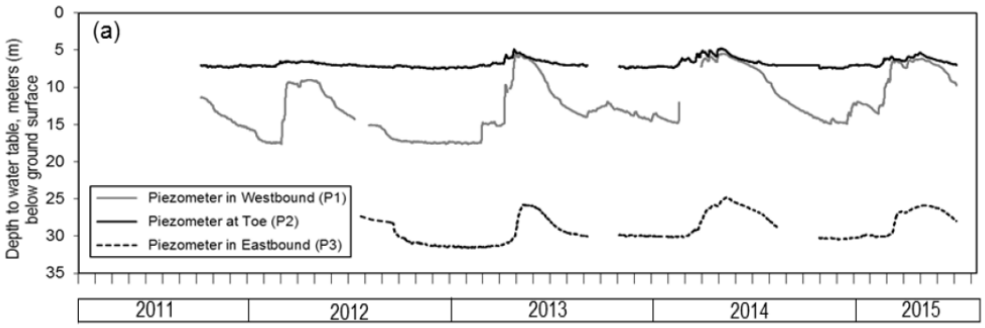

Figure 44 Piezometric reading from the case study [90]

Here are snippets of the saturation percentages throughout the year, and it is apparent from the snippets that the change in the groundwater behaves like the piezometric reading taken on site.

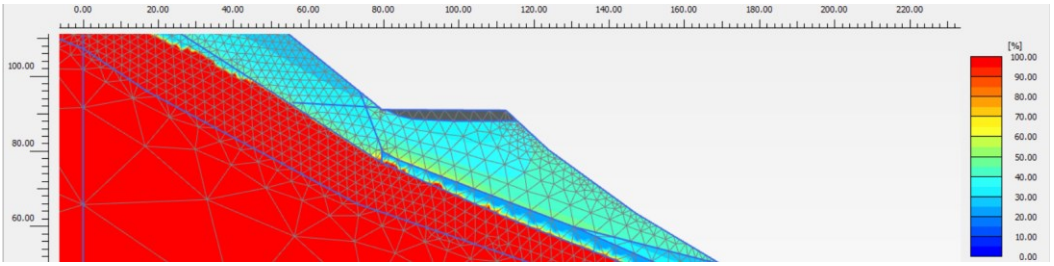

Figure 45 Distribution of Saturation after 90 days of the year 2010 without drains

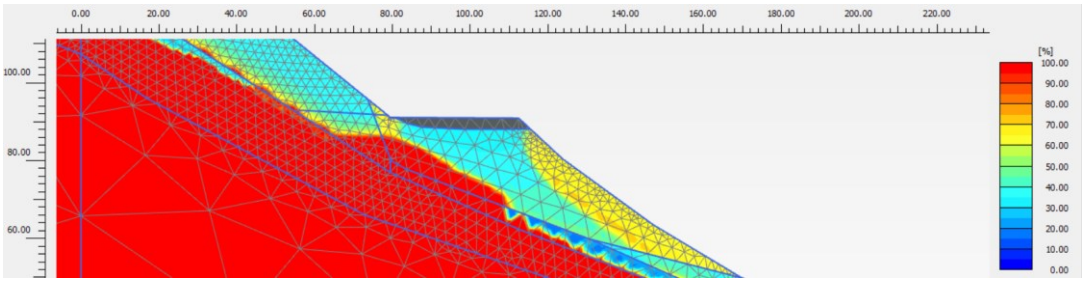

Figure 46 Distribution of Saturation after 168 days of the year 2010 without drains

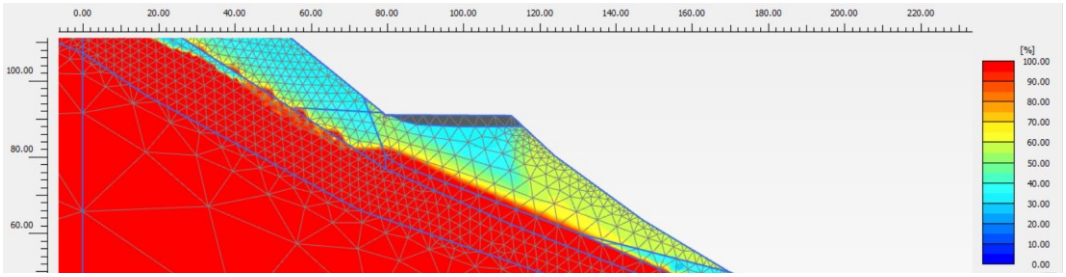

Figure 47 Distribution of Saturation after 295 days of the year 2010 without drains

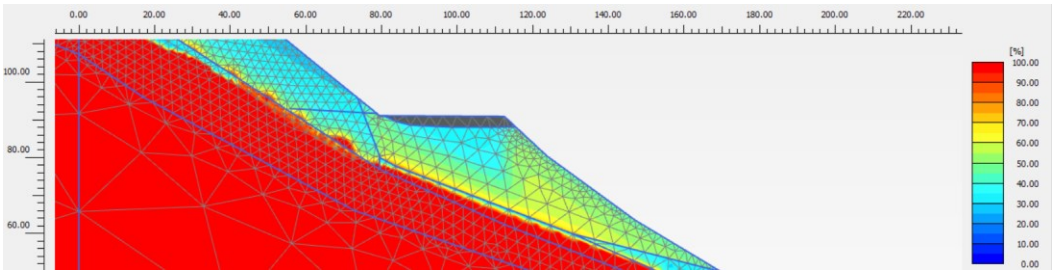

Figure 48 Distribution of Saturation after 365 days of the year 2010 without drains

1.36 North Drain

According to the remedy suggested by the case study, drain was made on north end of just above the westbound shoulder. The effect of drains was impressive and it intercepted the flow of water travelling from the higher elevations in the slope, thus increasing the stability of the slope.

Below snippets from the software show the effectiveness of the drain in intercepting the water, thus reducing the fluctuation in groundwater depth below the highway to contribute to stability of the slope. As seen from the figures there was considerable reduction in the saturation level in the slope after drains were installed. However, there is saturation of around 60% below the eastbound shoulder, and one

possible remedy can be drains in that area but it was not a wise choice because the drains were one the remedy already tried in that area and it had negligible impact on stability because of low permeability of soil.

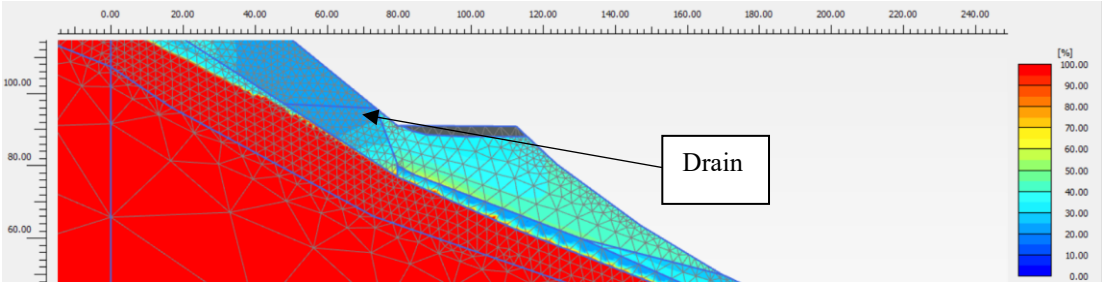

Figure 49 Distribution of Saturation after 90 days of the year 2010 with drains

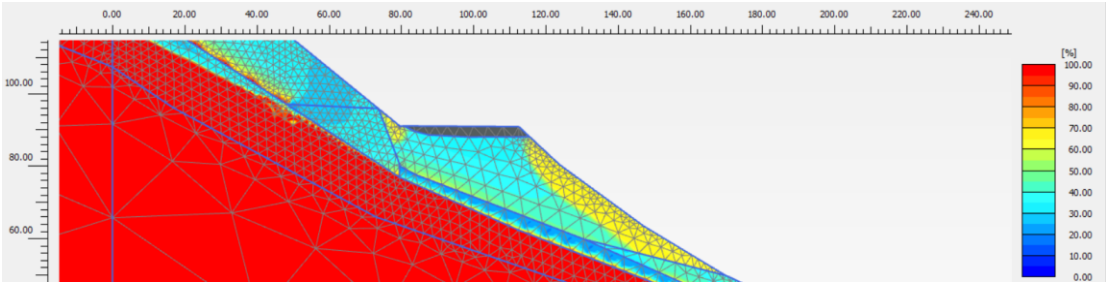

Figure 50 Distribution of Saturation after 168 days of the year 2010 with drains

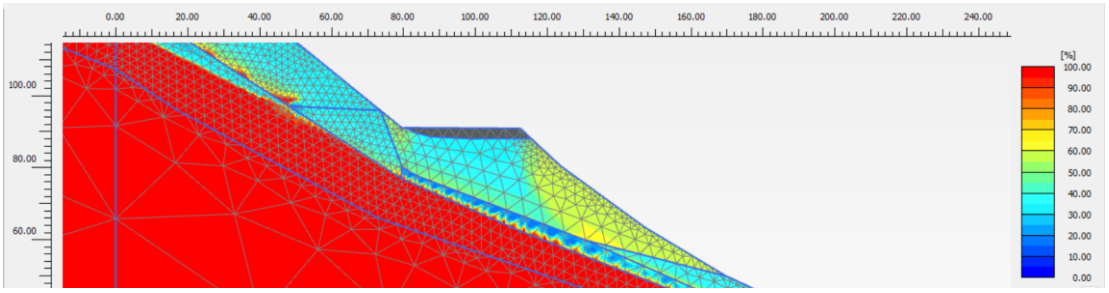

Figure 51 Distribution of Saturation after 295 days of the year 2010 with drains

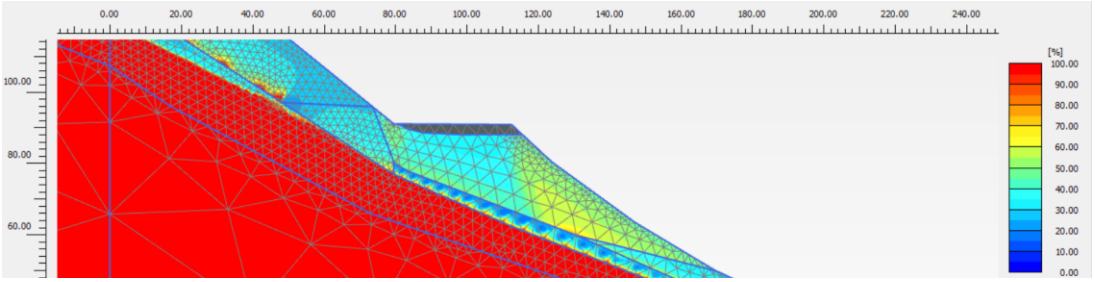

Figure 52 Distribution of Saturation after 365 days of the year 2010 with drains

1.36.1 Safety factor for slope having north drain and no drains.

After model validation safety factor changes for the slope were monitored. Here, in the graph their safety factors of slope with and without north drains are compared alongside the precipitation changes. One of the most significant uncertainties in the data is the assumption that the Grizzly Peak SNOTEL data is indicative of the atmospheric conditions at this site. As predicted, using infiltration data from another site does not provide the same water table response as found at the Straight Creek landslide. The more exposed location of the Straight Creek landslide is most likely experiencing a faster rate of snowpack melting that begins earlier than indicated by the Grizzly Peak SNOTEL, which may account for the lag in the arrival time of water table peaks seen in simulated data as well as some of the difference in the volume of water in the hillslope in simulation versus observed data [96].

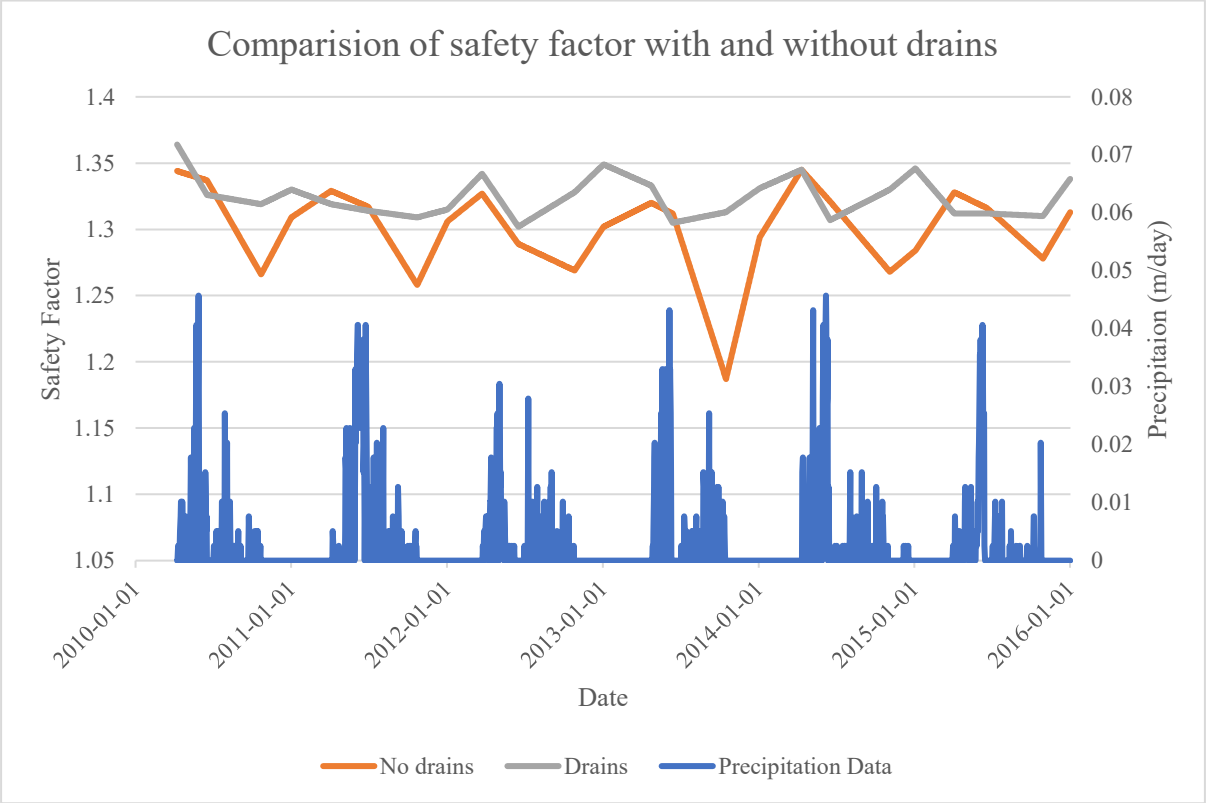

Figure 53 Comparison of safety factor with and without north drains, along with the precipitation data

The non-drained slope seemed to be more fluctuating in response to the precipitation, while the one having north drain is more stable and has safety factor of about 1.325 on average. Here since the highway is a busy one and failure of the slope can cause heavy casualties and long-term closure of the highway, for adequate safety, a safety factor of 1.5 was targeted.

The note here is that the safety factor for the non-drained slope drops to 1.2, which is below minimum requirement decided for slope to be stable. Even for temporary soil nail wall slope the requirement is 1.35. Moreover, the slope with north drains has shown good increase in the stability from the previous model without drains, but at the same time it does not suffice the condition of having a safety factor of 1.5.

1.37 Soil Nail

To further improve the safety factor of the slope soil nails were selected. Here soil nails of varying angles of 10°,15° and 20° were selected according to FHWA circular no 7. Moreover, the spacing was changed from 1.2, 1.5, 1.8 and 2.0 meters. Following images show the layout of soil nails.

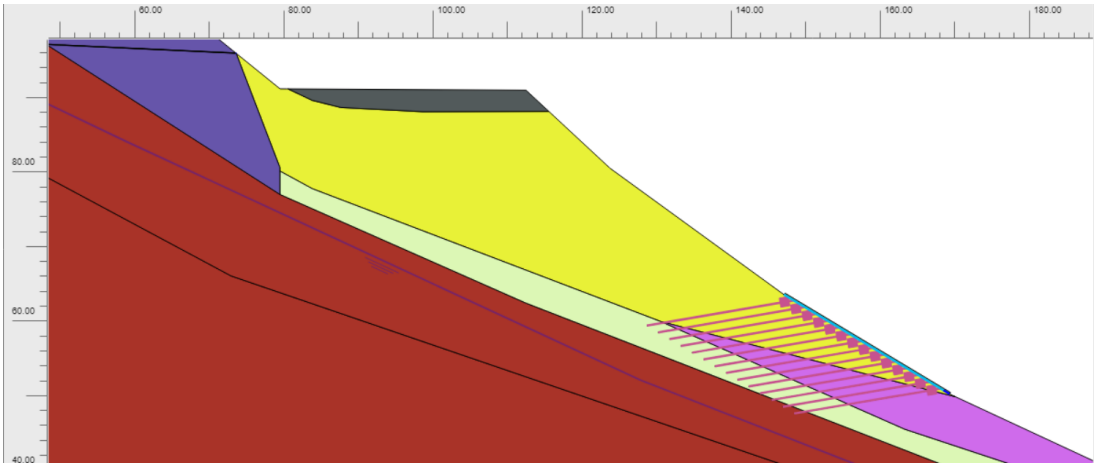

Figure 54 Soil Nail layout with 1.2m spacing and 10 degree inclination

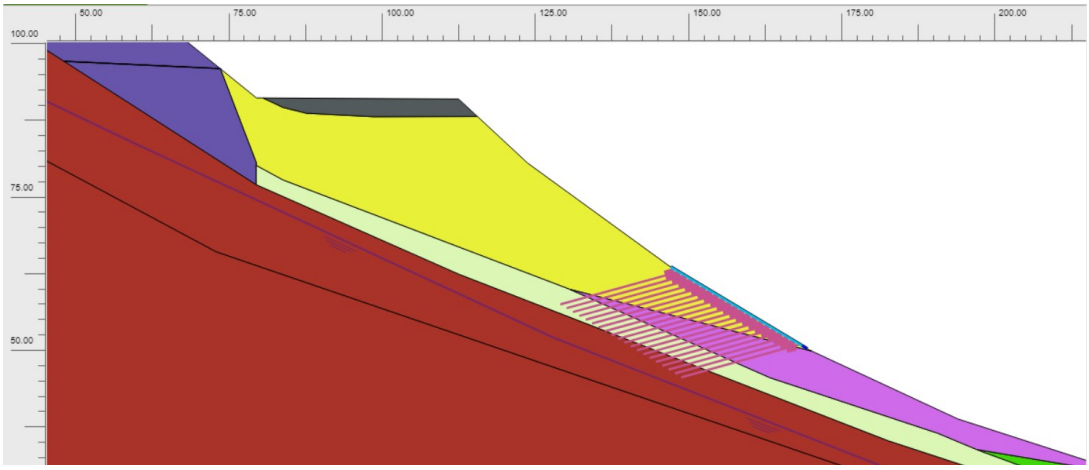

Figure 55 Soil Nail layout with 1.2m spacing and 15 degree inclination

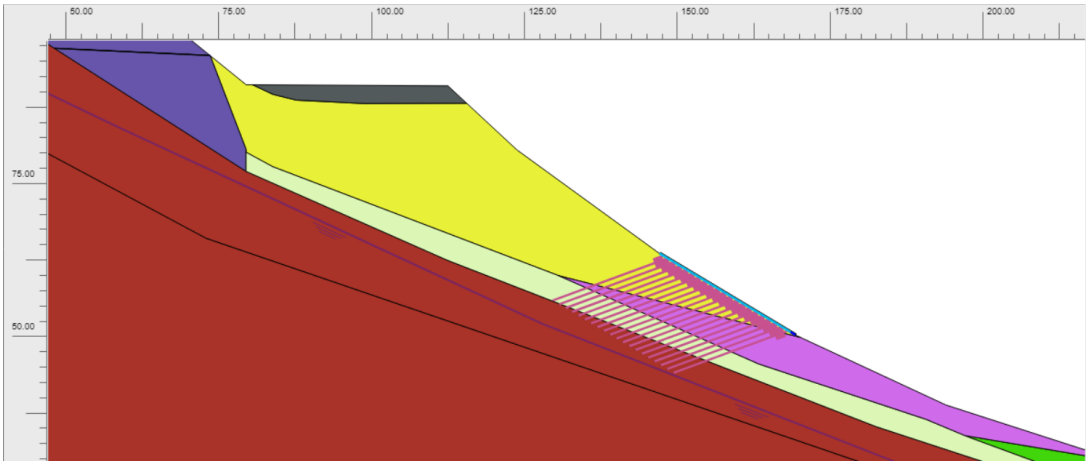

Figure 56 Soil Nail layout with 1.2m spacing and 20 degree inclination

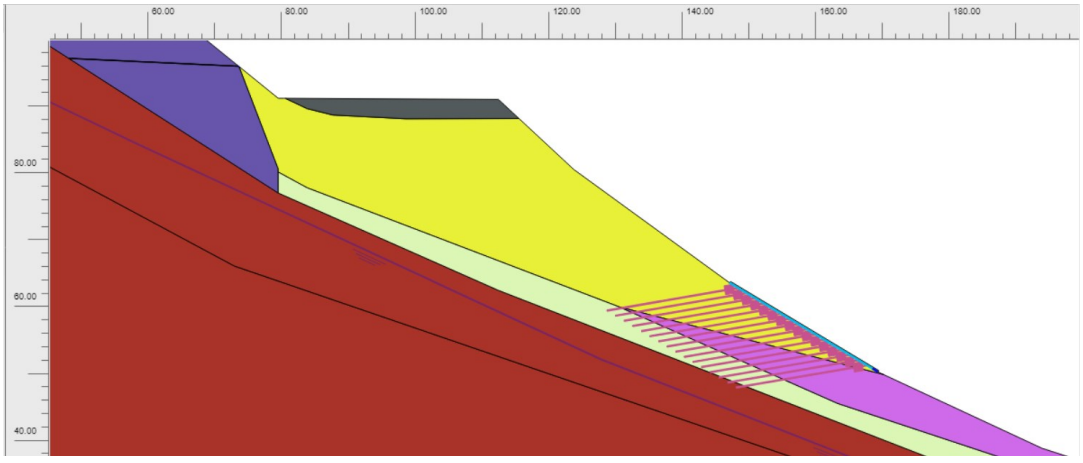

Figure 57 Soil Nail layout with 1.5m spacing and 10 degree inclination

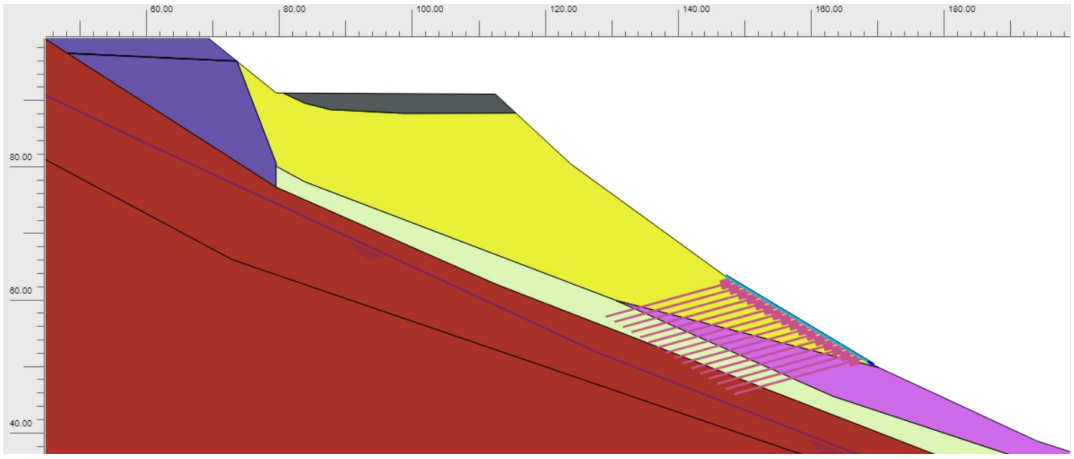

Figure 58 Soil Nail layout with 1.5m spacing and 15 degree inclination

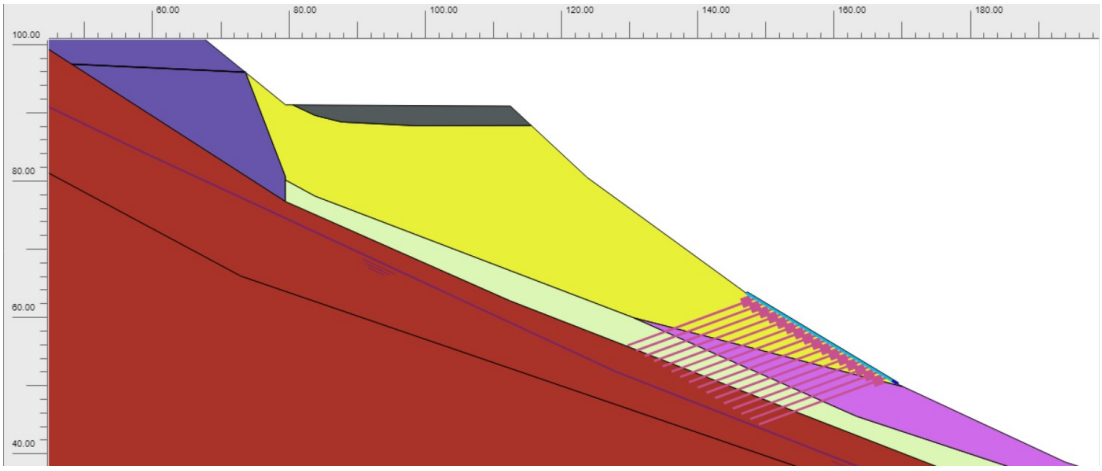

Figure 59 Soil Nail layout with 1.5m spacing and 20 degree inclination

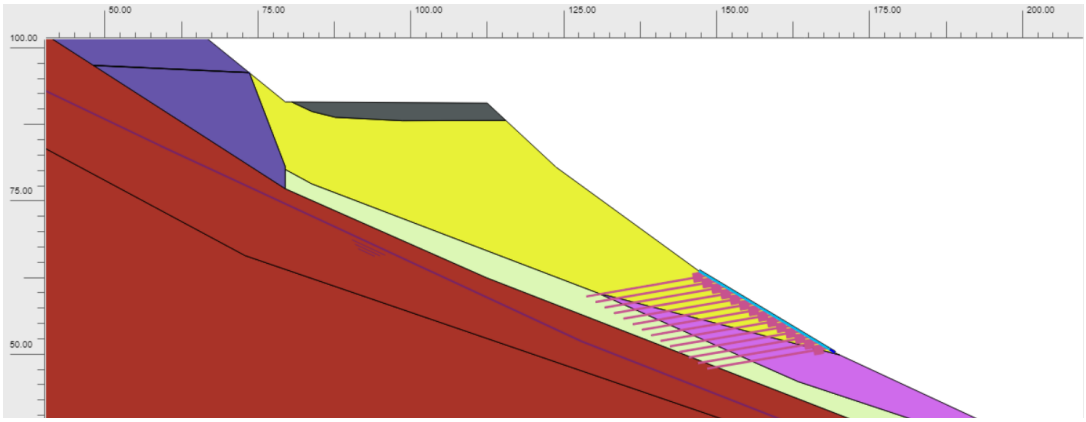

Figure 60 Soil Nail layout with 1.8m spacing and 10 degree inclination

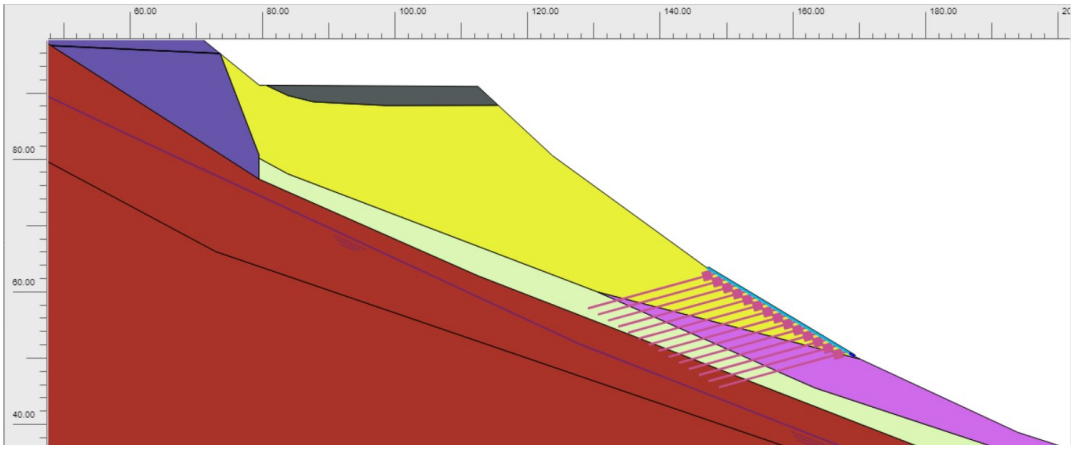

Figure 61 Soil Nail layout with 1.8m spacing and 15 degree inclination

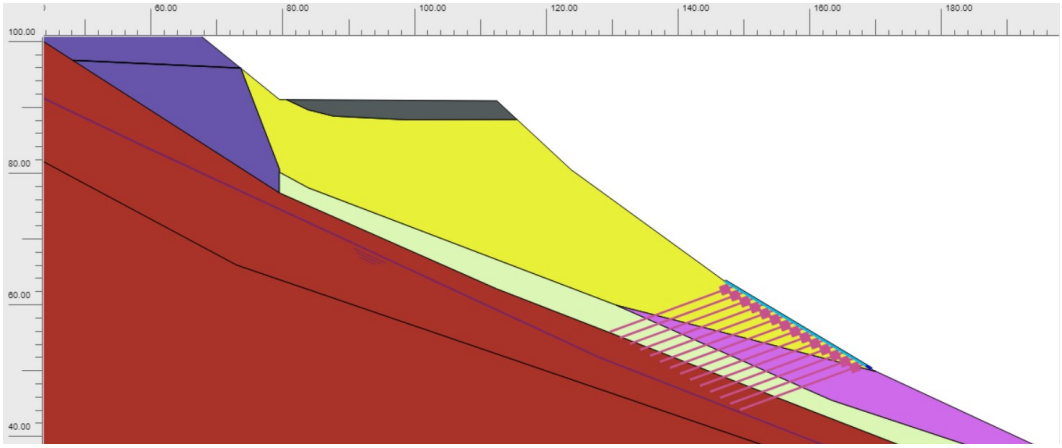

Figure 62 Soil Nail layout with 1.8m spacing and 20 degree inclination

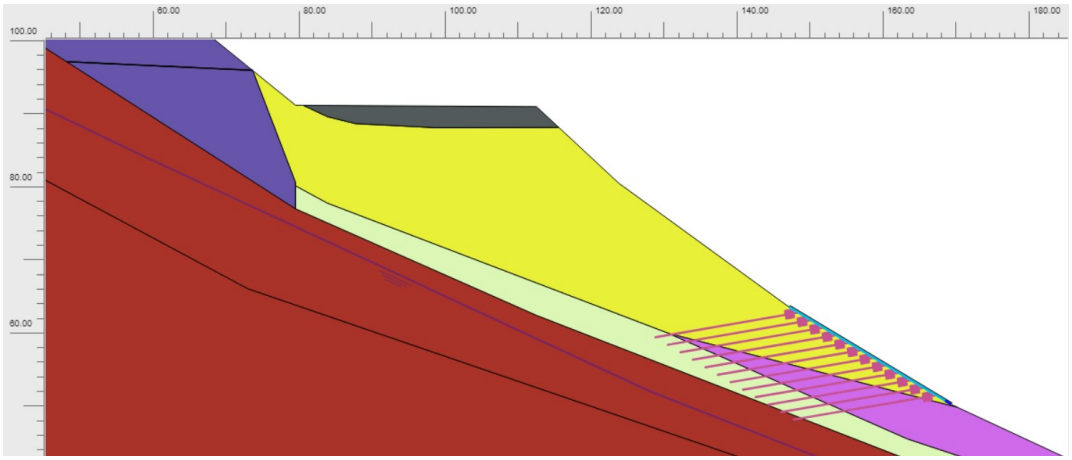

Figure 63 Soil Nail layout with 2.0m spacing and 10 degree inclination

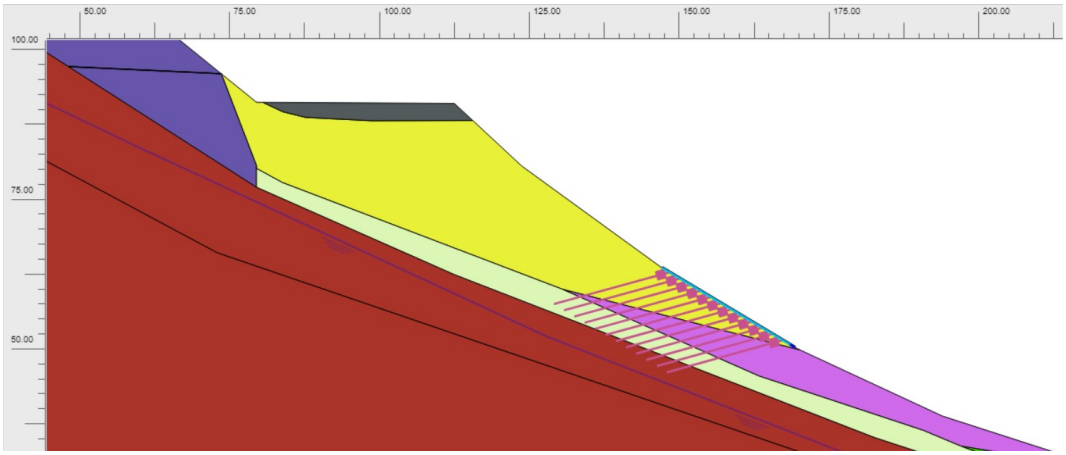

Figure 64 Soil Nail layout with 2.0m spacing and 15 degree inclination

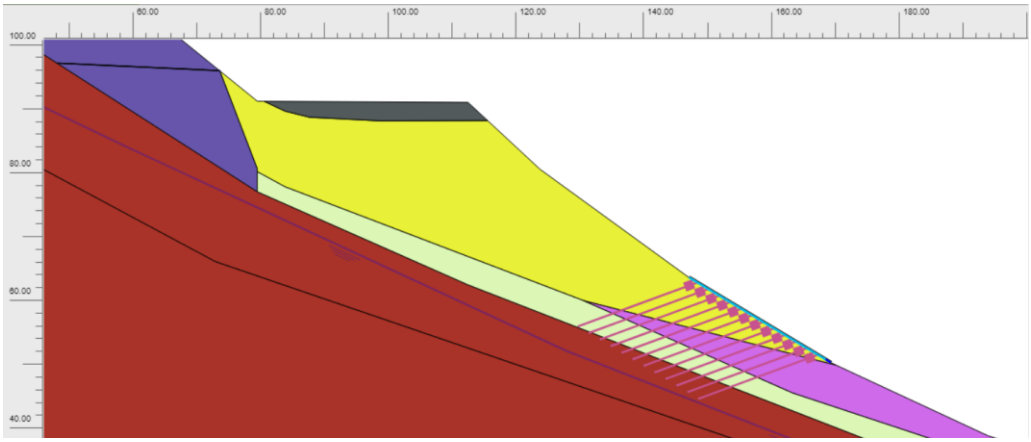

Figure 65 Soil Nail layout with 2.0m spacing and 20 degree inclination

1.38 Effect of Spacing and Inclination on Safety Factor

Here to compare the effect of inclination and spacing the average safety factor values were taken throughout the year and comparison was done. The 20° inclination soil nails have constant effect on the slope regardless of the spacing. A major reason can be due to relatively longer embedded depth in the bedrock. For the 15° inclination the value of safety factor remains same except it reduces marginally for 2.0m spacing. As the spacing between nails increases it reduces the soil holding capacity and hence causes to have lesser safety factor. The 10° inclination proved to be least effective as it had the lowest value of safety factor and looking closely at the values of the 10° inclination one can see that the safety factor increases at 1.5m and then gradually decreases to 2.0m spacing. This demonstrates similar behavior that is seen in the piles,

when piles are too close to each other then it reduces the efficiency of them due to interference and it they are too far it becomes too distributed to support the load.

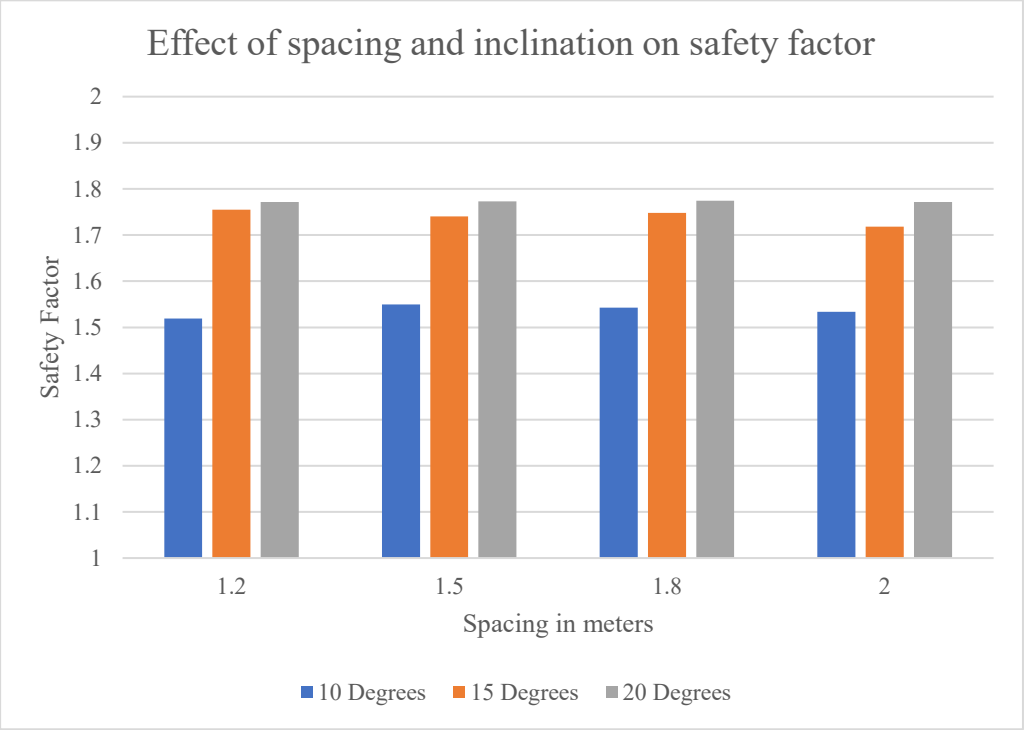

Figure 66 Effect of Spacing and Inclination on the safety factor of the slope

1.39 Yearly changes in Safety factors for all nail layouts

Due to infiltration of water into the soil the safety factor of soil decreases as it loses matric suction. Now it is apparent from the graphs that the safety factor periodically drops at the end of the year and again increases once certain water gets removed from the system. Also, the safety factors are highest during the beginning and end of the year, because its when the saturation percentages are at their lowest, albeit not zero, as the water will contribute to strength of the soil by the help of matric suction. In general, the saturation ranges from 30-40% at the end and beginning of the year. Lastly, the 10° inclination shows highest fluctuations, reaching below 1.5 value multiple times.

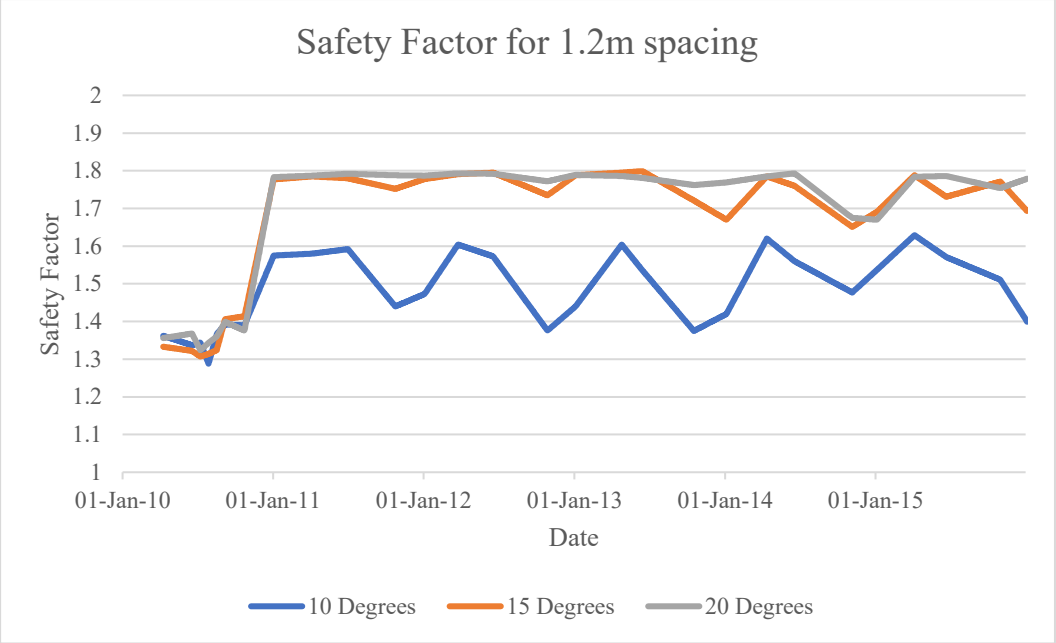

Figure 67 Change in Safety factor for 1.2m spacing.

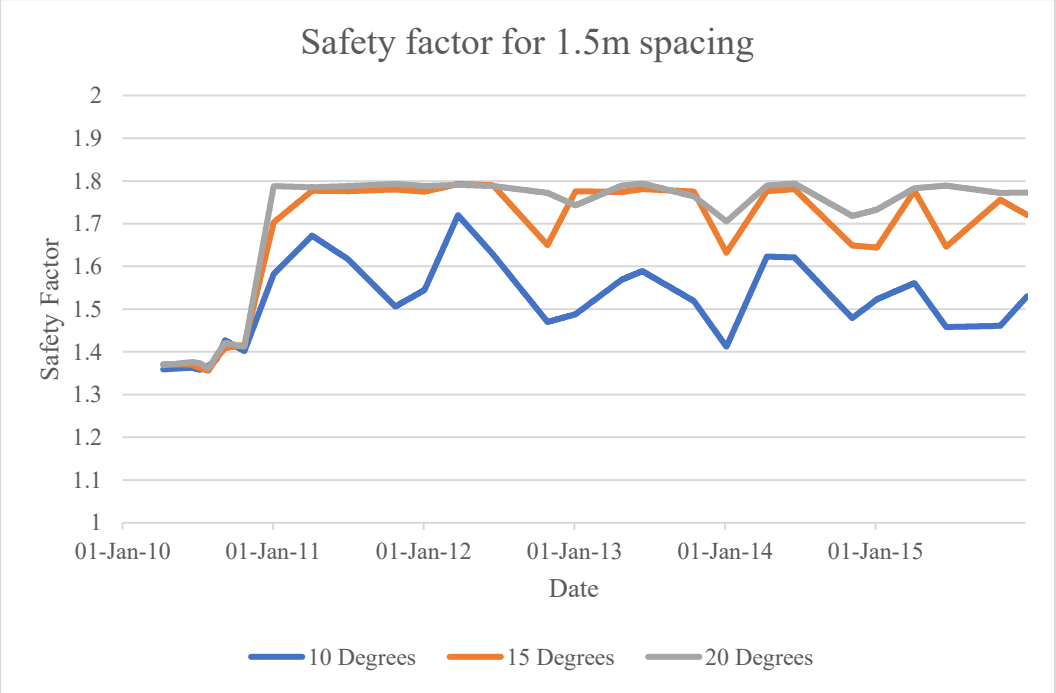

Figure 68 Change in Safety factor for 1.5m spacing.

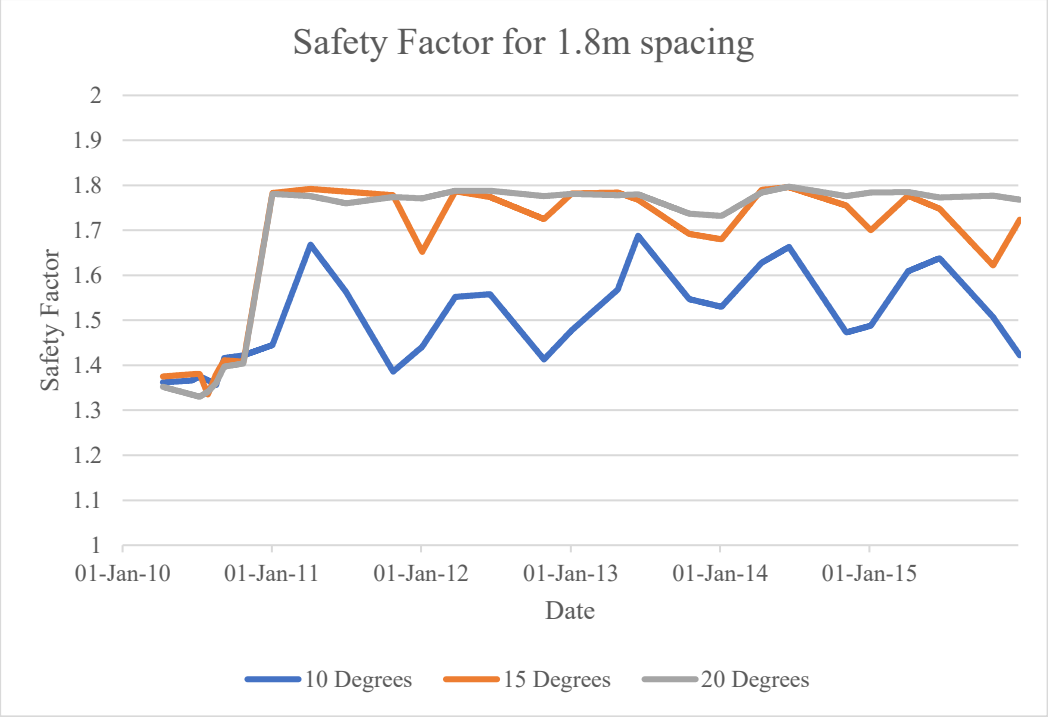

Figure 69 Change in Safety factor for 1.8m spacing.

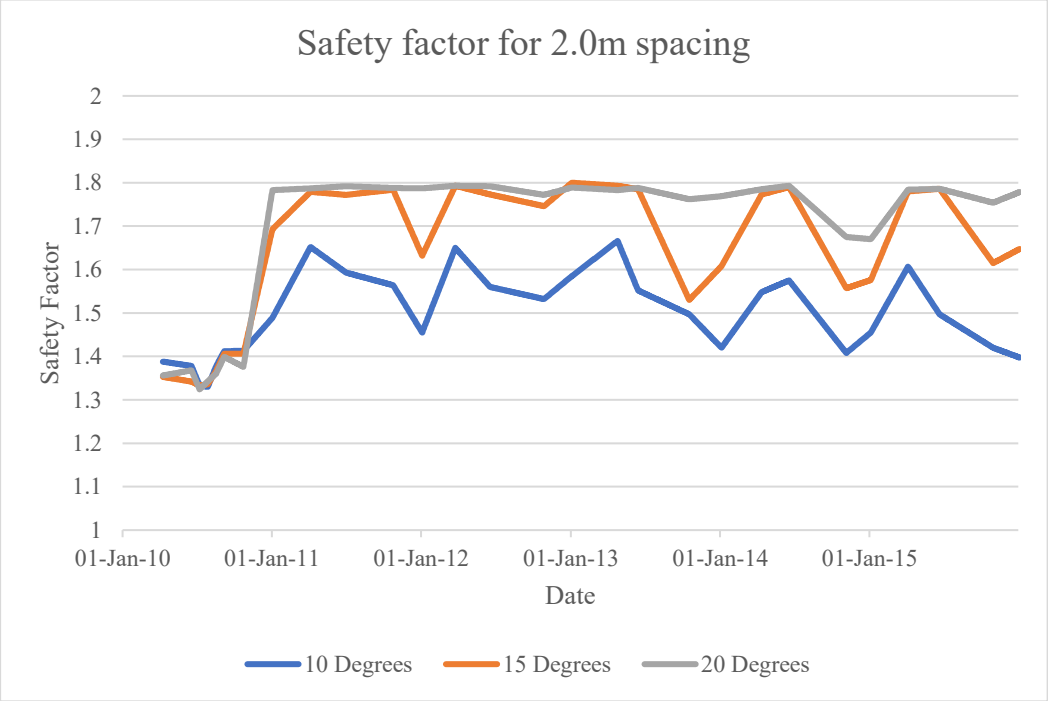

Figure 70 Change in Safety factor for 2.0m spacing.

1.40 Data forecasting for safety factors

In this study the data of safety factors were predicted for future using two methods, using excel and using LSTM deep learning algorithm. The purpose was not

to forecast for each combination but to see and compare the forecasts from excel and LSTM, hence only one of the data is predicted.

1.40.1 Excel forecasting

The excel predictions are little lower than the previously calculated data, but the data seems to follow a general trend, seasonality and it is not too skew from the original data. There is also a lower and upper confidence bound which changes with respect to time, as for certain data accurate predictions can only be made up to a certain point then the accuracy gets reduced.

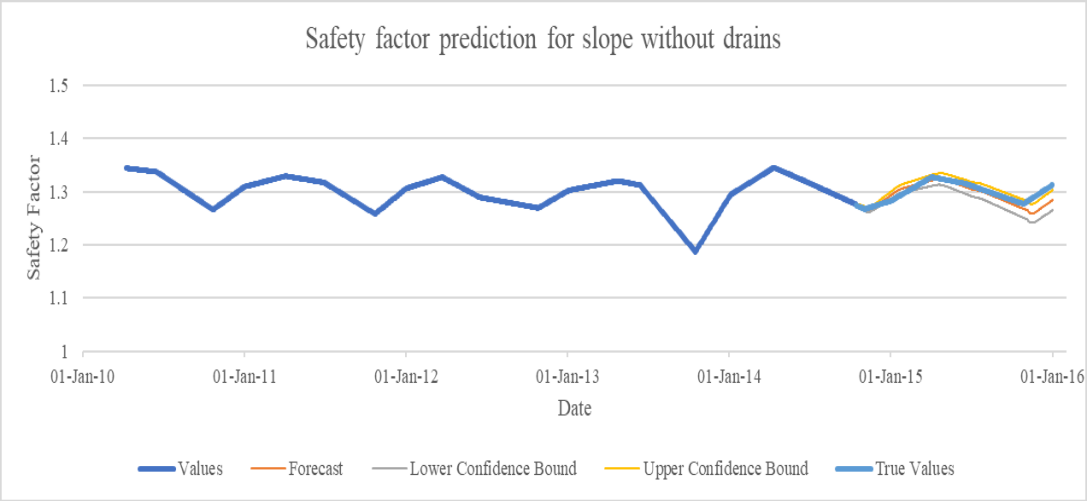

Figure 71 Data forecasting result in excel.

1.40.2 LSTM forecasting

The LSTM model successfully predicted the data like the original data. The model was trained for 80% of the given data and it predicted the rest of 20% values.

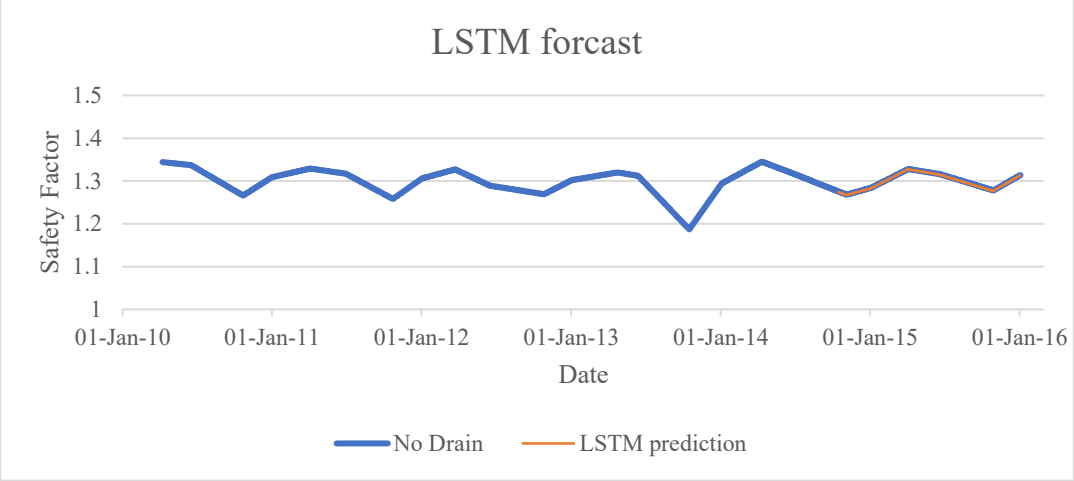

Figure 72 Data forecasting result from LSTM

The plot of the loss over epoch shows that once the epoch value reached just above 40, the trained value became closer to the test value i.e., original value.

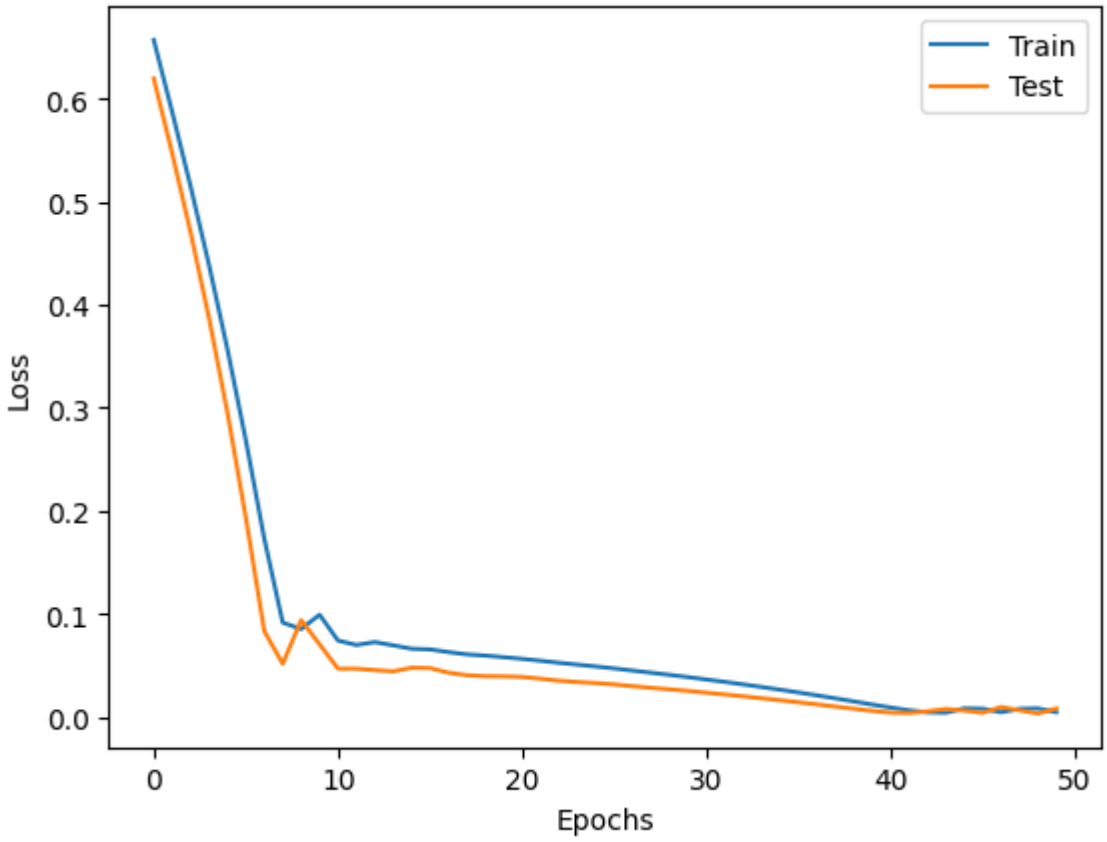

Figure 73 Plot of loss over epochs

6. **Conclusion**

The present study investigates the effectiveness of soil nails and drains for infiltration induced landslide stabilization. Furthermore, the study explores the use of excel forecasting and LSTM algorithm for prediction of future factors of safety value. Valuable insights have been gathered by an in-depth review of relevant literature, and computer modelling. In this part, we summarize the research's significant results and consequences.

The PLAXIS 2D successfully simulated the yearly precipitation cycle for the given slope. It further demonstrates that the north drains can dispel the majority of water and increase the factor of safety, but that won't be enough as we are targeting the safety factor of 1.5. So, to further increase the safety factor soil nails were used. The effect of soil nail was promising, and it increased the safety factor to a significantly safe value. In addition to that, various layouts of soil nails were tested out here, and parametric analysis was conducted to see what the effects are of spacing and inclination on the stability of the slope.

It was observed that nail inclinations of 15° and 20° are very effective and increased the safety factor, one of the main reasons for that was that the end of few nails were embedded in the bedrock which gave the nails necessary friction to hold onto and thereby holding the soil all together. For the spacing, the ideal spacing came out to be 1.5m, as the spacing closer than that caused interference of nails like that of piles, and farther the nails less effectively they would hold the soil together.

Moreover, the data was forecasted for a year using excel forecast function and using the LSTM deep learning model. The excel successfully predicted the trend, seasonal changes and level of the data using the previously inputted data. It not only

predicted the data but also displayed the upper and lower bound values which increased as the time progressed to show that the accuracy of the prediction decreased as the time progressed. The LSTM model is a very powerful tool to make predictions and in this study, it showed high accuracy in predicting the data.

To sum it up, this thesis gives contribution in understanding and implementation of soil nails for infiltration induced landslide stabilization and explores ideal layout of soil nails. It also predicts the future safety factor values using two methods, using excel and LSTM deep learning model. It is hoped that the study inspires further investigation in integration of deep learning in safety factor prediction and improved landslide mitigation techniques.

1.41 Future study recommendations

In this study the length and diameter of the soil nails were not changed so in future one can change them and observe what are their effects. For future study one can optimize the code further and calculate the preceding year's safety factor values to better predict the safety factor. Also, one can use different methods instead of LSTM, such as ARIMA, SARIMA and VARMAX, to predict the safety factors. Additionally, one can make the model multivariate and add the values such as precipitation, displacement, groundwater level etc. to help the model correlate better, at the same time caring for data types where there are lot of zeros for instance moments where there is no precipitation, as it will be difficult for model to correlate and will cause inaccuracy. For that the data should be normalized or augmented in such a way that it makes sense for model.

References

[1] G. F. Sower, "Natural Landslides," *Proc. ASCE Geotechnical Engineering Specialty Conference on Stability and Performance of Slopes and Embankments – II, Berkley, California, pp804-833*, 1992.

[2] E. W. Brand, "State-of-the-art report of landslides in Southeast Asian," *Proc., 4th Int. Symp. on Landslides.*, 1984.

[3] H. Rahardjo, A. Satyanaga, and E. C. Leong, "Unsaturated Soil Mechanics for Slope Stabilization," 2012.

[4] C. S. Brönnimann, "Effect of groundwater on landslide triggering," EPFL, 2011.

[5] R. Sidle and H. Ochiai, "Processes, prediction, and land use," *Water resources monograph. American Geophysical Union, Washington*, vol. 525, 2006.

[6] Government of Canada, "Landslides," https://www.nrcan.gc.ca/science-and-data/science-and-research/natural-hazards/landslides/10661.

[7] N. L. J. Dolojan, S. Moriguchi, M. Hashimoto, and K. Terada, "Mapping method of rainfall-induced landslide hazards by infiltration and slope stability analysis: A case study in Marumori, Miyagi, Japan, during the October 2019 Typhoon Hagibis," *Landslides*, vol. 18, no. 6, pp. 2039–2057, Jun. 2021, doi: 10.1007/s10346-020-01617-x.

[8] R. L. , and L. H. Schuster, *Socioeconomic and environmental impacts of landslides in the western hemisphere*. Denver (CO): US Department of the Interior, US Geological Survey, 2001.

[9] L. TANGENT Technologies, "Common Types of Slope Stabilization Methods," https://tangentmaterials.com/common-types-of-slope-stabilization-methods/.

[10] by Abdulrahman Alhabshi, M. A. Dissertation, and A. D. Budek Sanjaya Senadheera Charles Newhouse Accepted John Borrelli, "FINITE ELEMENT BASED DESIGN PROCEDURES FOR MSE/SOIL-NAIL HYBRID RETAINING WALL SYSTEMS Chairperson of the Committee," 2006.

[11] G. Shanmugam and Y. Wang, “The landslide problem,” *Journal of Palaeogeography*, vol. 4, no. 2, pp. 109–166, 2015.

[12] M. J. Hansen, “Strategies for classification of landslides,” *Slope instability*, pp. 1–25, 1984.

[13] S. Herath and Y. Wang, “Case studies and national experiences,” *Landslides–disaster risk reduction*, pp. 475–497, 2009.

[14] O. Kjekstad and L. Highland, “Economic and social impacts of landslides,” *Landslides–disaster risk reduction*, pp. 573–587, 2009.

[15] L. M. Highland, J. W. Godt, D. G. Howell, and W. Z. Savage, “El Nino 1997-98; damaging landslides in the San Francisco Bay area,” US Dept. of the Interior, US Geological Survey, National Landslide …, 1998.

[16] T. Li, “Landslide hazards and their mitigation in China,” *(No Title)*, 1992.

[17] S. Herath and Y. Wang, “Case studies and national experiences,” *Landslides–disaster risk reduction*, pp. 475–497, 2009.

[18] D. J. Varnes, “Slope movement types and processes,” *Special report*, vol. 176, pp. 11–33, 1978.

[19] D. M. Cruden and D. J. Varnes, “Landslides: Investigation and Mitigation. Chapter 3—Landslides Types and Processes,” *Transportation research board special report*, vol. 247, 1996.

[20] J. N. Hutchinson, “General report: morphological and geotechnical parameters of landslides in relation to geology and hydrogeology,” in *Proceedings of 5th International Symposium on Landslides, Balkema, Rotterdam, Netherlands, 1988*, 1988, pp. 3–35.

[21] S. G. EVANS, M. J. Bovis, and J. N. Hutchinson, “Landslides of the Flow Type,” *Environmental & Engineering Geoscience*, vol. 7, no. 3, pp. 221–238, 2001.

[22] O. Hungr, S. Leroueil, and L. Picarelli, “The Varnes classification of landslide types, an update,” *Landslides*, vol. 11, pp. 167–194, 2014.

[23] R. L. Schuster, *LANDSLIDES: INVESTIGATION AND MITIGATION. CHAPTER 2-SOCIOECONOMIC SIGNIFICANCE OF LANDSLIDES*, no. 247. 1996.

[24] Andrew Ridley, “Inclinometers,” https://www.field-monitoring.org/inclinometer.

[25] H. Wengui, “Stability of Unsaturated Soil Slopes under Rainfall and Seismic Loading,” 2017.

[26] J. E. B. Jennings and J. B. Burland, “Limitations to the Use of Effective Stresses in Partly Saturated Soils,” *Géotechnique*, vol. 12, no. 2. Thomas Telford Ltd., pp. 125–144, 1962.

[27] D. G. Fredlund, “State variables in saturated-unsaturated soil mechanics,” *Soils Rocks São Paulo*, vol. 39, pp. 3–17, 2016.

[28] C. A. Coulomb, “Essai sur une application des regles des maximis et minimis a quelquels problemesde statique relatifs, a la architecture,” *Mem. Acad. Roy. Div. Sav.*, vol. 7, pp. 343–347, 1776.

[29] K. Terzaghi, *Theoretical Soil Mechanics*. New York: John Wiley and Sons, 1943.

[30] W. J. Likos, X. Song, M. Xiao, A. Cerato, and N. Lu, “Fundamental Challenges in Unsaturated Soil Mechanics,” 2019, pp. 209–236. doi: 10.1007/978-3-030-06249-1_8.

[31] B. Fatahi, U. Pathirage, B. Indraratna, M. Pallewattha, and H. Khabbaz, “The role of native vegetation in stabilizing formation soil for transport corridors: an Australian experience,” in *Ground Improvement Case Histories*, Elsevier, 2015, pp. 591–628.

[32] A. Farouk, L. Lamboj, and J. Kos, “A Numerical Model to Predict Matric Suction Inside Unsaturated Soils,” *Acta Polytechnica*, vol. 44, no. 4, 2004, [Online]. Available: http://ctn.cvut.cz/ap/

[33] K. M. H. Ismail Ibrahim, “Effect of percentage of low plastic fines on the unsaturated shear strength of compacted gravel soil,” *Ain Shams Engineering Journal*, vol. 6, no. 2, pp. 413–419, 2015.

[34] T. Nishimura, Y. Hirabayashi, D. G. Fredlund, and J. K. M. Gan, “Influence of stress history on the strength parameters of an unsaturated statically compacted soil,” *Canadian Geotechnical Journal*, vol. 36, no. 2, pp. 251–261, 1999.

[35] Charles W. W. Ng and Bruce Menzies, *Advanced Unsaturated Soil Mechanics and Engineering*. Spon Press, 2007.

[36] H. Rahardjo, Y. Kim, and A. Satyanaga, “Role of unsaturated soil mechanics in geotechnical engineering,” *International Journal of Geo-Engineering*, vol. 10, no. 1, Dec. 2019, doi: 10.1186/s40703-019-0104-8.

[37] A. B. Fourie, “Predicting rainfall-induced slope instability.,” *Proceedings of the Institution of Civil Engineers-Geotechnical Engineering*, vol. 119, no. 4, pp. 211–218, 1996.

[38] D. G. Fredlund and H. Rahardjo, *Soil mechanics for unsaturated soils*. John Wiley & Sons, 1993.

[39] L. L. Zhang, J. Zhang, L. M. Zhang, and W. H. Tang, “Stability analysis of rainfall-induced slope failure: a review,” *Proceedings of the Institution of Civil Engineers-Geotechnical Engineering*, vol. 164, no. 5, pp. 299–316, 2011.

[40] B. D. Collins, S. M. Asce, D. Znidarcic, and M. Asce, “Stability Analyses of Rainfall Induced Landslides”, doi: 10.1061/ASCE1090-02412004130:4362.

[41] S. Utili and G. B. Crosta, “Analysis tools for mass movement assessment,” in *Landslide Hazards, Risks, and Disasters*, Elsevier, 2015, pp. 479–503.

[42] Y. Beyene, “Comparison of Finite Element and Limit Equilibrium Methods for Slope Stability Analysis COLLEGE OF ARCHITECTURE AND CIVIL ENGINEERING COMPARISON OF FINITE ELEMENT AND LIMIT EQUILIBRIUM METHODS FOR SLOPE STABILITY ANALYSIS.”

[43] “Slope Stability ENGINEER MANUAL,” 2003. [Online]. Available: http://www.usace.army.mil/inet/usace-docs/.

[44] C. A. Lazarte, H. Robinson, J. E. Gómez, A. Baxter, A. Cadden, and R. Berg, “Soil nail walls reference manual,” 2015.

[45] CA Lazarte, “Soil Nail Walls Reference Manual Developed following: AASHTO LRFD Bridge Design Specifications, 7 th Edition,” 2015. Accessed: Jul. 03, 2023. [Online]. Available: https://www.fhwa.dot.gov/engineering/geotech/pubs/nhi14007.pdf

[46] T. F. E. Wikipedia, “Soil Nailing,” https://en.wikipedia.org/wiki/Soil_nailing.

[47] C. C. Ikeagwuani and D. C. Nwonu, “Emerging trends in expansive soil stabilisation: A review,” *Journal of rock mechanics and geotechnical engineering*, vol. 11, no. 2, pp. 423–440, 2019.

[48] S. Saleh, N. Z. Mohd Yunus, K. Ahmad, and K. N. Mat Said, “Numerical simulation with hardening soil model parameters of marine clay obtained from conventional tests,” *SN Appl Sci*, vol. 3, pp. 1–13, 2021.

[49] Plaxis 2D, “Scientific Manual 2D,” https://communities.bentley.com/cfs-file/__key/communityserver-wikis-components-files/00-00-00-05-58/PLAXIS_5F00_2D_5F00_2023.1_5F00_2D_5F00_4_5F00_Scientific-Manual.pdf.

[50] Plaxis 2D, “Reference Manual 2D,” https://communities.bentley.com/cfs-file/__key/communityserver-wikis-components-files/00-00-00-05-58/PLAXIS_5F00_2D_5F00_2023.1_5F00_2D_5F00_2_5F00_Reference-Manual.pdf.

[51] S. Naseer, M. Sarfraz Faiz, S. Iqbal, and S. M. Jamil, “Laboratory and numerical based analysis of floating sand columns in clayey soil,” *International Journal of Geo-Engineering*, vol. 10, pp. 1–16, 2019.

[52] E. El Kahi, O. Deck, M. Khouri, R. Mehdizadeh, and P. Rahme, “A new simplified meta-model to evaluate the transmission of ground movements to structures integrating the elastoplastic soil behavior,” in *Structures*, Elsevier, 2020, pp. 324–334.

[53] R. Acharyya, “Finite element investigation and ANN-based prediction of the bearing capacity of strip footings resting on sloping ground,” *International Journal of Geo-Engineering*, vol. 10, no. 1, p. 5, 2019.

[54] B. J. Abbas, H. Y. Aziz, B. H. Maula, and R. T. Alkateeb, “Finite element analysis of spread footing near slops,” in *IOP Conference Series: Materials Science and Engineering*, IOP Publishing, 2019, p. 022055.

[55] R. P. Munirwan, “Escape hill as geotechnical quick response method in facing upcoming tsunami disaster,” in *IOP Conference Series: Earth and Environmental Science*, IOP Publishing, 2019, p. 012053.

[56] S. ÇELİK, “Comparison of Mohr-Coulomb and Hardening Soil Models’ Numerical Estimation of Ground Surface Settlement Caused by Tunneling.,” *Journal of the Institute of Science & Technology/Fen Bilimleri Estitüsü Dergisi*, vol. 7, no. 4, 2017.

[57] V. P. Singh and G. L. Sivakumar Babu, “2D numerical simulations of soil nail walls,” *Geotechnical and Geological Engineering*, vol. 28, pp. 299–309, 2010.

[58] ScienceDirect Topics, “Finite Element Analysis - An Overview,” https://www.sciencedirect.com/topics/physics-and-astronomy/finite-element-modeling.

[59] C. Mosser, “Numerical Study on the Behaviour of Soil Nails,” 2016.

[60] R. B. J. Brinkgreve, S. Kumarswamy, W. M. Swolfs, D. Waterman, A. Chesaru, and P. G. Bonnier, “PLAXIS 2016,” *PLAXIS bv, the Netherlands*, 2016.

[61] G. S. Babu and V. P. Singh, “Simulation of soil nail structures using PLAXIS 2D,” *Plaxis Bulletin*, vol. 25, pp. 16–21, 2009.

[62] T. P. T. Dao, “Validation of PLAXIS embedded piles for lateral loading,” 2011.

[63] E. S. Gardner Jr, “Exponential smoothing: The state of the art,” *J Forecast*, vol. 4, no. 1, pp. 1–28, 1985.

[64] N. Vandeput, *Data science for supply chain forecasting*. Walter de Gruyter GmbH & Co KG, 2021.

[65] “FORECAST.ETS function,” https://support.microsoft.com/en-us/office/forecast-ets-function-15389b8b-677e-4fbd-bd95-21d464333f41.

[66] https://www.ibm.com/topics/deep-learning, “What is deep learning?”

[67] Tanishk Parihar, “Grocery Sales Forecasting,” https://github.com/tan305/Grocery-Sales-Forecasting.

[68] S. Hochreiter and J. Schmidhuber, “Long short-term memory,” *Neural Comput*, vol. 9, no. 8, pp. 1735–1780, 1997.

[69] “Time Series Forecasting Using Deep Learning,” https://www.mathworks.com/help/deeplearning/ug/time-series-forecasting-using-deep-learning.html.

[70] Gaurav Singhal, “Introduction to LSTM Units in RNN,” https://www.pluralsight.com/guides/introduction-to-lstm-units-in-rnn.

[71] Shi Yan, “Understanding LSTM and its diagrams,” https://blog.mlreview.com/understanding-lstm-and-its-diagrams-37e2f46f1714.

[72] Jason Brownlee, “Multivariate Time Series Forecasting with LSTMs in Keras,” https://machinelearningmastery.com/multivariate-time-series-forecasting-lstms-keras/?source=post_page.

[73] Jason Brownlee, “How to Choose an Activation Function for Deep Learning,” https://machinelearningmastery.com/choose-an-activation-function-for-deep-learning/.

[74] NumPy, “Mathematical functions,” https://numpy.org/doc/stable/reference/routines.math.html.

[75] L. Zhang, J. Li, X. Li, J. Zhang, and H. Zhu, “Rainfall-induced soil slope failure,” *Florida: Taylor&Francis Group*, 2016.

[76] S. Elsevier, “International Journal of Sediment Research,” *收錄起迄年: 2008-Present*, 2009.

[77] H. Yang and R. F. Adler, “Predicting global landslide spatiotemporal distribution: integrating landslide susceptibility zoning techniques and real-time satellite rainfall estimates,” *International Journal of Sediment Research*, vol. 23, no. 3, pp. 249–257, 2008.

[78] G. F. Wieczorek, Ls. Eaton, B. A. Morgan, R. M. Wooten, and M. Morrissey, “An examination of selected historical rainfall-induced debris-flow events within the central and southern Appalachian Mountains of the eastern United States,” 2009.

[79] J. J. Hemphill, “Assessing landslide hazard over a 130-year period for La Conchita, California,” in *Proceedings of the Association of Pacific Coast Geographers Annual Meeting. Santa Barbara, CA*, 2001, pp. 12–15.

[80] J. O’Tousa, “La Conchita landslide, Ventura County, California,” *AEG News, Association of Engineering Geologists*, vol. 38, no. 4, pp. 22–24, 1995.

[81] National Oceanic and Atmospheric Administration, “Climatological data,” California, 1995.

[82] National Oceanic and Atmospheric Administration, “Climatological data annual summary,” California, 1995.

[83] M. Wofford, “Ventura,” *California weather conditions: http://www. venturaweather. com/daily. htm, last visited January*, vol. 28, p. 2005, 2005.

[84] R. W. Jibson, *Landslide hazards at La Conchita, California*. US Department of the Interior, US Geological Survey, 2005.

[85] S. A. REGION, “FINAL REPORT OF THE COMMISSION OF INQUIRY INTO THE RAINSTORM DISASTERS 1972”, [Online]. Available: https://www.cedd.gov.hk/filemanager/eng/content_414/er229links.pdf

[86] R. L. Schuster and L. M. Highland, “The Third Hans Cloos Lecture. Urban landslides: socioeconomic impacts and overview of mitigative strategies,” *Bulletin of Engineering Geology and the Environment*, vol. 66, no. 1, pp. 1–27, 2007.

[87] S. Oh and N. Lu, “Slope stability analysis under unsaturated conditions: Case studies of rainfall-induced failure of cut slopes,” *Eng Geol*, vol. 184, pp. 96–103, Jan. 2015, doi: 10.1016/j.enggeo.2014.11.007.

[88] B. S. Pai DS, “IMD (2012) Monsoon 2012: a report,” Pune, India, 2012. Accessed: Jan. 05, 2023. [Online]. Available: https://www.tropmet.res.in/~kolli/MOL/Monsoon/year2012/Monsoon-2012-NEW.pdf

[89] M. Raj and A. Sengupta, “Rain-triggered slope failure of the railway embankment at Malda, India,” *Acta Geotech*, vol. 9, no. 5, pp. 789–798, Oct. 2014, doi: 10.1007/s11440-014-0345-9.

[90] B. Thunder, “THE HYDRO-MECHANICAL ANALYSIS OF AN INFILTRATION-INDUCED LANDSLIDE ALONG I-70 IN SUMMIT COUNTY, CO.”

[91] N. Lu, A. Wayllace, and S. Oh, “Infiltration-induced seasonally reactivated instability of a highway embankment near the Eisenhower Tunnel, Colorado, USA,” *Eng Geol*, vol. 162, pp. 22–32, Jul. 2013, doi: 10.1016/j.enggeo.2013.05.002.

[92] E. Hinds, N. Lu, B. Mirus, and A. Wayllace, “Effects of Infiltration Characteristics on Spatial-Temporal Evolution of Stability of an Interstate Highway Embankment,” *Journal of Geotechnical and Geoenvironmental Engineering*, vol. 145, no. 9, Sep. 2019, doi: 10.1061/(asce)gt.1943-5606.0002127.

[93] Robert k Barret and Dale M Cochran, “Straight Creek Landslides, Colorado Division of Highways,” Colorado, 1971.

[94] A. Wayllace, N. Lu, and J. Godt, “IN-SITU MONITORING OF INFILTRATION-INDUCED INSTABILITY OF I-70 EMBANKMENT

WEST OF THE EISENHOWER-JOHNSON MEMORIAL TUNNELS, PHASE II," 2017.

[95] E. S. Hinds, N. Lu, B. B. Mirus, J. W. Godt, and A. Wayllace, "Evaluation of techniques for mitigating snowmelt infiltration-induced landsliding in a highway embankment," *Eng Geol*, vol. 291, p. 106240, 2021.

[96] B. Thunder, *The hydro-mechanical analysis of an infiltration-induced landslide along I-70 in Summit County, CO*. Colorado School of Mines, 2016.

[97] A. Wayllace, N. Lu, and B. Mirus, "IN-SITU MONITORING OF INFILTRATION-INDUCED INSTABILITY OF I-70 EMBANKMENT WEST OF THE EISENHOWER-JOHNSON MEMORIAL TUNNELS, PHASE III APPLIED RESEARCH & INNOVATION BRANCH," 2021. [Online]. Available: www.coloradodot.info/programs/research/pdfs

[98] Robinson & Associates. 1971, "The geologic investigation of the Straight Creek landslides.," Denver, 1971.

[99] A. Wayllace, B. Thunder, N. Lu, A. Khan, and J. W. Godt, "Hydrological behavior of an infiltration-induced landslide in Colorado, USA," *Geofluids*, vol. 2019, 2019, doi: 10.1155/2019/1659303.

[100] S. Saleh, N. Z. Mohd Yunus, K. Ahmad, and K. N. Mat Said, "Numerical simulation with hardening soil model parameters of marine clay obtained from conventional tests," *SN Appl Sci*, vol. 3, no. 2, Feb. 2021, doi: 10.1007/s42452-020-04115-w.

[101] M. Kahlström, "Plaxis 2D comparison of Mohr-Coulomb and soft soil material models." 2013.

[102] Micha van der Sloot, "Hardening Soil Model," https://communities.bentley.com/products/geotech-analysis/w/wiki/45461/hardening-soil-model.

[103] E. U. Eyo, S. Ng'ambi, and S. J. Abbey, "An overview of soil–water characteristic curves of stabilised soils and their influential factors," *Journal of King Saud University-Engineering Sciences*, vol. 34, no. 1, pp. 31–45, 2022.

[104] M. T. Van Genuchten, "A closed-form equation for predicting the hydraulic conductivity of unsaturated soils," *Soil science society of America journal*, vol. 44, no. 5, pp. 892–898, 1980.

[105] pkraljnovak, “DM_course,” http://source.ijs.si/pkraljnovak/DM_course.

Appendix

Python code for data forecasting using LSTM method

```
import pandas as pd
import numpy as np
from math import sqrt
from sklearn.preprocessing import MinMaxScaler
from keras.models import Sequential
from keras.layers import Dense
from keras.layers import LSTM
from sklearn.metrics import mean_squared_error, mean_absolute_error
import matplotlib.pyplot as plt




# Read the data from excel1.xlsx
df1 = pd.read_excel("d:/excel for python/excel3.xlsx")

# Add a date column as the index starting from April 7, 2010
df1["Date"] = pd.date_range(start="2010-04-07", periods=len(df1))
df1.set_index("Date", inplace=True)


# Frame the inputs as a supervised learning problem
def lstm_super(data, n_in=1, n_out=1, dropnan=True):
    df = pd.DataFrame(data)
    columns, names = list(), list()

    # Input sequence (t-n, ..., t-1)
    for i in range(n_in, 0, -1):
        columns.append(df.shift(i))
        names += [("var(t-%d)" % i)]

    # Forecast sequence (t, t+1, ..., t+n)
    for i in range(0, n_out):
        columns.append(df.shift(-i))
        if i == 0:
            names += [("var(t)")]
        else:
            names += [("var(t+%d)" % i)]

    # Put it all together
    final = pd.concat(columns, axis=1)
    final.columns = names
    return final

# Load the values from the training dataset
```

```
values = df1["Safety Factor"].values

# Convert all data to float data type
values = values.astype("float32")

# Normalize features using MinMaxScaler
scaler = MinMaxScaler(feature_range=(0, 1))
scaled = scaler.fit_transform(values.reshape(-1, 1))

# Frame the inputs as a supervised learning problem
lstm_input = lstm_super(scaled, 1, 1)

# splitting data into train and test set according to 80:20 policy
train = scaled[:1652]
test = scaled[1652:]

# split the train and test further into inputs represented by X and
outputs represented by Y
train_X, train_y = train[:-1], train[1:]
test_X, test_y = test[:-1], test[1:]

# reshape the input to be 3D [samples, timesteps, features] as LSTM
requires inputs in 3D format
train_X = train_X.reshape((train_X.shape[0], 1, train_X.shape[1]))
test_X = test_X.reshape((test_X.shape[0], 1, test_X.shape[1]))

# Design the LSTM model using the Adam optimizer and mean absolute error
(MAE) as the loss function
model = Sequential()
model.add(LSTM(365, input_shape=(train_X.shape[1], train_X.shape[2])))
model.add(Dense(1))
model.compile(loss="mae", optimizer="adam")

# Train the model using 50 epochs
history = model.fit(
    train_X,
    train_y,
    epochs=50,
    batch_size=365,
    validation_data=(test_X, test_y),
    verbose=4,
    shuffle=False,
)



# Save the trained model for future predictions
model.save("safety_factor_model.h5")
```

```
# Make predictions for future unknown values using the trained model
future_predictions = model.predict(future_X)

# Invert the scaling for the forecasted predictions
future_predictions = scaler.inverse_transform(future_predictions)

# Plot the training loss and validation loss over epochs
plt.plot(history.history["loss"], label="Train")
plt.plot(history.history["val_loss"], label="Test")
plt.xlabel("Epochs")
plt.ylabel("Loss")
plt.legend()
plt.show()

# Convert the NumPy array to a DataFrame
test_predicted = pd.DataFrame({'Predicted Safety Factor':
test_predictions.flatten()})




# Save the DataFrame to an Excel file
test_predicted.to_excel('E:/New folder (2)/soil mode/excel for
predictions/Pythonpredicted_data5.xlsx', index=False)
```